CENTRO DE INVESTIGACION Y DE ESTUDIOS AVANZADOS DEL INSTITUTO POLITECNICO NACIONAL

Programa Interdepartamental de

Nanociencias y Nanotecnología

Quitosano/plata nanocompositos para aplicaciones biomédicas

Tesis que presenta:

Siva Kumar - Krishnan

Para obtener el grado de
Doctor en Ciencias en

Nanociencias y Nanotecnología

Director de Tesis:
Dr. J. Gabriel Luna Bárcenas
Dr. Evgen Prokhorov

México, D.F. **Marzo, 2015**

CENTER FOR RESEARCH AND ADVANCED STUDIES OF THE NATIONAL POLYTECHNIC INSTITUTE

Interdepartmental program in

Nanoscience and Nanotechnology

Chitosan/silver nanocomposite for biomedical applications

Presented by:

Siva Kumar - Krishnan

To obtain the degree of
Doctor of sciences in

Nanoscience and Nanotecnology

Thesis supervisor:
Dr. J. Gabriel Luna Bárcenas
Dr. Evgen Prokhorov

Mexico city. **March, 2015**

Acknowledgement

First and foremost I would like to express my deep and sincere gratitude to **Prof. Gabriel Luna Barcenas**, my supervisor, whose deep concern, friendliness and unlimited help. I am deeply grateful to my other supervisor, **Dr. Evgen Prokhorov**, for his direction, guidance, encouragement and support for completing this thesis. I must mention that without his help during my study, this thesis could not have been completed. I would like to thank **Dra. Olimpia Arias**, Institute of Materials Science and Technology, University of Havana, Ciudad de La Habana, Cuba for helping me for biosensor application studies.

I am grateful to express my sincere gratitude and appreciation the reason behind my PhD in Mexico to Dr. Velumani Subramaniam for his faith, guidance and encouragement. Also, I would like to thank the other members of my thesis committee, Dr. Arturo Maldonado, Prof. Mauricio Ortega, Prof. Yasuhiro Matsumoto for their keen eye and new ideas of my work during my advances. I wish to extend my warmest thanks to Dra. Montserrat Hernández Iturriaga**,** Profesor Investigador, Universidad Autónoma de Querétaro, Mexico for helping me out for antibacterial studies. Ultimatley, I would like to take a moment to thank all the workers, students of CINVESTAV, Qro unit for their time with me.

I would like to thank Coordinator **Dr. Jose Gerardo Cabanas Moreno** and academic Secretary **Jessica Márquez Dueñas** of Nanoscience program for their unlimited support. My very special thanks to my colleagues J.A. Muñoz-Salas, Martín A. Hernandez-Landaverde and R. A. Mauricio Sánchez for their continuous support throughout my PhD and my friends Adriana

Hernández Rangel, Diana Zarate, Jose Juan Gervacio and Rodrigo Fernandez Loyola are kindly acknowledged for their valuable friendship.

Most importantly, I acknowledge the economical support of CONACyT Fellowship (Registration No of CVU. **404750**) provided by Mexico government, this research wouldn't be successful. Truly this support brought me so much of smile, happiness to my family.

Finally, I would like to thank Gods abundant blessing in my life that have allowed me to be where I am today. I owe my loving thanks to my family especially to my father, mother and my brother for their years of constant love, support and their prayers.

SIVA KUMAR - KRISHNAN

This thesis is dedicated to
My father, mother and my family.

for their endless love, support, and encouragement.

Contents

List of Figures

List of Tables

Abbreviations

NPs	Nanoparticles
nm	Nanometer
CS	Chitosan
PVP	polyvinylpyrrolidone
PVA	poly(vinyl alcohol)
SDS	Sodium dodocyl sulfate
S.aureus	Staphylococcus aureus
E.coli	Escherichia coli
MIC	Minimum inhibitory concentration
CFU	Colony Forming Unit
ROS	Reactive Oxygen Species
PEG	Poly ethylene Glycol
DD	Degree of deacetylation
Mw	Molecular Weight
MMT	Montmorillonite
NWs	Nanowires
GOx	Glucose Oxidase
UV-Vis	Ultraviolet-Visible
FTIR	Fourier transformed infrared spectroscopy
HR-SEM	High resolution-Scanning Electron Microscopy
EDS	Energy dispersive analysis
TGA	Thermo gravimetric analysis
XPS	X-ray photoelectron spectroscopy
XRD	X-ray diffraction
TEM	Transmission Electron Microscopy
SAED	Selected Area Electron diffraction
SPR	Surface plasmon resonance
DC	Direct current
VFT	Vogel–Fulcher–Tammann
BE	Binding Energy
GHz	Giga Hertz
T_g	Glass transition temperature
T	Tendon or hydrated Form I
L-2	Hydrated
An	Annealed
DE	Dey-Engley
SERS	Surface- enhanced Raman scattering
LEDs	Light Emitting Diodes
EG	Ethylene glycol
1-D	One dimensional
SPR	Surface Plasmon resonance
GCE	Glassy Carbon Electrode
ME	Modified Electrode
CV	Cyclic voltamettery

AEMB	Anaerobic enriched mixed bacteria
PCR-DGGE	Polymerase chain reaction-denaturing gradient gel electrophoresis
NCBI	National center for biotechnology information
CS/AgNPs/GOx	Chitosan/silver nanoparticles/Glucose oxidase
CS/AgNWs/GOx	Chitosan/silver nanowires/Glucose oxidase

Resumen

Se sintetizaron nanocompositos quitosano/nanopartículas de plata (CS/AgNPs) mediante cuatro métodos diferentes. Las propiedades estructurales y de relajación fueron analizadas con mediciones de SEM, TEM, XRD, TGA, infrarrojo, espectroscopia dieléctrica y XPS. Dos procesos de relajación fueron detectados; en las películas húmedas la relajación α asociada con la temperatura de transición vítrea se encontró en el intervalo de temperatura entre 25 y 70°C y se observó una segunda relajación en el intervalo de temperatura entre 80 y 160°C, la cual fue definida como una relajación σ, que frecuentemente se asocia con el movimiento de salto de los iones en la estructura desordenada del composito. Además de las relajaciones α y β, se encontraron por primera vez dos procesos más de relajación a alta frecuencia (en el intervalo 10^8-3 10^9 Hz). Estos dos procesos de relajación se relacionan con la rotación de los grupos –OH y $-NH_2/NH_3^+$. Para las películas CS/AgNPs, la libertad de rotación de los grupos laterales del CS es significativamente modificada debido a la interacción entre dichos grupos y las AgNPs. También, se correlacionaron por primera vez las propiedades eléctricas con la actividad antibacteriana de las AgNPs. Finalmente, se fabricó un electrodo enzimático modificado a base de CS/AgNPs y quitosano/nanohilos de plata (CS/AgNWs) para biosensor glucosa. Se encontró que el biosensor CS/AgNWs es más sensible y estable que el CS/AgNPs. De esta forma, el ajuste de las características fisicoquímicas y la química superficial mediante diferentes rutas de síntesis, el entendimiento más profundo de las propiedades estructurales y el mecanismo de interacción y actividad antibacteriana son factores críticos en el diseño de nanocompositos para aplicaciones biomédicas potenciales.

Palabras clave: *quitosano, nanopartículas de plata, nanohilos de plata, estructura y propiedades, percolación, propiedades antibacterianas y biosensor de glucosa.*

Abstract

Chitosan/silver nanoparticles (CS/AgNP's) composite films have been synthesized by four different methods. Structure and relaxation properties of nanocomposites films have been analyzed by SEM, TEM, XRD, TGA, infrared, dielectric spectroscopy and XPS measurements. Two relaxation processes have been detected; in the wet films in the temperature range 25-70°C, the α-relaxation associated with the glass-rubber transition and the second relaxation was observed in the temperature range 80-160°C and it has been identified as the σ-relaxation which is often associated with the hopping motion of ions in the disordered structure of the composite. In addition to the low frequency relaxations α and β, for the first time, two high-frequency relaxation processes (in the range 10^8-3x10^9 Hz) are reported. These two relaxation processes are related to the rotation of side groups -OH and -NH_2/NH_3^+, respectively. For CS/AgNPs composite films, the freedom of side group rotation is significantly modified due to the interaction between side groups of CS and AgNPs. Furthermore, for the first time, correlation between electrical properties and the antibacterial activity of CS/AgNP's composite has been found. Finally, we have developed the enzymatic glucose biosensor based on CS/AgNPs and chitosan/Ag nanowire (CS/AgNWs).The CS/AgNWs was found to have superior sensitivity, stability compared to CS/AgNPs. In this way, the tailoring the physicochemical characteristics and surface chemistry via different green synthesis routes, deeper understanding the structural properties, interaction and antibacterial mechanism will be shown to have significant impact on designing of nanocomposite for the potential biomedical applications.

***Key words**: Chitosan, silver nanoparticles, Silver nanowires, structure and properties, percolation, antibacterial properties and glucose biosensor applications.*

Introduction

Bacterial infections are a constant threat to human health, and it is a great challenge to the healthcare and scientific community. With the increasing number of infectious diseases caused by different pathogenic bacteria, the studies are orientating towards development of new and effective antibacterial materials which are of great demand. Polymer nanocomposites have attracted significant interest in recent years and have become key functional materials in modern nano science and nanotechnology due to their unique properties and broad range of potential applications. This interest arises as a result of their unprecedented performance, improved properties compared to the individual components, design flexibility, lower costs and extensive applicability in various industrial and wide ranges of biomedical applications. Due to the above properties, it is promising to biomaterial to solve the future demand of antibacterial material. Polymer nanocomposites are advanced functional materials composed of nanoparticles dispersed via direct incorporation or *in situ* generation inside the polymer matrix and/ or coated or functionalized by polymer, thus forming a core-shell structure. As a result, the produced material combines the unique properties of both counter parts.

Among the numerous nanoparticles including noble metals (e.g. Au, Ag) semiconductors (e.g. CdSe, CdS, ZnS, TiO_2, PbS, InP, Si) magnetic compounds (e.g. Fe_3O_4, Co, $CoFe_2O_4$, FePt, CoPt) that have been used as polymer functionalizing agent, silver nanoparticles represents the most promising and extensively used nanomaterial for biomedical and biosensor application. This is mainly due to their unique electric, optical, catalytic and particularly, antimicrobial properties. The synthesis of silver nanoparticles with specific size and shape for antibacterial properties is an important challenge, although it is only the first step towards their successful use in biomedical applications. Typically, AgNPs are likely to undergo significant modifications

when transferred to physiological media, such as aggregation, surface oxidation, which may limit their desired antibacterial properties. On the other hand, numerous practical applications of silver nanoparticles require their entrapment or stabilize them with various substarate and matrices in order to overcome current challenges such as surface oxidation, aggregation and instability which limit their practical applicability in antibacterial and biomedical field. Therefore, biopolymers are the materials of the first choice because of their chemical and structural nature with the long polymeric chains allowing incorporation and through dispersion of nanoparticles. Additionally, the functional groups of such biopolymer provide the platform to obtain highly stable nanocomposite via co-ordination of these side group with nanoparticle surface, as well as it can be used as targeted reactive sites for the controlled one-step synthesis of nanoparticles.

Great efforts have been devoted to investigating the antibacterial properties of silver nanoparticles and polymer based silver nanoparticles nanocomposites. Majority of the previous research on antibacterial studies of silver based nanocomposites are simple preparation, characterization and study their antibacterial activity. The generation of extracellular reactive oxygen species (ROS) by AgNPs oxidation and Ag^+ ion release from the nanoparticle surface were typically proposed for antibacterial mechanism of AgNPs but the exact mechanism of antibacterial activity is not clearly understood yet. Most of the previous studies proposed smaller AgNPs (less than 10 nm) demonstrating significant antibacterial performance due to high specific surface area, facilitates fast release of Ag^+ ions from the surface which could significantly contribute to the antibacterial activity. Therefore recently, new efforts have been attempted to enhance the antibacterial activity by increasing specific surface area using Ag with 1-D (High aspect ratio) nanostructures and nanowires decorated with nanoparticles, which are found to have remarkable enhancement in antibacterial activity. The knowledge about the

chitosan based silver nanocomposites is very few due to their complex nature, difficulties in controlling the size and shape of the nanoparticles. However, both chitosan and silver nanoparticles possess their own antibacterial properties and more interestingly, a synergetic antibacterial activity becomes operational when both components acts together. Thus, this thesis is focused to develop a novel chiotsan based silver bio-nanocomposite and to study their antibacterial potential via preparing different synthesis strategies.

Additionally, glucose detection is of great importance in the biomedical application. Particularly in clinical medicine, diabetes is one of the leading causes of death and disability in the world. The quantitative monitoring of blood glucose is of great clinical importance, which can greatly reduce the risks of diabetes, heart diseases, kidney failure or blindness. GOx enzyme based amperometric glucose biosensor is expected to be ideal models for the fabrication of the biosensors. Therefore, we fabricated CS/AgNPs and CS/AgNWs based modified electrodes for detection of glucose.

Besides literature review and experimental part, five major chapters narrating the experimental results present in this study. The first part is about biosynthesis of AgNPs via anaerobic enriched mixed bacteria culture and characterization. The second part describes structure and properties of CS/AgNPs nanocomposites prepared by different synthesis methods. Third part, for the first time, novel high frequency relaxation process of chiotsan and CS/AgNPs nanocomposites have been investigated. Subsequently other chapter is preparation of bionancomposite based on CS/AgNPs and study the mode of antibacterial action, and its relationship with the electrical properties.The fifth major part talks about the preparation of AgNPs and high aspect ratio Ag nanowires for the electrochemical glucose biosensor based on fabricated CS/AgNPs/GOx and CS/AgNWs/GOx modified electrodes.

Thesis organization

The research organized in this thesis consists of nine chapters. First chapter describe the introduction and literature review of the state of research on antibacterial action of silver nanoparticles and chitosan/silver nanoparticles nanocomposites is summarized. Chapter two provides a justification and objectives of this thesis. Chapter three gives the meaterials, methods and characterization techniques. Chapter four provide the results and discussion of green synthesis method of AgNPs using AEMB culture. Chapter five provides a detail description of the three different synthesis strategies to abtain CS/AgNPs nanocomposite films using simple solution casting techniques. The effect of preparation methods, AgNPs concentration, stabilizing and reducing agent on structure and dielectric relaxation properties are investigated by using scanning electron microscopy (SEM), thermo gravimetry analysis (TGA), infrared (FTIR), dielectric spectroscopy and X-ray photoelectron spectroscopy (XPS) techniques.

Chapter six provides the high frequency relaxation properties of CS films. Additional to the low frequency relaxation process, for the first time giga hertz frequency (GHz) dielectric relaxation of chitosan and CS/AgNPs composites is reported for the first time. Chapter seven describes the chitosan mediated synthesis of CS/AgNPs composite by facile *in situ* preparation without using additional reducing agents. The antibacterial properties and electrical conductivity are crucial in understanding the relationship between antibacterial and electrical conductivity. Chapter eight gives the details of the electrochemical detection of glucose based on chitosan stabilized silver nanoparticles (CS/AgNPs) and silver nanowires (CS/AgNWs) modified glassy carbon electrode (GCE) is presented. Chapter nine conclude the thesis with the new results obtained in this work with some suggestions for the future work.

Chapter 1. Literature review

The development of new material to treat human diseases caused by several pathogenic bacteria has become serious problem recently. Significant efforts have been attempted to find solutions for this serious concern, including vaccination, improvement of hygienic conditions, and antibiotics development. For example, the treatment of infectious diseases has been estimated to cost more than 120 billion dollars per year to the U.S. society as direct healthcare expenses. Moreover, the health care costs associated with the treatment of resistant pathogens is around 5 billion dollars annually [1].

In recent years, nanomaterials (NMs) have received extraordinary attention due to long-term solutions for successful control of such diseases as well as wide range of biomedical applications. The materials composing the nanoparticles produce fascinating and diverse functionalities as a result of their exceptionally small size (1-100 nm). Among different nanoparticles (NPs), silver nanoparticles (AgNPs) have been recognized as ideal candidates for treating such pathogenic bacteria because of their unique antibacterial properties towards broad spectrum of bacterias. Moreover, highly sensitive and specific sensor based on AgNPs have opened up the possibility of creating new diagnostic platforms for disease markers, biological and infectious agents in the early-stage detection of disease and other physiological threats [2]. Additionally, the applications of AgNPs have the highest degree of commercialization. For instance, AgNPs applications have emerged in consumer products ranging from disinfecting medical devices and home appliances to water treatment [3]. Futher more, their unique surface plasmon-resonance scattering (SPR) properties allow AgNPs use in bio-sensing and imaging applications [4].

1.1. Bactericidal effects of silver nanoparticles

Silver nanoparticles (colloidal) have been known for about 120 years [5]. The antibacterial activity of AgNPs was extensively reported previously, which has been demonstrated to have effective antibacterial action against broad-spectrum of bacteria including both *Gram-positive* and *Gram-negative* bacteria [6-8]. The antibacterial activity of silver nanoparticles is highly modulated by their physico- chemical characteristics such as size, shape, surface chemistry and importantly concentration of metallic and ionic content.

Morones et al. showed the size-dependent (1-100 nm range) bactericidal effects of AgNPs toward *Gram-positive* and *Gram-negative* bacteria [7]. They found that AgNPs with small particle size (1-10 nm) exhibits significantly higher affinity and drastically perturbing the membrance function of bacterial cell wall as compared to bigger nanoparticles [7]. Such behavior can be ascribed by high specific surface area of smaller NPs and also fast release of Ag^+ ions. In another study, they have suggested that the toxicity of the AgNPs is strictly related to a reactive oxygen species (ROS) mediated cell death [9]. However, it is not clear whether AgNPs or Ag^+ ions are more effective for the ROS production. On the other hand, many studies tried to correlate the physico chemical properties of AgNPs such as surface modification, surface charge with the bactericidal effects [10]. Moreover, it is evident that the results of the antibacterial effect of AgNPs and Ag^+ ions depends on the method of antibacterial assay.Therefore, need of highly standardized methodlogies to perform the antibacterial activity. Therefore, *Sondi et al.*reported the antibacterial activity in both solid and liquid media [11]. They found that the antibacterial activity is more effective in liquid media compared to the solid media. **Table 1.1** summarizes the exhibited antibacterial activities of AgNPs and Ag^+ ions, the data were collected from the recent published articles.

Table 1.1. The biological effect of silver nanoparticles and Silver ions on microorganisms.

Silver species	Particle size	Functionalization	Organism	Major outcomes	Ref
Ag NPs	75±20 nm	PVP	*Staphylococcus aureus*	MBC=20 mgL^{-1} for 103 cells at cultivation in RPMI/FCS	12
Ag NPs	6.5-43.8 nm	Not reported	*S. epidermidis*	MIC90=6.25 mgL^{-1}; MBC99.9=12.5 mgL^{-1}	13
Ag NPs	7 nm	Gallic acid	*S. aureus*	MIC=7.5 mgL^{-1}	14
Ag NPs	14-16 nm	PVA	Nitrifying bacteria	1 mgL^{-1} inhibits respiratory activity by 86±3%	15
Ag NPs	10 nm	Citrate	*B.subtilis*	no growth inhibition at 50 mgL^{-1};EC50 (CFU assay)>10 mgL^{-1}	16
Ag NPs	25 ±13 nm	Carbonate	*C. reinhardtii*	EC50 (1 h)=0.36 mgL^{-1}: EC50 (5 h) =0.089 mgL^{-1}	17
Ag NPs	25 nm	PVP	*C. albicans*	MIC=0.1 mgL^{-1}	18
Ag NPs	75±20 nm	PVP	*E. coli*	MBC=12.5–20 mgL^{-1} for 103 cells	12
Ag NPs	14–16 nm	PVA	*E.coli*	0.5 mgL^{-1}inhibits bacterial growth by 55±8%	15
Ag NPs	12 nm	None	*E. coli*	50–60μg cm−3(105 CFU), and 20μg cm^{-3}(104 CFU)	11
Ag NPs Powder	1-100 nm	Carbon matrix	*E. coli; V. cholera, P. aeruginosa Salmonella typhus*	MIC: 75μg ml^{-1}	7
Ag NPs	13.4 nm	None	*E. coli and S.aureus*	MIC: 3.3nM (*E. coli*) and >33nM (*S. aureus*)	19
Ag NPs	10–15 nm	None	*E. coli, S. typhi, S. aureaus*	MIC :25μg ml^{-1} for *E. coli,*	20
Ag NPs	9-10 nm	Oleate ions	*E coli and V. cholerae*	MIC: 3μg ml^{-1}	21
Ag NPs	8–50 nm	SDS	*E. coli, P. aeruginosa, S. aureus*	MIC <7 ppm	22
Ag NPs	3 nm	None	*T. mentagrophytes, C. albicans*	IC80: 1–7μg ml^{-1}	23
Ag NPs	25 nm	SDS	*Candida spp*	MIC:210μg ml^{-1} Ag-NPs; 50μg ml^{-1} for SDS Modified	24
Ag NPs	5 nm	None	*C. albicans, Candida glabrata*	MIC: 0.4–3.3μg ml^{-1}	25
Ag^{+}	N/A	- N/A	*E. coli*	0.5 mgL^{-1} inhibits bacterial growth by 100%	15
Ag^{+}	N/A	N/A	*E. coli*	MIC=3.5 mgL^{-1} for 103 cells; MBC=3.5-5 mgL^{-1}	12
Ag^{+}	N/A	N/A	*L.pneumophila*	Complete inactivation at 0.1 mgL^{-1};	26
Ag^{+}	N/A	N/A	Nitrifying bacteria	1 mgL^{-1} inhibits respiratory activity by 42±7%	15
Ag^{+}	N/A	N/A	*S. aureus*	MIC=2.5 mgL^{-1} for 103 cells	12
Ag^{+}	N/A	N/A	*P. aeruginosa ATCC 10145*	complete inactivation at 0.1 mgL^{-1}; survival after 7 days at 0.1 mgL^{-1} as endosymbiont in A. polyphage	26

IC_{80}: 80% inhibitory concentration; SDS: sodium dodecyl sulfate MIC: minimum inhibitory concentration; PVP: poly (*N*-vinyl-2-pyrrolidone); NA: not available.

1.2. Mechanism of antibacterial action of AgNPs and Ag^+ ions

There are several reports proposed the possible mode of antibacterial activity of AgNPs. However, the generation extracellular reactive oxygen species (ROS) by AgNPs oxidation and Ag^+ ion release from the nanoparticle surface were typically proposed for antibacterial mechanism of AgNPs. Due to high specific surface area of the AgNPs, the better contact with the microorganisms is facilitated. The AgNPs gets attached to the cell membrane and also penetrate inside the bacteria [27, 28]. In particular, smaller AgNPs (less than 10 nm) were shown to induce a stronger inhibition of microorganism growth compared to large NPs. The bactericide effect was mainly ascribed to the direct membrane damage, ROS production and block of respiration induced by both AgNPs and Ag^+ ions which seem to have same mechanism.

The antibacterial effect of AgNPs can be significantly contributed by the Ag^+ ion release. But the action of mechanism of silver ions is still not completely understood. There are some hypothesized mechanisms, mainly there different interactions have been elucidated such as direct Ag^+ induced membrane damage, Ag^+ related reactive Oxygen species (ROS) generation, and cellular uptake of Ag^+ ions, with consequent disruption of ATP production and hindering of DNA replication activities. Several previous reports have proposed the direct membrane damage by Ag^+ ions [7, 15, 29-31]. They proposed silver ions may interact with sulfur containing membrane proteins (e.g. with the thiol groups of respiratory chain proteins), causing physical damage to the membrane by visualizing small pits or holes with in the bacterial membranes via TEM analysis. Apart from sulfur containing membrane peptides and proteins, Ag^+ may be also involved in Ag-N and Ag-O bonds with preferential linear co-ordination with the Ag^+ ions [32].

The toxicity of Ag^+ ions are also been ascribed to the generation of ROS. The excess of ROS leads toxicity related to the oxidative stress due to additional generation of free radicals that

may damage both lipids and DNA. In particular, Ag^+ ions may act as catalyst in generating high level of ROS [33] Furthermore, the free radicals may arise from direct impairing of the respiratory chain enzymes carried out by silver, which can be induced photocatalytically or by Ag-promoted fenton reactions [34].

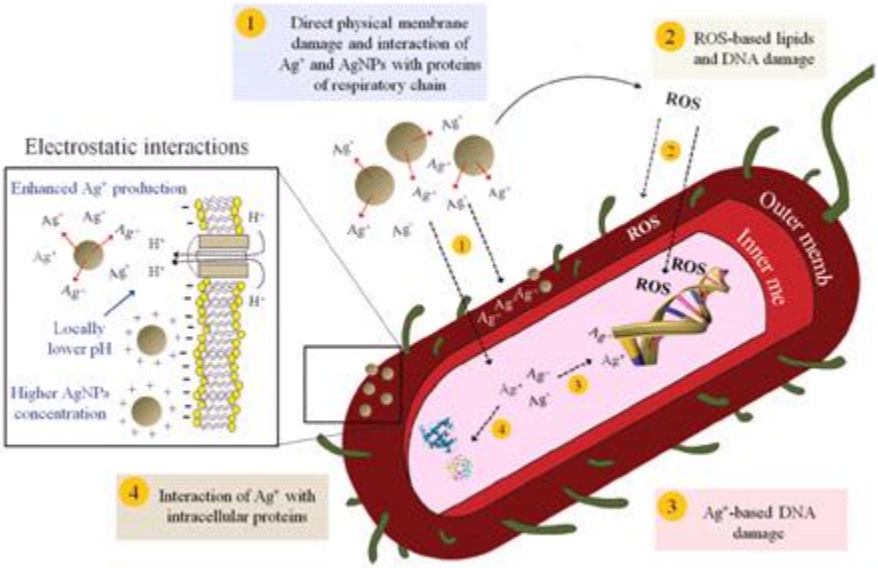

Fig. 1.1 Antibacterial mechanism of AgNPs and Ag^+ ions with the bacteria.

1.3. Functionalization and stabilization of metal nanoparticles

The stabilization of nanoparticles is very important issue to solve the problems related to the aggregation, surface oxidation, and potential use in biomedical application. It is well known that, aggregated nanoparticles reduced the specific surface area and their interfacial free energy, thereby diminishing particle reactivity. Thus, it's extremely important to increase the stability of the nanoparticle during storage and when applied to biological systems. Therefore, there is a need to seek environmental friendly, non-toxic, chemically not reactive stabilizing agents.

Various stabilizing agents are used to prevent the nanoparticle aggregation as well as functionalization of nanoparticle surface for the desired application. However, usually reactive and toxic chemicals may not be suitable for the biomedical applications. Currently, there are several green stabilizing agents such as polyphenols, enzymes, citric acid, vitamins, biodegradable polymers and silica can be used for stabilize or functionalize the nanoparticles without the undesirable consequences on the environment. Among, biopolymers are highly suitable for the biomedical applications.

1.4. Biopolymer is an exciting matrix to stabilize NPs.

Among different polymers known to be widely used for biomedical applications, the most commonly applied polymers are poly(ethylene glycol) and carbohydrates such as starch [35] dextran [36] and chitosan [37]. In particular, chitosan biopolymer attracted much attention for stabilization of metal nanoparticles because of its functional groups $-NH_3^+/NH_2$ and -OH exhibits strong co-ordination with the metal nanoparticle surface leading to high stability of the obtained nanocomposite. In addition, chitosan based nanocomposite exhibitis potential biomedical applications including wound dressing [38], carriers for drug or gene delivery [39], tissue engineering [40] and cancer diagnosis [41]. The above promising applications of CS is mainly due to its excellent properties such as minimum foreign body reaction, biocompatibility and biodegradability in a physcologically relavent environment, intrinsic antibacterial nature, prepared in different forms (e.g. fibres, membranes, scaffolds, sponges, tubes). Also CS was shown to have ability to reduce metal ions ($AgNO_3$, $HAuCl_4$) into metallic nanoparticles without additional toxic reducing agents [42].

1.5. Chitosan biopolymer

Biopolymers are an important class of polymeric materials that have intensively attracted the attention of the scientific community. Chitosan is typically obtained by deacetylation of chitin under alkaline conditions, which is the second most abundant polysaccride after cellulose. (Fig.1). Chitosan is a linear polysaccride, composed of glucosamine and N-acetyl glucosamine units lined by (1-4) glycosidic bonds. As a result, the polymer does not have a single well-defined structure and may have different molecular weight (Mw) and sequences. The content of glucosamine is called degree of deacetylation, depending on the conditions of the deacetylation process, different forms of chitosan are available. Those forms vary in the deacetylation degree (DD) and average molecular weight (Mw) of the polymer. In fact, in a general way, it is considered that when the DD of chitin is higher than about 50% (depending on the origin of the polymers and on the distribution of the acetyl groups along the chains), it becomes soluble in an aqueous acidic medium, and in these conditions, it is named as chitosan. The DD and Mw of the chitosan affect the physico chemical properties and their applications.

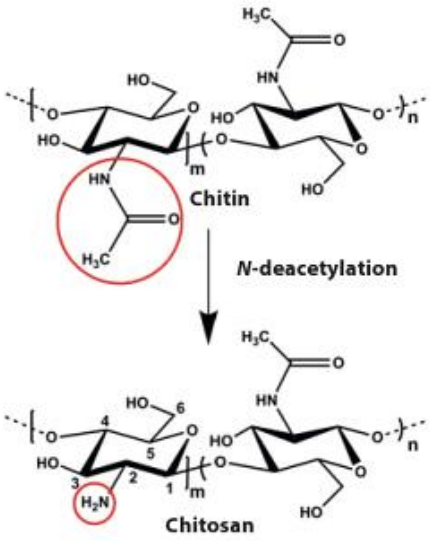

Fig.1.2. Structure of Chitin and Chitosan

1.5.1. Physicochemical properties of chitosan and its applications

Chitosan displays interesting properties such as biocompatibility, biodegradability and its degradation products are non-toxic, non-immunogenic and non-carcinogenic [43]. Chitosan contains two reactive hydroxyl groups (C-3 and C-6) and an amino group at the C-2 position of the glucosamine residue which is responsible for the unique properties of chitosan. The reactivity of chitosan is largely dependent on pH which affects its charged state and properties Due to the presence of strong intra and intermolecular hydrogen bonds; the polymer does not dissolve in most organic or aqueous solvents. This poor solubility restricts the possible applications of the polymer. In order to increase polymer solubility, derivatives of chitosan have been synthesized by attaching hydrophilic or hydrophobic groups to the polymer backbone. One particular route to increase solubility, involves the conversion of the C-6 hydroxyl groups into a carboxy or amino group, thereby increasing solubility in organic and aqueous solvents.

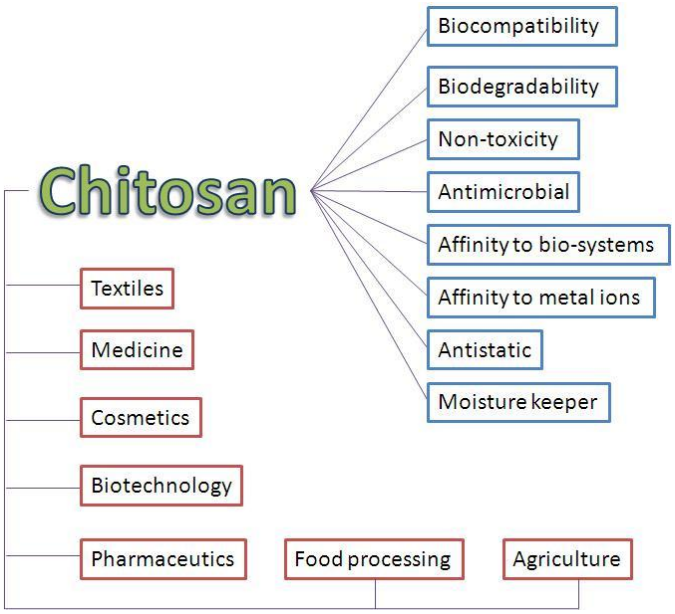

Fig.1.3. properties of chitosan and their applications.

1.5.2. Structural characteristics of chitosan

The chitosan structural forms correspond to the hydrated crystals in which the water molecules may or may not be located in the crystallographically defined position in the unit cell. Upon heating chitosan samples in water, the crystals were converted into anhydrous form. The crystal nature of the chitosan structure was first reported by *Sakurai et al*. [44]. Later, *Ogawa et al.* studied extensively different polymorphs [45]. Mainly two important structures have been reported. The hydrated form or tendon form chitosan have identified in both non-neutralized and neutralized form. The dehydrated (annealed) form has been observed by removing of structurally bound water as well as the free water. In case of non-neutralized film it is difficult to obtain dehydrated form which is either too unstable due to presence of week acids (acetic acid). Such physical properties of chitosan, arising from the crystalline nature might be correlated to its chemical and biological activities.

1.5.3. Molecular motion and dielectric relaxation of chitosan

Dielectric relaxation studies on polysaccharides have been reported in literature, for example *Einfeldt et al*. have reported the molecular motions and commonly observed relaxation process for various polysaccharides which exhibits similar relaxation process as CS [46, 47]. The increasing numbers of studies of dielectric measurements in polysaccharides are controversially discussed about the shape of the dielectric spectra, number of relaxation process and their interpretation. Among the main causes for the discussion are the very complex supramolecular structures of chitosan such as intra and intermolecular hydrogen bonds and the strong influence of water content [48]. The presence of water can significantly distort the results, giving rise to additional relaxation process in the material.

The β-relaxation is the main one found in all polysaccharides, including chitosan, at temperatures between -135 to 120^{o}C; this relaxation is related to segmental motions of the chains via the glycoside bond and therefore, it corresponds to local chain dynamics appearing just above 10^6 Hz [46]. The σ-relaxation process at higher temperature (80-180^{0}C) and low frequency range (about of 100-1000 Hz) is associated with the hopping motion of ions in the disordered structure of the biomaterial and it is independent on water content. Additionally, an α-relaxation assigned to the motion of a water-polymer complex has been observed in wet chitosan and wet cellulose materials in the 1k Hz-6 MHz range between 20-70^{o}C; this relaxation is traceable to a plasticizing effect of water [49]. It is noteworthy that in hydrated samples of polysaccharides, proteins and biopolymers water molecules can be directly bounded to give rise to additional relaxations. The polymer chain restricts the orientation of water molecules such that the collective motions of the macromolecule-water are distorted giving rise to relaxation times about 100 fold as slow as that of pure water [50].

1.6. Chitosan/silver nanocomposites

Polymer nanocomposites are advanced, functional material have attracted significant interest in recent years due to their unique physico-chemical properties and broad range of potential applications. Silver nanoparticles (AgNPs) polymeric nanocomposites are particularly sought after due to the combination of their optical, catalytic and antibacterial properties [51]. Most of the practical application of silver nanoparticle (AgNPs) demand the polymeric functionalized or stabilized by homogeneously dispersed polymer matrix. Biopolymer such as chitosan (CS) are usually the most suitable matrix due to a specific surface morphology, chain structure, functional side groups (-NH_3^+/NH_2 or -OH) enabling nanoparticles chemically

interacts with the functional groups of these biopolymers and their homogeneous dispersion. In some cases, the functional groups of polymers may be responsible for the synthesis and stabilization of silver nanoparticles.

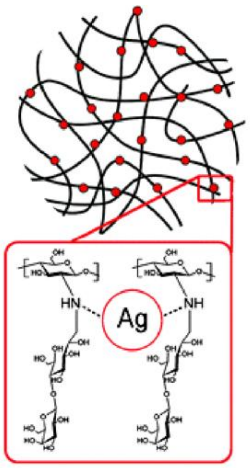

Fig.1.3 Interaction of Silver nanoparticles with the Chitosan functional groups

1.7. Synthesis strategies of CS/AgNPs nanocomposites.

Different routes of synthesis of chitosan/AgNP composite have been prepared such as chemical reduction using different reducing agents, direct *in situ* reduction; also, separately prepared AgNPs have been mechanically incorporated within chiotsan films were summarized in Table 1.2. Among different routes to obtain stable CS/AgNPs composites, most applied synthesis methods are chemical reduction and *in situ* formation of AgNPs using chitosan as reductant and stabilizing agent.

1.7.1. Chemical reduction

The chemical reduction method is the most extensively applied method to prepare AgNPs with high yield. Several previous studies exploited the synthesis of CS/AgNPs composite by chemical reduction methods as shown in the Table 1.2. For instance, most pioneering work by *Potara et.al.* showed CS/AgNPs composite obtained by two step chemical reduction process

using sodiumbhrohydrate and sodium citrate as reducing and stabilizing agents [52]. However, they obtained triangular and truncated triangular shape together with some spherical particles. *X. L. Cao et al.* [53] reported ascorbic acid based chemical synthesis of CS/AgNPs composite. Also, *Jin An et al* [54] prepared using $NaBH_4$. Most of these studies showed that the resultant composite exhibites by-products from the chemical reaction that significantly affect the biomedical potential of the resultant nanocomposite.

1.7.2. Chitosan biopolymer as reductant

The *in-situ* reduction methods using the chitosan as reducer and also as stabilizer have become very popular because they are easy to implement. The major advantage of the *in situ* reduction method is that they usually yield a homogeneous distribution of nanoparticles in the polymer matrix. This *in situ* synthesis is highly favorable due to increase the effectiveness and to avoid the necessity of employing additional toxic reducing agents. Recently, many groups have demonstrated that *in situ* synthesis methods can be used to generate highly stable nanocomposite for various applications [55-58]. However, by *in situ* reduction methods it remains a challenge to control nanoparticle size and efficiency of reduction process which possess limitations on the fabrication of nanocomposite with tunable functionalities.

1.8 Antibacterial and proliferative activities of CS/AgNPs composites

The antibacterial activities of AgNPs have been reported in numerous reports previously. (see table 1.2). However, the mechanism of antibacterial activity of CS/AgNPs is not completely understood. *Potara et al* [52] reported the synergetic antibacterial activity of CS/AgNPs composites is combination of different mechanism of action of two components. i) The strong interaction between AgNPs surface and the functional groups (- NH_3/NH_2 and -OH) of chitosan, the AgNPs surface is covered by the CS which leads to steric stabilization and decrease of

aggregation potential. Consequently, the AgNPs exhibits higher effective surface area capable of interacting with the cellular surface; in our studies we experimentally verified this effect; the fact is acceptable only below percolation threshold concentration. Above percolation threshold concentration the AgNPs tend to agglomerate which highly decreases the antibacterial activity [59] ii) The positive charge conferred to the particles by the CS enhances their binding to negative charges present at the cell surface. In spite of excellent antibacterial properties of CS/AgNPs composite, it has been successfully applied in therapeutic applications such as impregnated catheters and wound dressing. Tran and co-workers demonstrated that CS/AgNPs remarkably inhibited the growth of MCF-7, HepG2 (human hepatocellular carcinoma), Lu (human lung carcinoma) and KB (human epidermic carcinoma) cancer cell lines [60].

Table 1.2. The biological effect of chitosan/silver nanoparticle (CS/AgNPs) nanocomposites on microbial strains.

Type	Method Of preparation	Reaction Temp	Particle Size	Microbial strains	Major outcomes	Ref
CS/AgNPs composite	In-situ reduction	95^{O}C	3-22 nm	*S.aureus*	MIC 52 mM (1.7E^{2} CFU)	58
CS/AgNPs composite	Two step Chemical reduction	35^{o}C and 0^{o}C	28-55 nm	*S. aureus*	MIC 4µg ml^{-1}	52
CS/AgNPs composite	Direct incorporation	26^{o}C	25 nm	*S. thyphimurium, S.aureus,E. coli, Listeria monocytogenes.*	MIC 2 Wt%	59
CS/AgNPs Colloidal suspension	gamma-ray irradiation	26^{o}C	7-30 nm	*E. coli and S. aureus*	Clear Zone 0.354 and 0.092 cm	61
CS/AgNPs Composite	In-situ reduction	30-100^{o}C	5-30nm	*E. coli, P. aeruginosa, L. fermentum, E. faecium, S. aureus, B. subtilis, C. albicans*	MIC 10 µg ml^{-1}	62
CS/AgNPs composite	Chemical reduction	N/A	3-18 nm	*E. coli, B. subtilis, S. aureus, and P. aeruginosa.*	MIC 150-400 µg ml^{-1}	54
CS/AgNPs composite.	Chemical reduction.	N/A	16-53 nm	*S.aureus, K.pmeumoniae, E.coli*	Inhibition zone (mm) 1.5-2 mm	63
CS/AgNPs composite	Chemical reduction	4-25 ^{o}C	22-175 nm	*S.aureus*	Inhibition zone (mm) 19-20 mm	64
CS/AgNPs composite	Chemical reduction	N/A	50 nm	*E.coli*	Inhibition zone 0.5 cm	65
CS/AgNPs composite	In-situ reduction	95 ^{o}C and 60 ^{o}C	4-18 nm	*S.aureus, E.coli*	MIC :10 µg ml^{-1}	56
CS/AgNPs composite	Chemical reduction	2-100 ^{o}C	21.0-110 nm	*S.aureus, E.coli*	Inhibition zone 2.0 and 1.5 mm	53
CS/AgNPs composite	In-situ reuction	95 ^{o}C	2-4nm	*E. coli,*	MIC :100 µg ml^{-1}	66
CS/AgNPs composite	In-situ reuction	95 ^{o}C	10 nm.	*GFP-expressing E. coli*	MIC :48.8 µg ml^{-1}	67
CS/AgNPs composite	Chemical reduction	30 ^{o}C (Tamp)	10-15 nm	*S. aureus, P. aeroginosa, Salmonella entrica*	No Inhibition zone	68
CS/PEG/AgNPs	In-situ reduction	80^{o}C	5-50nm	*E. coli, Pseudomonas aeroginosa, S. Aureus,methicillin-resistant S. aureus*	Inhibition zone 15-18mm	69
CS/ MMT/ AgNPs	UV irradiation	N/A	3-26 nm	*S. aureus, E.coli.*	Inhibition zone (mm) 8.2 to 8.6	70
CS/MWCNTs/AgNPs	Chemical reduction	120^{o}C	2-16 nm	*S. aureus E. coli*	MIC 5 µg ml^{-1}	71

CS: Chitosan; MIC: Minimum inhibitory concentration; MMT: montmorillonite; N/A: not available.

1.9. Applications of CS/AgNPs nanocomposites

1.9.1 Advanced tissue regeneration and wound dressing applications.

Chitosan is an important class of biomaterial due its biological properties. It was shown that chitosan can accelerate wound healing by activating and modulating the function of inflammatory cells such as neutrophils, macrophages, fibroblasts and endothelial cells [72]. Therefore, chitosan has been successfully applied to the tissue regeneration. In order to enhance the tissue regeneration property, it has been used in different physical forms such as scaffolds, hydrogells, fibres, membranes etc. [73]. Additionally, the design of nanomaterials which possess not only excellent mechanical properties, but also shown to have strong cell adhesion properties which makes them popular to improve bone and tissue regenerative functions [74].

In number of studies, the application of chitosan based materials for treat burns and wounds have been reported [75]. Recently emergence of silver nanoparticle is found to be used in diverse medical application such as silver based dressing, treatment of chronic wounds. *Sibbald et al*. [76] showed that silver nanoparticle based dressing on variety of choronic non-healing wounds. In addition, incorporation of silver nanoparticles with the chitosan biopolymer are promising matrices providing good cell attachment besides their antibacterial properties, which is ideal candidate for wound dressing and wound healing applications.

1.9.2 Biosensors.

A growing demand of integration nanomaterials based biosensor platforms with minimal costs, potential real time monitoring and point-of-care applications. Different nanomaterials have been emerged recent times for the integration of biosensors and biomarkers. Among metal nanoparticles, silver nanoparticles have proven to be one of the most important groups of

nonomaterials for biosensing applications. In particular, a novel hydrogen peroxide sensor based on AgNPs on a glassy carbon electrode with superior electrocatalytic abilities for H_2O_2 reduction have been constructed [77]. *W. Shi et al*. have reported amperometric glucose biosensor based on a triangle silver nanoprism/chitosan composite film as immobilization matrix [78]. Silver nanowires stabilized with chitosan for sensing glucose are also reported [79]. Chitosan biopolymer displays an ideal matrix to stabilize Ag nanostructures and immobilize enzymes stably with efficient electrical communication while maintaining their biological activities due to its excellent film-forming ability and good biocompatibility. Therefore, highly sensitive and stable sensor based on chitosan/silver system has opened up the possibility to creating new biosensing platforms for early stage detection of various diseases.

1.9.3 Cancer treatment

The cancer disease has become the second most likely cause of death worldwide. In 2004; approximately 7.4 million peoples were killed by cancer, most of them from developed countries. By 2030, this number estimated to reach 12 million. Therefore, it is extremely important to find anticancer material to resolve the demand. It is well known that chitosan biopolymer exhibits intirsic antibacterial activity and interaction with the mammalian cells. Recently, *H. H. Shuai* reported that surface modulated chitosan membranes exhibits distinct structurally based interaction and distruction of NIH-3T3 fibroblast cells [80]. Also, chitosan based nanocomposites showed to be excellent candidate to drug targeting to cancer cells. For example, chitosan/Fe_3O_4 nanocomposite has been used to enhance the intravenous delivery of the anticancer agent gemcitabine to the cancer tissue [81]. The metal nanoparticles (Au and Ag) and semiconducting quantum dots (CdS, CdSe) potentially applied to early detection and targeting of

cancer cells due their unique size dependent surface plasmon resonance (SPR) properties [82]. Recently, Ag nanorods were used in detecting cancer as a multivalent binding in order to increase binding strengths of the aptamers in cancer cell recognition [83]. Therefore, there is a potential platform to use chitosan-silver based nanocomposite for detecting and targeting cancer cells.

1.10. Chitosan /silver nanocomposites – a promising biomaterial for advanced biomedical applications

The constantly expanding field of polymer /AgNPs composite has been proven to become significant functional materials due to their well proven antibacterial properties and great potential for biomedical applications. It is evident from the previously published literatures; the chitosan based silver nanoparticles nanocomposite is emerging generating simple and cost effective powerful methodologies with a variety of morphologies, compositions and surface modification for the various advanced biomedical applications such as antibacterial and antinflamation, cancer diagnosis, advanced tissue regeneration and drug and gene delivery applications. Additionally, AgNPs demonstrate localized plasmon resonance that is promising for next generation optical imaging and sensing applications. For research based chitosan-silver nanocompsites containing different size, shape and modifying surface chemistry, large emphasis has been made. In particular, I-D nanostructures recently have been developed for the potential use as assembly and integration of molecular-scale components into electronic devices and wide range of antibacterial and biomedical applications. As synthesis of very small well defiend nanostructures and polymer based synthetic methodology advancement and become more mainstream, exciting new opportunities will emerge for the fabrication of next generation smart nanocomposite that have multible functionalities and tunable physical properties.

Despite of massive use of chitosan based AgNPs for different advanced applications and the numerous studies regarding their mechanism of antibacterial action, there is still a significant level of controversy. Several reports proposed that direct interaction of NPs with the cell wall. Other publications explained antibacterial activity mainly contributed due to Ag^+ ions. But there is lack of direct evidence and standard methodology to quantify the Ag^+ ion release in the biological medium in order to confirm the hypothesis. On the other hand, the unique characteristic of AgNPs depends on the synthesis methods and were exploited in many biomedical applications. However, the complexity arises when change the AgNPs characteristics such as size, shape, surface chemistry and charge. Different experimental methods have been proposed for preparation nanocompsites, still there are search for new green and environmental friendly synthesis route that allows the preparation of composite with biocompatible, biodegradable, and non-toxic with silver nanoparticles attached homogeneously and narrow size distribution.

Chapter 2. Justification and Objectives

2.1. Justification

Over the last decade the development and implications of nanomaterials in various biomedical and clinical applications has risen exponentially due to their unique physicochemical characteristics. Noble metal nanoparticles (Ag, Au) have already proven to be one of the most important classes of nanomaterials for biomedical applications as well as for biosensing platforms [2, 84]. It is well known that the toxicity of AgNPs is strongly associated to their physicochemical parameters such as particle size, shape, surface charge, compositions and subsequent stability of the nanoparticles. Significant advances have been made in the synthesis methodologies to prepare AgNPs with controlled size and shape, surface charge and physicochemical characteristics.

In the literature there are many reports focusing on the preparation and characterization of CS/AgNP's nanocomposite (**see chapter 1**). From these reports it is possible to conclude that the properties of nanocomposite films depend not only on the dimension of nanoparticles but also on their concentration, distribution, methods of preparation and the type of interaction with chitosan matrix. However, to the best of our knowledge, there are no reports about influence of preparation methodology and concentration of AgNP's on the structure, electrical and dielectric relaxation properties of CS/AgNP's nanocomposites. It is noteworthy that the relation between electrical, structure and concentration of nanoparticles is of primary importance on the design and optimization of such nanocomposite for their application in different fields. Another important question is how to compare materials obtained using different method of synthesis? For our knowledge in the literature there is no answer on this question.

As fundamental understanding of the structure and various other properties such as DC conductivity,glass transition and molecular relaxation properties of the CS/AgNPs composite have been studied by the broad band dielectric spectroscopy. Dielectric spectroscopy have shown to be more effective technique to investigate the molecular motion, conductivity, glass transition temperature, etc. In many cases, the nature of the molecular interaction of side groups with other polymers and nanoparticles is still not known. Furthermore, to the best of our knowledge in the literature there are no publications about application of dielectric spectroscopy for investigation of CS/AgNPs nanocomposites.Furthermore, the electrochemical measurements provide powerful analytical techniques due to their instrumental simplicity, significantly higher sensitivity and low cost. A number of experimental electrochemical strategies have been explored in the development of nanomaterils based sensors for biomedical applications. In this context, we have taken advantage of this technique to explore and to develop biosensors for effective detection of glucose.

In this thesis the physicochemical and structural properties of CS/AgNPs composites using different synthesis methods have been investigated and elucidated with an aim to obtain highly efficient biomaterials and then to design high performance enzymatic electrochemical glucose biosensors, which will open new platforms to early detection of diseases. That is why the research proposed in this work are innovative and will provide new information about structure, dielectric relaxation, physicochemical properties and possible application of CS/Ag nanocomposites.

2.2. Objectives of the thesis

2.2.1 General Objective

The overall aim of this thesis is to develop and investigate a feasible bionanocomposites based on chitosan/silver nanoparticles, and to propose methods to compare properties and optimize the materials obtained by different methods for biomedical application.

2.2.2 Specific objectives

- Green synthesis of AgNPs using anaerobic enriched mixed bacteria (AEMB).
- Synthesis of CS/AgNPs via four different methods (including chemical reduction using different reduction agents and *in situ* reduction method).
- Structural characterization of the resultant bionanocomposites via different conventional characterization techniques as: ultraviolet-visible spectroscopy (UV-Vis), scanning electron microscopy (SEM), transmission electron microscopy (TEM), Fourier transform-infrared spectroscopy (FTIR), X-ray diffraction (XRD), X-ray photoelectron spectroscopy (XPS), Termogravimmetry (TGA) and energy-dispersive analysis (EDS).
- Investigate electrical properties of chiotsan biopolymer and CS/AgNPs nanocomposites using dielectric spectroscopy (particularly in GHz frequency range).
- Proposed method to compare properties of nanocomposites obtained using different method of synthesis.
- Investigate interaction of AgNPs with chitosan matrix using the high frequency dielectric (GHz) spectroscopy.
- Antibacterial evaluation of CS/AgNPs toward Gram positive and Gram negative bacteria.
- To develop enzymatic biosensor based on the CS/AgNPs/GO_X and CS/AgNWs/GOx and evaluate their electrochemical glucose biosensor performance.

Chapter 3. Materials and methods

3. Materials preparation

Because of such wide range of applications of silver nanoparticles numerous methods concerning the fabrication of silver nanoparticles, as well as various silver-based compounds containing ionic silver (Ag^{+}) or metallic silver (Ag^{0}) have been developed [85, 86]. There are many reports focusing on the preparation and characterization of CS/AgNPs nanocomposite [59, 87]. From these reports one can conclude that the properties of the nanocomposites depends not only on the dimension of nanoparticles but also on their concentration, distribution, methods of preparation, type of interaction with chitosan matrix, etc. However, in the literature, from our knowledge, there are no reports about influence of preparation methodology and concentration of AgNPs on the structure, electrical and dielectric relaxation properties on CS/AgNPs nanocomposite. Necessary to note, that relation between electrical, structure and concentration of nanoparticles are primary importance on the design and optimization of such nanocomposite for applications in different fields. Due to the above, the aim of this chapter is to present the synthesis of CS/AgNPs films using different methods and to investigate the influence of the nanoparticles concentration on structure, electrical and relaxation properties.

3.1 Preparation of CS (neutralized and non-neutralized) films.

Chitosan (CS), 86% of degree of deacetylation (DD) and molecular weight of *ca.* 350 kDa from Sigma-Aldrich was used as received. CS films were obtained by dissolving 1 wt % of CS in a 1 wt % aqueous acetic acid solution with subsequent stirring to promote dissolution. Films were prepared by the solvent cast method by pouring the solution into a plastic Petri dish and

allowing the solvent to evaporate at 60^{o}C. To obtain the neutralized films and to remove acetic acid, chitosan films were immersed into a 0.1M NaOH solution for 30 min and washed with distilled water until neutral pH is obtained; a subsequent drying step in furnace at 60^{o}C for 14 hours was performed. A thin layer of gold was vacuum-deposited onto both sides of the films to serve as electrodes.

3.2 Green synthesis of silver nanoparticles

Different innovative approaches have been developed to synthesize silver nanoparticles particularly chemical reduction methods using different reducing agents such as $NaBH_4$, citrate, and ascorbic acid. [54, 60]. However, these chemical reduction processes have its own drawbacks such as toxic issues, stability and agglomeration effect without additional stabilizing agent and difficulties in handling chemical reagents. Therefore, the greener environmentally friendly biological approaches to produce metal nanoparticles are encouraging due to their growing success, ease in the formation of nanoparticles without any additional reducing agents and minimize the problem associated with environmental contamination [88].

Numerous green synthesis methods have been exploited to prepare silver and gold nanoparticles such as vitamins, sugars, plant extract biopolymers and microorganisms as reducing and capping agents [89]. Among these, microorganism is preferred to synthesis metal nanoparticles because of ease in handling, large scale possibilities and exhibits potential applications in various areas of nanotechnology [90]. Several microorganisms have been utilized intracelluraly and extracellularly to produce metal nanoparticles [91].

In the literature there are reports about synthesis of silver nanoparticles using individual bacteria culture. There are no reports available, about the mixed bacterial culture being used for biosynthesis of silver nanoparticles. In this chapter new strategy to *in situ* reduction of AgNPs

mediated by anaerobic enriched mixed bacteria culture as well as it can be used to formation of biofilms containing NPs on the electrode surface. In contrast to conventional biosynthesis methods, AEMB synthesize method are non-toxic, environmentally friendly and have additional advantages like easy and rapid preparation, high stability and low cost industrial applications.

3.2.1 Preparation of anaerobic enriched mixed culture

The enriched mixed culture was prepared from the swine manure collected in Central Mexico. Initially, the swine manure was cultivated in the nutrient medium. The basal nutrient medium was followed Endo formulation and contained the following ingredients (g/L): NH_4CO_3 5.24, $NaHCO_3$ 6.72, K_2HPO_4 0.125, $MgCl_2{\cdot}6H_2O$ 0.1, $MnSO_4{\cdot}6H_2O$ 0.015, $FeSO_4{\cdot}7H_2O$0.025, $CuSO_4{\cdot}5H_2O$ 0.005, $CoCl_2{\cdot}5H_2O$ 0.00012. After 3 transfers in the medium, the enriched mixed culture obtained was used for further synthesis work. The dominant bacterial population present in the consortia was revealed by PCR-DGGE.

3.2.2 Bio-synthesis of Ag nanoparticles

In a typical synthesis procedure, 2 mL of 0.2mM $AgNO_3$ precursor solution were added to 10 mL of freshly prepared anaerobic enriched mixed culture. The pH of the AEMB has been kept as neutral (7.0), since the neutral pH is supportive for the growth and maintain as active bacterial culture. The solution mixture was allowed for plurge by N_2 gas for 5 min to achieve strict anaerobic environment. The final solution mixture closed tightly and magnetically stirred at 35^{o}C. Important to note, the mixture were stirred without any exposer of light. Within 30 min the transparent colloidal suspension turns into light yellow in color and the reaction was completed in 2-3 hrs by obtaining stable dark yellow color colloidal suspension. Upon completion of the reaction, the nanoparticles were isolated by centrifugation at 2500 rpm for 20 min and

subsequently washed with copious amount of de-ionized water to remove the excess surface bounded bacteria culture filtrate.

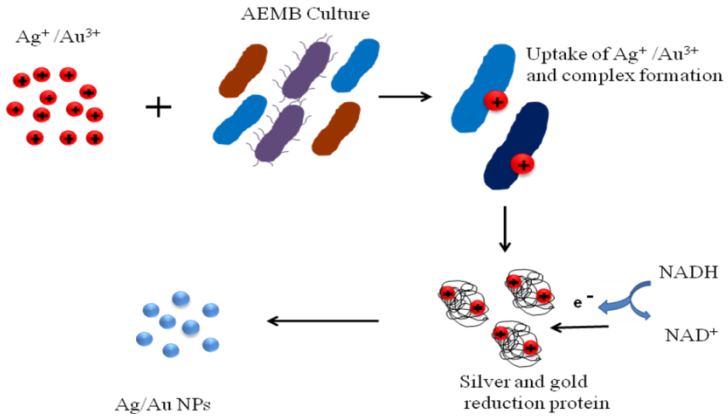

Fig.3.1 Reduction mechanism of AgNPs from AEMB culture

3.3 Preparation of CS/AgNPs films.

3.3.1 Method 1 (direct dispersion of AgNPs)

The proper quantity of AgNP's powder (1, 3, 5 and 10% wt % respect to CS dry based) was poured into a 1 wt % aqueous acetic acid solution and further sonicated for 30 min to obtain the nanoparticle dispersion. Then the pristine CS film as- prepared was dissolved into the AgNPs solution and further sonicated for 10 min to eliminate the formation of bubbles. The final solution was poured into a Petri dish and allowed to the solvent to evaporate for 24 h at 60°C to obtain the CS/AgNPs nanocomposite films.

3.3.2 Method 2 (Chemical reduction)

CS/AgNPs colloidal suspension was obtained by chemical reduction of $AgNO_3$. Ascorbic acid, sodium citrate were used as reducing agent and stabilizing agent respectively. In a typical preparation, 10 ml of a solution of chitosan and freshly prepared 0.01M to 0.5M of $AgNO_3$ solution were mixed and stirred until homogenization. Then 4 ml of 3 mM of sodium citrate and 0.2 mM of ascorbic acid were added to the reaction system and stirred for 20 min at 1000 rpm in room temperature. The transparent colorless solution was converted to the characteristic pale yellow in color. It is important to note that sodium citrate can play the role of reducing agent at high temperature (above 80°C) in this case, sodium citrate acting as stabilizer of nanoparticles. The final solution was poured into a Petri dish allowing the solvent to evaporate for 24 h at 60°C to obtain the CS/AgNPs nanocomposite films.

3.3.3 Method 3 (chemical reduction)

CS/AgNPs colloidal suspension was obtained by chemical reduction of $AgNO_3$ as precursor and ascorbic acid as reducing agent and sodium dodecil sulfate (SDS) as stabilizing agent. In a typical preparation, various concentration of 0.01M to 0.5M of $AgNO_3$ solution were mixed with 200 µl of 0.1 M SDS. The reducing agent (ascorbic acid) was added to the reaction system in one step during stirring at 200 rpm, in ratio 1:1 without excess of reducer. The SDS was kept constant in all concentrations of $AgNO_3$ solution. The reduction was initiated in 30 min after addition of reducing agent at room temperature. To this SDS coated AgNP's solution, 10 ml of CS solution (1 wt %) was added and stirred for 1 hr, in order to obtain homogeneously dispersed CS/AgNPs suspension. The main purpose of introducing SDS to the solution was to prevent the silver nanoparticles from growth and aggregation. The final solution was poured into

a Petri dish and allowing the solvent to evaporate for 24 h at 60°C to obtain the CS/AgNPs nanocomposite films.

3.4. Chitosan mediated synthesis of CS/AgNPs nanocomposite

In recent years the development of efficient and greener routes for metal nanoparticles syntheses has gained considerable interest in various areas of nanotechnology. Several physical and chemical approaches have been established to prepare CS/AgNP composite films. Common methods involve the chemical reduction of silver salts by different reducing agents such as $NaBH_4$, sodium citrate, or ascorbic acid [54, 60]. However, in these chemical processes the nanoparticles tend to aggregate due to the high surface energy during the synthesis. The reducing agents used for the preparation might exhibit environmental toxicity. Therefore, in this paragraph we developed the green method to synthesis CS/AgNPs nanocomposites using biopolymer CS.

The synthesis was carried out by adding 100 µl of different concentrations of silver precursor $AgNO_3$ (0.01, 0.05, 0.1, 0.2, 0.3, 0.4, 0.5, 0.6 and 0.8 M) to 10 ml of chitosan solution in acetic acid (1%) and the final solution was sirred magnetically at 95°C, then allowed to react for an additional 8 hours. The color of the solution progressed from colorless to light yellow within 30 minutes and finally to dark yellow after the reaction is completed. This change of color indicates the formation of AgNP. The temperature of the reaction plays an important role and has a strong influence of the particles size and dispersity of AgNP in the chitosan solution. CS/AgNP films were obtained by the solvent casting method pouring the final solution into a plastic Petri dish and allowing the solvent to evaporate for 24 h at 60°C.

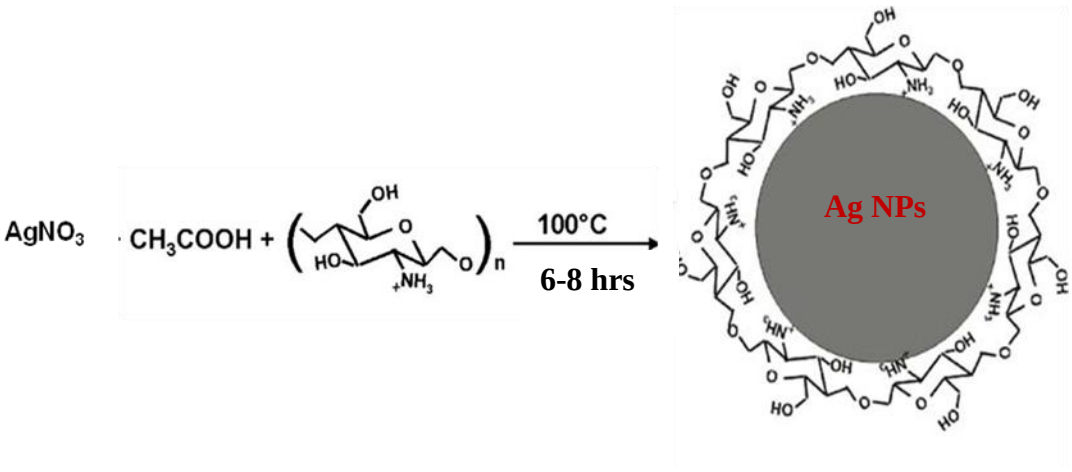

Fig 3.2. Reaction mechanism of chitosan mediated synthesis of CS/AgNPs nanocomposites

3.5 Polyol synthesis of Ag nanowires.

Additionally, in this work CS/Ag nanowires composite has been synthesis for biosensor applications. In recent years, one-dimensional (1D) metallic nanostructured materials owing their unique size and shape dependent properties, have attracted considerable attention because of their potential use as assembly and integration of molecular-scale components into electronic devices and wide range of antibacterial and biomedical applications [92]. Among all metals nanostructures, silver nanowires (AgNWs) have drawn intensive attention due to its highest electrical, thermal conductivity and remarkable antibacterial performances to broad-spectrum of bacterial species and relatively lower toxicity to human cells [93]. Due to these attractive properties AgNWs have successfully been applied to microelectronics such as transistors, LEDs, solar cells, catalysis, SERS and in the biomedical field as biosensors and effective and long term antibacterial applications [94].

Several approaches are exploited for the preparation of polymer/silver nanowire nanocomposites [95, 96], such as direct incorporation to polymer such as dispersion of AgNWs powder in polymer solution or AgNWs can be generated by *in situ* reduction of silver salts in

Polyaniline based nanocompsites. In this work uniform silver nanowires (AgNWs) with high yield through a modified polyol process have been prepared.

3.5.1 Preparation of Ag Nanowire

High yield uniform silver nanowires were synthesized by modified polyol process according to *J. J. Zhu et al* [97]. Briefly, 0.204 g of $AgNO_3$ and 0.1332 g of PVP were dissolved in 5 ml of ethylene glycol (EG) solvent separately. Then both solutions were simultaneously injected drop wise into 25 ml of EG solvent which is magnetically stirred at 170^{o}C for 1 hr. The injection time lasted about 3 minutes. The color of the solution turned into white color after 1 hour of reaction time. The final colloidal suspension is cooled to room temperature, then subsequently washed with acetone to remove excess PVP and the unreacted Ag^{+} ions by centrifugation at 6000 rpm for 30 min. These silver nanowires were then redispersed in water and then the AgNWs powder was collected by centrifugation and used for the further work.

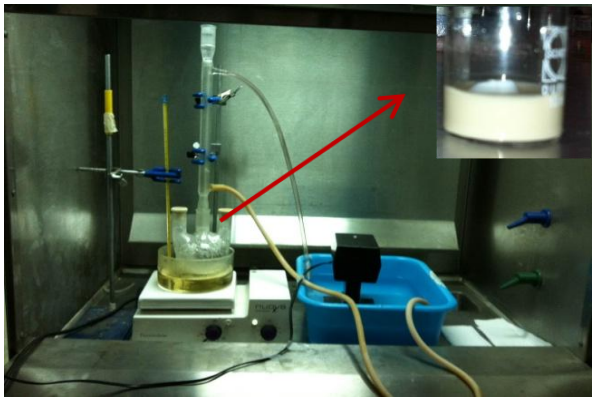

Fig. 3.3. Experimental set-up to preparepare AgNWs via polyol process

3.6 Characterization techniques

3.6.1. UV-vis analysis

The ultraviolet visible spectrum (UV-Vis spectrometer Agilent 8453) was used in order to determine the formation and size of the AgNP's in the CS matrix by the detection of the maximum absorption band in the UV-visible region (300-1100 nm).

3.6.2. Structural characterization (SEM, TEM and EDS)

CS/AgNPs films morphology was analyzed by JEOL JSM7401F Field emission scanning electron microscope (SEM) and transmission electron microscopy (TEM) using JEOL 2010 operated at 200 kV. The weight percent of AgNP's in the chitosan film were obtained by Energy dispersive analysis (EDS).

3.6.3 Infra-red spectroscopy

FTIR measurements were used in order to determine the interaction of the AgNP's with the CS matrix. The FT-IR spectra were obtained by FTIR spectroscopy (Perkin–Elmer spectrophotometer) using an ATR accessory in the range 4000– 400 cm^{-1}, resolution was set to 4cm^{-1}, and the spectra shown are an average of 16 scans. *In situ* FTIR spectra with different temperature were obtained from FTIR spectroscopy, (Perkin–Elmer) using an ATR accessory in the range 4000– 400 cm^{-1}; resolution was set to 4 cm^{-1}; it is equipped with MiRacle Heated ZnSe system and *in situ* temperature controller in the temperature range of $25^{o}C$ to $110^{o}C$.

3.6.4. Dielectric characterization

The aim of dielectric measurements was to investigate the electrical (conduction, permittivity, their dependencies on frequency and temperature) and relaxation properties of CS/AgNPs nanocomposites. Dielectric spectroscopy measurements were carried out using three Impedance Analyzers: Solartron 1260 (in the frequency range 1-10^4 Hz); Agilent 4249A (in the

frequency range 10^2-10^7 Hz) and Agilent E4991A (in the frequency range 10^6-3x10^9 Hz). The amplitude of measuring signal was 100 mV. Temperature measurements were performed in the cell with temperature controller from 20° C to 200° C, and in the bench-top temperature chamber SU-261 which was programmed to produce a constant heating rate of 5°C/min. The measurement of each temperature was left for 3 min to ensure thermal equilibrium. Measurements were carried out on sandwich structure with sputtering on both sides of films with gold contacts to serve as electrode.

3.6.5. Thermogravimetric analysis (TGA)

The amount of free water was determined by thermogravimetric analysis (TGA) (Metler Toledo 851e Model). The measurement was made with a dry air flow from 25 to 330º C with heating rate of 10 ºC/min.

3.6.6. X-ray diffraction (XRD)

The crystalline nature of the samples were investigated using *in situ* X-ray diffraction measurements using a Rigaku Ultima-IV diffractometer with temperature chamber (Rigaku HT-1500) to evaluate structural changes as a function of temperature.

3.6.7. XPS analysis

XPS was used to determine the chemical states of the functional groups in CS/AgNPs films. Data were collected with Alpha 110 instrument from Thermo Fischer Scientific (East Grinstead, UK) with monochromatic Al-k_α ($h\nu$=1486.7 eV) radiation with a pass energy of 20 eV. The calibration of the binding energy of the spectra was performed with the C *1s* peak of the carbon due to atmospheric contamination at 284.8 eV. The XPS peaks were fitting with the software AAnalyzer v1.12.

3.6.8. Bactericidal analysis of CS/AgNP composite films

For investigating the antibacterial properties of CS/AgNPs composites bactericidal analysis has been done. Strains of Gram-positive *Sthapylococcus aureus* (ATCC 8923) and Gram-negative *Escherichia coli* (ATCC 25922) were tested. Squares of each film (1 x 1 cm) were aseptically obtained with a sanitized scalpel. Each square was inoculated with 10 µl (8 log CFU/square) and placed inside sterile glass tubes, and incubated at 22°C with the time interval of 0, 24 and 48 hrs. Films were removed from storage and placed in tubes containing 3 ml of Dey-Engley (DE) neutralizing broth (pH 7.6; BBL/Difco) and were homogenized using vortex for 1 min. Inocula and inoculated CS/AgNP films were analyzed for populations of bacteria. Cell suspensions were serially diluted in sterile 0.1% peptone and surface plated (0.1 ml) on tryptic soy agar supplemented with rifampicin (TSAR, 100 mg/ml). Inoculated plates were incubated at 35°C for 24 h before colonies were counted. Colonies from each sample were chosen randomly and subjected to biochemical confirmation.

3.6.9. Electrochemical measurements

The possibilities of application of CS/silver nanocomposites in glucose detection have been investigated using electrochemical measurements. Glassy carbon electrodes (GCE) were used as working electrode which is home-made. Prior to use, the GCE were carefully polished until obtain a mirror surface was obtained and corroborated their cleanliness and their reversible electrons transfer. Cleaned GCE were dried with nitrogen stream. After that, 30 µl of AgNPs solution (1.5 mg mL^{-1}) was dropped onto the surface of the pretreated GCE and left to dry at room temperature to obtain a AgNPs-modified GCE. The immobilization of GOx onto the surface of the AgNPs/GCE was obtained by dropping 5 µL of 30 mg mL^{-1} GOx aqueous solution mixed with 5 µL of chitosan (CS) and left to dry at $4^{o}C$ for at least 2 h, it was referred to as the

CS/AgNPs/GOx/GCE. Similar fashion, enzyme electrode based on AgNWs modified electrode was constructed using 35 µl of CS/AgNWs solution (1.5 mg mL^{-1}) was dropped onto the surface of the pretreated GCE and left to dry at room temperature to obtain a CS/AgNWs-modified GCE, referred to as CS/AgNWs/GCE. The immobilization of GOx onto the surface of the CS/AgNWs/GCE was obtained by dropping 5 µL of 30 mg mL^{-1} GOx aqueous solution onto the resultant CS/AgNWs/GCE and left to dry for at least 2 h, it was referred to as the CS/AgNWs/GOx/GCE. The enzyme modified electrode was stored at 4^{o}C when not in use.

Fig. 3.4. Experimental set-up of the electrochemical cell.

All electrochemical measurements were performed at room temperature using a VoltaLab 40 PGZ 301 instrument. Three-electrode conventional electrochemical cell with the modified GCE as working electrode (WE), platinum foil as counter electrode (CE), and saturated calomel electrode (SCE) as reference electrode (RE) was employed. Ultrapure water with resistivity 18 MΩ cm was used throughout the experiments.

Chapter 4. Characterization of bio-synthesized AgNPs

4.1 Identification of dominant bacterial species in anaerobic enriched mixed bacteria (AEMB) culture.

It is necessary to know the dominant bacterial species present in the mixed cultures to draw the mechanism to fully understand the background of the nanoparticles synthesis. Thus, widely known PCR-DGGE based 16s rDNA sequence has been employed for the identification of V3-V6 regions of 424 bp long nucleotide sequence. Three major bands were detected and they were sequenced and closely related match search was performed via NCBI database. The bands representation was shown in Table 4.1 and Figure 4.1.

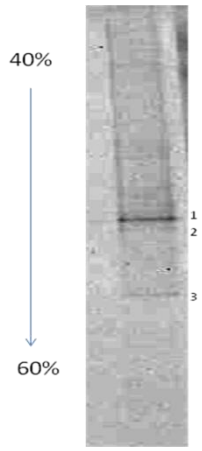

Fig.4.1. PCR-DGGE, DNA sequencing and phylogenetic analysis of anaerobic enriched mixed bacteria culture.

Table 4.1. Affiliation of DGGE fragments determined by their 16S rDNA and isolated microorganisms.

Sequence no.	Family	Closest match	Homology (%)	Sequence length (bp)
1	Gamma proteobacateria	*Klebsiella pneumonia* (Accession no. NR_074913)	99	418
2	Firmicutes	*Lactobacillus amylotrophicious* (Accession no. NR_042511)	98	416
3	Gamma proteobacateria	*Salmonella entérica* (Accession no. NR_074935)	99	414

4.2 Characterization of Ag nanoparticles

It is widely known that UV-vis spectroscopy is used to examine the shape and size of the metal nanoparticles by carefully observing of the peak position and shape of the peak. Fig. 4.2 shows the UV-vis absorption spectra of biosynthesized colloidal AgNPs exhibit the absorption peak at 425 nm corresponding to the characteristic absorption profile of spherical silver nanoparticles regime [98]. The appearance of a high intensity absorption peak of AgNPs suggesting the conversion of AgNPs is significantly higher (*ca.* 80-90%). Notably, in comparison with other microbial based synthesis, the present synthesis showed high yield. In addition, the color of the final solution turns into dark yellow, reveled the higher conversion of the nanparticle within the culture medium (inset of Fig. 4.2). Further confirmation of shape and size of as-prepared nanoparticles were subjected to transmission electron microscopy (TEM) imaging.

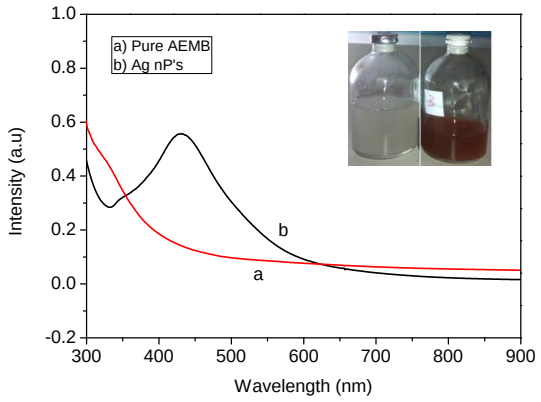

Fig. 4.2.UV-vis spectra of bio-synthesized silver nanoparticles colloids. Inset shows photographs of a) Pure AEMB culture solution b) as-prepared AgNPs colloidal suspension.

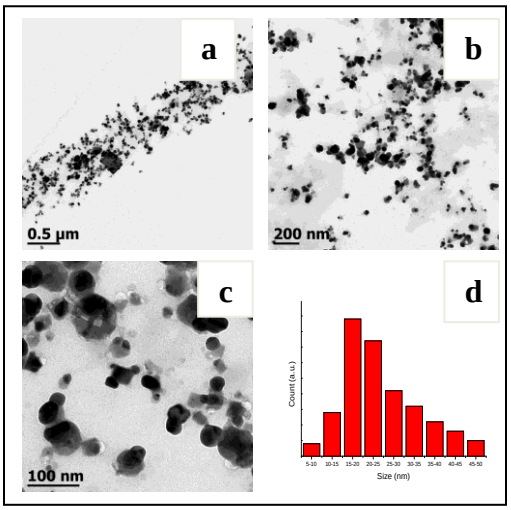

Fig.4.3. a) TEM images of as-prepared silver nanoparticles. b) and c) Magnified image of silver nanoparticles. d) Size distribution of AgNPs average of four different images.

Transmission electron microscopy images of as-prepared AgNPs colloidal suspensions is shown in Fig. 4.3. It is observed that silver nanoparticles are spherical and are homogeneously dispersed with an average particle size of 5-50 nm. The particle size distributions are presented in Fig. 4.3d. The crystalline nature of biosynthesized AgNPs was confirmed by X-ray diffraction (XRD) analysis. Fig. 4.4 shows the XRD patterns of dried powder samples of biosynthesized silver and gold nanoparticles. Typical XRD patterns of AgNPs show peaks at 2θ values of 38º, 44.2º, 64.3º and 77.7º corresponding to the (111), (200), (220) and (311) planes of face centered cubic (fcc) for Ag^0 [99]. XRD pattern showed that silver nanoparticles are essentially presented in crystalline in nature. The crystalline size of silver nanoparticles *d* was estimated from XRD measurements using well known Scherer formula. The calculated value of *d* was about of 35±9.4 nm, which is close to TEM measurements.

To gain insight into the specific interactions between nanoparticle surface and the active bacterial species, FTIR measurement has been carried out. Fig. 4.5 shows two representative FTIR spectra of synthesized AgNPs that exhibit strong bands at 1657 cm^{-1}, 1539 cm^{-1}, 1235 cm^{-1} and 1062 cm^{-1}. The most prominent bands at 1657 cm^{-1} and 1539 cm^{-1} correspond to the characteristic vibrations of amide I (C=O stretching vibration) and amide II vibrations of the protein [100]. Other bands at 1235 cm^{-1} and 1062 cm^{-1} can be assigned to the C-N stretching vibrations of NH bending of peptide linkage. From FTIR measurement, one can conclude that AgNPs could bind to free amino or carboxylate groups in the protein; these groups may be responsible for the reduction and stabilization of nanoparticles. Such interaction of silver nanoparticles with the amine and carboxyl groups is consistent with the previous reports [101]. Additionally, TEM analysis revealed the attachment of silver nanoparticles with bacteria and formation of stabilization layer on the AgNPs surface (see Fig. 4.3a).

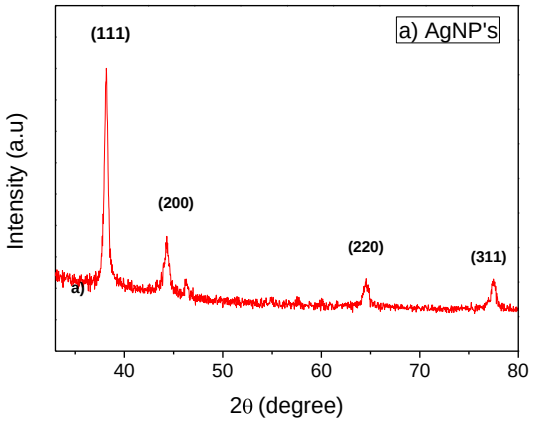

Fig. 4.4. XRD spectra of as-prepared silver nanoparticles.

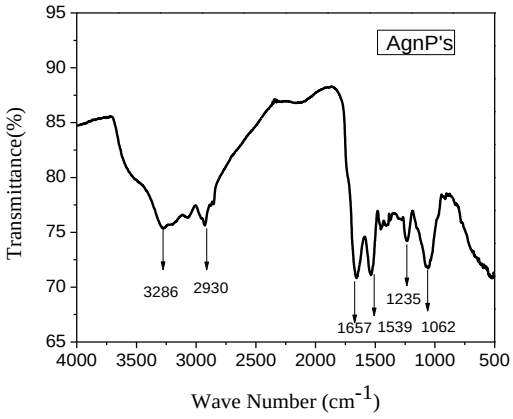

Fig.4.5. FTIR spectra of dried samples of AgNPs

4.3. Reduction mechanism of AgNPs from AEMB.

In the literature different mechanisms have been proposed for reduction of metal nanoparticles using different bacterial cultures. Most of the previous investigations showed that NADH dependent electron shuttle enzymatic metal reduction process is responsible for bio-reduction of nanoparticles [102]. Other studies demonstrated that nitrate reductase enzyme system can be responsible for formation of silver nanoparticles from silver ions. Recently, *Ramanathan et al.* experimentally demonstrated the possible mechanism of extracellular bio-reduction of silver and copper nanoparticles [103, 104]. They found that the silver binding gene in the silver-resistant bacteria is responsible for the reduction and stabilization of AgNPs via sulphur containing amino acids (cysteine/methionine) in the protein. However, the exact reduction mechanism of metal ions (Ag^{+}) into metal nanoparticles either extracellular or intracellular way is poorly understood. In our present study based upon FTIR and TEM observation, the possible mechanism involved in the bio-reduction of AgNPs could be, the first step involves the uptake of Ag^{+} and formation of complex formation with the AEMB. The

second step, the NADH-dependent reductase which may secreted from the AEMB culture may responsible for the bio-reduction of Ag^{+} into AgNPs, respectively. A similar hypothesize has been observed for AgNPs reduction using different bacteria previously Notably, surface binded to proteins through either free amine groups or carboxyl groups from the cysteine residues in the protein; which may be confer stability of the AgNPs.

4.4. Summary

Bio-genic approach to synthesize AgNPs using anaerobic enriched mixed bacteria (AEMB) culture has been described. Three dominant bacterial species *Klebsiella pneumoniae, Lactobacillus amylotrophicious* and *Salmonella enteric* have been identified in the mixed culture which were responsible for effective bio-reduction of AgNPs. The reduction of metal ions and stabilization is more likely mediated by enzymatic process. However, the prepared AgNPs exhibits few drawbacks to use in biomedical applications. 1. Bio-synthesized nanoparticeles exhibits higher particle size (20-60 nm) and not homogenious distribution. 2. The stability of the as-prepared AgNPs is low (stable for 30 days). 3. The above mixed bacterial culture used in this preparation was the pathogenic bacteria, thus needs careful washing and centrifugation cycles to remove surface coated bacterial culture. Therefore, in the next chapter we described about the feasible direct and chemical reduction starategy to obtain CS/AgNPs composite films via different methods and their structure and properties were elucidated.

Chapter 5. Structure and properties of chitosan-silver nanoparticles nanocomposites

The aim of this chapter is to investigate structure, electrical and relaxation properties of CS/AgNP's films synthesize using different methods. To shed light on these properties detailed analyses using dielectric spectroscopy, Fourier transformed infrared spectroscopy (FTIR), high resolution scanning electron microscopy with energy dispersive analysis (HR SEM-EDS), thermogravimetric analysis (TGA) and X-ray photoelectron spectroscopy (XPS) have be done.

5.1 UV-vis analysis of CS/AgNPs composites

The UV-vis spectra of CS/AgNPs composite films prepared by three different methods (described above in the chapter 3) with the same concentration are shown in Fig. 5.1a. The absorption peaks at 400-440 nm corresponded to that of AgNPs. In Fig. 5.1a, it can be seen the UV-vis absorption spectra of each films displaying the characteristics surface plasmon resonance (SPR) band at 416, 426 and 408 nm for method 1, 2 and 3 respectively. The shape of the plasmon band is symmetrical and narrow, suggesting that AgNPs are spherical [105]. It is observed that, in method 2 the intensity of SPR peak increased and broadening toward higher wavelengths (red shifted) indicates higher the particle sizes due to aggregation [105].

5.2 Morphology and EDS Analysis

The size and dispersion of AgNP's on CS matrix were analyzed by field emission scanning electron microscopy (SEM) and are shown in Fig. 5.1b. The representative SEM image recorded from CS/AgNP's composites shows the homogeneous distribution of AgNP's; the particles

exhibited a regular spherical shape in the chitosan matrix. The size of the AgNP's observed in the SEM micrographs for method 1, 2 and 3 are approximately 25, 40 and 20 nm respectively. Since method 2 and 3 involve the chemical reduction of Ag^+ to prepare AgNP's, the aggregation affects the dispersion and size of the AgNP's.

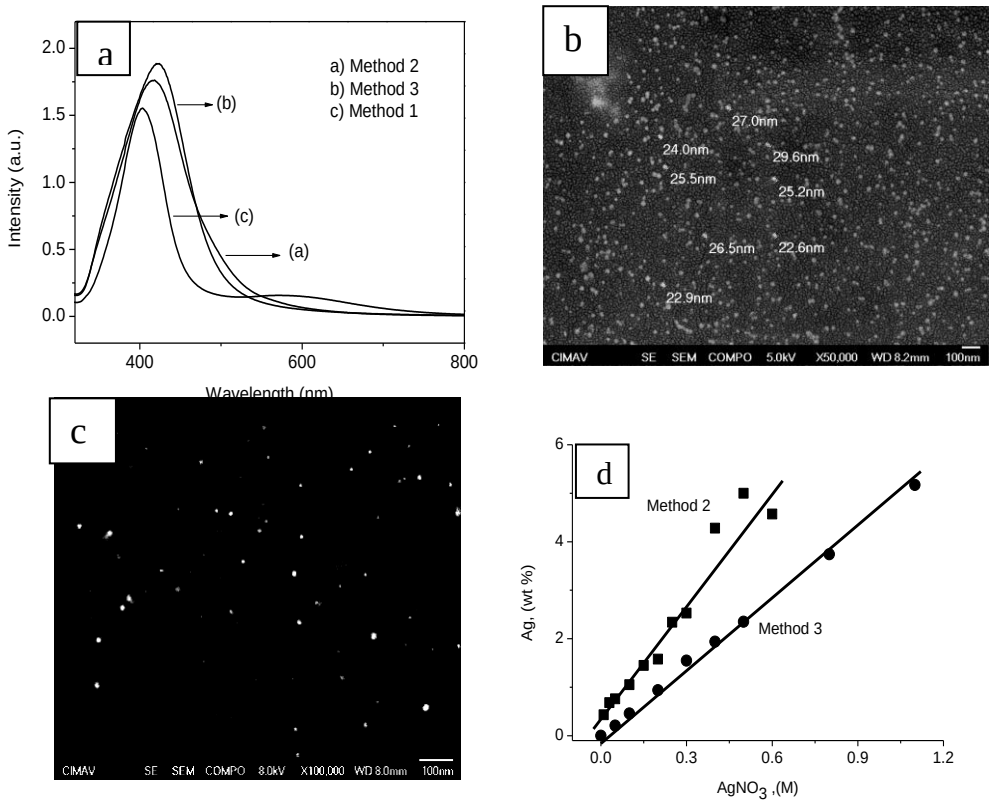

Fig. 5.1 a) UV-vis absorption spectra of CS/AgNPs composite films (1 wt. %) by three different methods. b, c) SEM image of CS/AgNPs obtained by (b) direct dissolution of AgnP's (1 wt %) in chitosan matrix, method I, and (c) by chemical reduction by method 2 (0.1 M $AgNO_3$). d) EDS analysis. Dependence of AgNPs wt. % in the films on the $AgNO_3$ concentration in the solution.

In the first preparation method exact wt % of AgNP's respect to dry- based chitosan has been taken. To compare properties of films obtained using second and third methods (chemical reduction with the different molar concentration of $AgNO_3$ precursor), the wt % of AgNP's have been obtained from energy dispersive analysis (EDS). EDS analysis shows that the weight

percent of AgNP's in the CS film was linearly dependent on molar concentration and on the method of preparation (Fig. 5.1d). It was also observed that the concentrations of AgNP's in the third method is lower when compared to second method due to presence of surfactants (SDS), which slows down the reduction process.

5.3 Infrared Spectroscopy (FTIR)

The chemical interactions between pure CS and CS/AgNP composite films (three different methods) obtained by FTIR measurements are shown in Fig. 5.2. The spectrum of pure CS film shows the absorption bands at 1650 cm^{-1} (amide I group), 1556 cm^{-1} (bending vibrations of NH_3^+), as well as bands at 1326 cm^{-1}(OH bending vibrations), 1157 cm^{-1} (anti-symmetrical stretching of C-O-C bridge),1083 and 1031 cm^{-1} (for skeletal vibration of C-O stretching) [106].

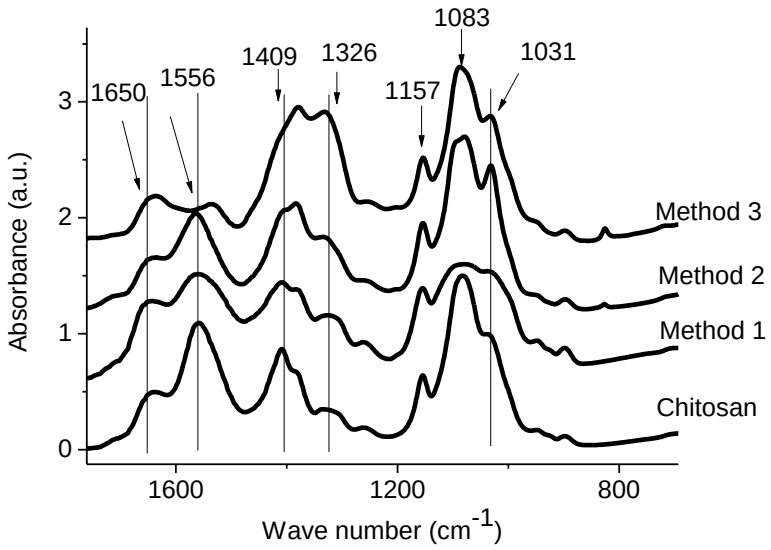

Fig. 5.2 FTIR spectra of neat CS and CS/AgNP's films (2 wt. %) obtained from first, second and third method respectively.

It could be seen in Fig. 5.2 the main difference between the CS/AgNPs composite films and the pure chitosan spectra is the change in the relative intensities of the infrared bands

positioned at 1650 cm^{-1} and 1556 cm^{-1}, indicating that the N-H vibration was affected by the interaction with silver nanoparticle. At the same time, in the method 3, the band due to asymmetric bending vibration of NH_3^+ band at about 1556 cm^{-1} was shifted to 1533 cm^{-1} with the decrease in intensity. Such reduction in intensity and shifts in the IR values could be considered that $–NH_3^+$ or –OH groups of CS combinated with Ag^+/Ag^0 by electrostatic bond [107]. Additionally, the intensity of O-H bending vibration band at 1326 cm^{-1} and C-O stretching bond at 1083 cm^{-1} decreased when AgNPs loaded to the chitosan chains, evidencing that the $-NH_3$ and -OH groups of chitosan interact with silver nanoparticles. The above results confirm that the strong interaction exists between CS and AgNPs, which depend on the method of preparation.

5.4 TGA measurements

For understanding the thermal relaxation properties, free moisture content have been investigated by TGA analysis in films obtained by three different preparation methods. The amount of free water can be evaluated by the decrease of sample weight during the heating scan. The loss in weight at the temperature 120ºC was taken to be the result of water evaporation. From TGA measurements has been observed that the free water content on wet as-prepare samples depends on Ag nanoparticles concentration and the method of preparation of CS/AgNPs nanocomposite (Fig. 5.3): the higher the Ag nanoparticles weight percent, the lower the moisture content. As it was shown by FTIR analysis (Fig. 5.2), the NH_3 and OH groups can be interaction with AgNPs affecting their vibration characteristics; this effect is related to the formation of a polymeric composite structure with nanoparticles and decreases the water absorption ability with increasing AgNPs concentration in composites [108]. Additional, in films prepared by method 2 (with ascorbic acid and sodium citrate as reducing agent and stabilizing agent respectively) at the low nanoparticles concentration water absorption initially increase but further decrease in

contrast to films prepared by methods 1 and 3. Such difference in water absorption can be relate to fact that neat sodium citrate has shown higher water absorbtion compare with neat chitosan films [109]. This difference in moisture content between neat chitosan and in films with sodium citrate can explained increasing of water content in films with low nanoparticles concentration. Further decreases the water absorption relates to increasing AgNP's concentration were same as films prepared by methods 1 and 3.

5.5 DC Conductivity Measurements

The DC conductivity (σ_{dc}) of pure CS and CS/AgNPs composites by different methods were calculated by dielectric measurements using the methodology previously described elsewhere [49, 108]. The DC resistance (R_{dc}) was obtained from the intersection of the semicircle and the real-part axis on the impedance plane (at Z" = 0) as it is shown in the insert in Fig.5.4, hence σ_{dc} can be calculated by the following relationship: $\sigma_{dc} = d/(R_{dc} \times A)$ where d–is film thickness and A-is area of film, respectively. In the typical complex impedance spectra (Z" versus Z') all films exhibit the characteristic semicircles at high frequencies and a quasi-linear response at low frequencies (Fig. 5.4 insert). The linear response at low frequencies can be associated with interfacial polarization or metal contact effects [49].

The ambient conditions moisture content in the films is (7-11 wt %), reduces film resistance and mask the real conductivity behavior of composites. This is a critical issue that needs to be considered when performing dielectric measurements especially in chitosan films. The previous measurements on composite film the DC conductivity were carried out by heating the film till 120^0C inside the vacuum cell and cooled to room temperature [49]. In this case, the water content absorbed on the surface of films is reduced by thermal treatment at 40^0C for 20

minutes inside the measuring cell. After this thermal treatment, the films are cooled down at room temperature (25^0C) without opening the measuring cell and then the measurement is carried out. Fig. 5.4. shows dependence of DC conductivity (at room temperature) of the CS/AgNPs composites on wt % of AgNPs (obtained from EDS measurements) prepared by three different methods. The DC conductivity increases with the addition of AgNP's in the CS film. In method 1 and 2, the conductivity increases with increasing of concentration and subsequent saturation. In the films, prepared by method 3, initially conductivity decreases with increasing of AgNPs wt % but at the concentration of nanoparticles higher than 3 wt %, the same as in another films, increase with subsequent saturation.

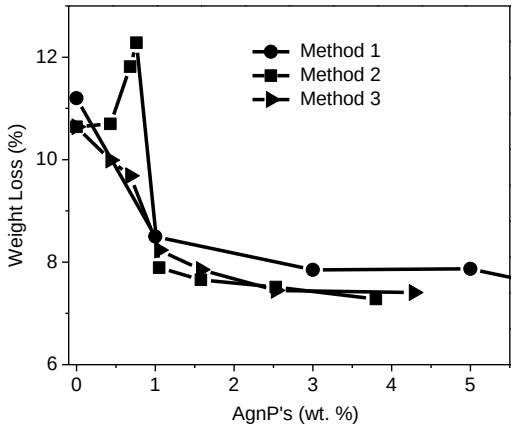

Fig. 5.3

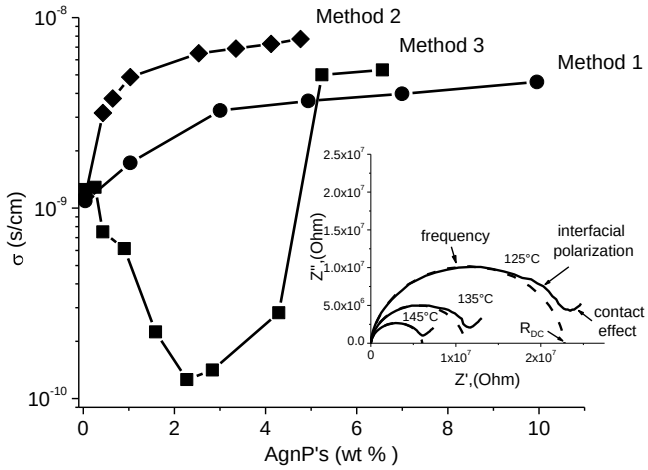

Fig. 5.4

Fig. 5.3 Dependence of weight loss of CS/AgNPs film on Ag nanoparticles wt% (TGA measurements). Fig.5.4 DC conductivity of CS/AgNPs nanocomposite at 25° C obtained by first, second and third methods as function of AgNPs wt %. Insert window shows impedance spectra (points) and results of fitting for calculation of DC conductivity.

The ionic conductivity of neat chitosan films can be related to the presence little concentration of conductive species in the form of NH_3^+ groups, H^+ and OH^- ions [110]. The

addition of AgNPs increases DC conductivity of nanocomposites. The higher DC conductivity values of CS/AgNPs nanocomposites films when compared to the pristine CS are ascribed to the motion of Ag mobile charge carriers. So, with increasing of AgNPs concentration conductivity must increase (as in films prepared by methods 1 and 2) and saturate due to the specific percolation effect. Low conductivity in the saturation region can be explained by the existence of a thin polymer layer that coexists between silver nanoparicles [111]. Confirmation of this hypothesis can be obtained from fourier transformed infrared (FTIR) spectroscopy analysis which shows that the silver nanoparticles have strong interaction with OH, NH_2, $CO.NH_2$ and C-O-C groups of chitosan matrix [111]. But in films prepared by method 3, conductivity first decreases with increasing of AgNPs wt % but at the concentration of nanoparticles higher than 3 wt %, the same as in another films, increase with subsequent saturation (Fig. 5.4). Such difference in conductivity in material obtained by method 3 with low wt % of nanoparticles (with sodium dodecil sulfate (SDS) as stabilizing agent can be related with coating of AgNPs by SDS and interaction of SDS with chitosan matrix which leads to decreasing the number of free NH_3 groups (that have been observed in FTIR measurements) which responsible for decrease ionic conductivity of chitosan [111].

5.6 Low frequency dielectric relaxation

The dielectric relaxation processes of CS/AgNPs composites were obtained from temperature dependence of DC conductivity and electrical modulus measurements. Generally in composites with conductive inclusions, ionic current and interfacial polarization could often mask the real dielectric relaxation processes in the low frequency range. Therefore, to analyze the dielectric process in detail, the complex permittivity ε^* has been converted to the complex electric modulus M^* by the following equation:

$$M^* = \frac{1}{\varepsilon^*} = M' + iM'' = \frac{\varepsilon'}{\varepsilon'^2 + \varepsilon''^2} + i\frac{\varepsilon''}{\varepsilon'^2 + \varepsilon''^2}$$

where *M'* is the real and *M''* the imaginary part of electric modulus, *ε'* is the real and *ε''* the imaginary part of permittivity. In this representation, interfacial polarization and electrode contributions are essentially suppressed. The corresponding relaxation time can be calculated by the relation $\tau = 1/(2\pi f_p)$, were f_p is the peak frequency in the dependence of *M''* on frequency (insert on Fig. 4.5).

The relaxation time dependence on temperature shown in Fig. 5.5 was obtained from the maximum of the imaginary part of the dielectric modulus *(M*), with the *M*'' peak ($\tau = 1/(2\pi f_{max})$ calculated at each temperature. The wet films of all three different methods display a nonlinear behaviors in the temperature range of 25-70° C. This behavior is well described by the Vogel–Fulcher–Tammann (VFT) relationship: $\sigma = \sigma_0 \exp(-\frac{DT_0}{T - T_0})$ and $\tau = \tau_0 \exp(\frac{DT_0}{T - T_0})$ (where σ_0 and τ_0 are the pre-exponential factors, *D* is a material constant, and T_0 is the so called Vogel temperature).

The nonlinear VFT behavior in wet films is a well known feature of the α-relaxation process related to the glass transition. The Vogel temperature is the apparent activation temperature of the α-relaxation and in many polymers T_0 is usually 50 K lower than glass transition temperature [108]. The α-relaxation process is strongly dependent on both moisture content and AgNPs wt %. Result obtained suggest a plasticizing effect of water on CS composites which shifting to lower values the Vogel and the glass transition temperatures as moisture content increases (Fig. 5.6). In dry films (annealed at the temperature 120^0C) with water content less than 0.2 wt % α-relaxation disappeared. On the other hand, the addition of

AgNPs leads to CS-CS intra chain interactions facilitating segments motion and thus reducing the glass transition temperature as AgNP's wt % increases.

Necessary to note, that dependencies of glass transition temperature Tg ($Tg=T_0+50$ K) in films prepared by 1 and 2 methods (Fig. 5.6) demonstrated inverse properties compare with dependence of water content in films (Fig. 5.3). The decreasing of moisture content in the films is responsible for increasing of glass transition temperature which confirms a plasticizing effect of water on CS/AgNPs composites. In contrast in films prepared by method 3 (with sodium dodecil sulfate as stabilizing agent) the Vogel temperature shifts to higher values as AgNPs concentration increases. This effect can be related to presence of surfactant (SDS) which affected on the CS-CS intra chain interactions and reduce the segments motion.

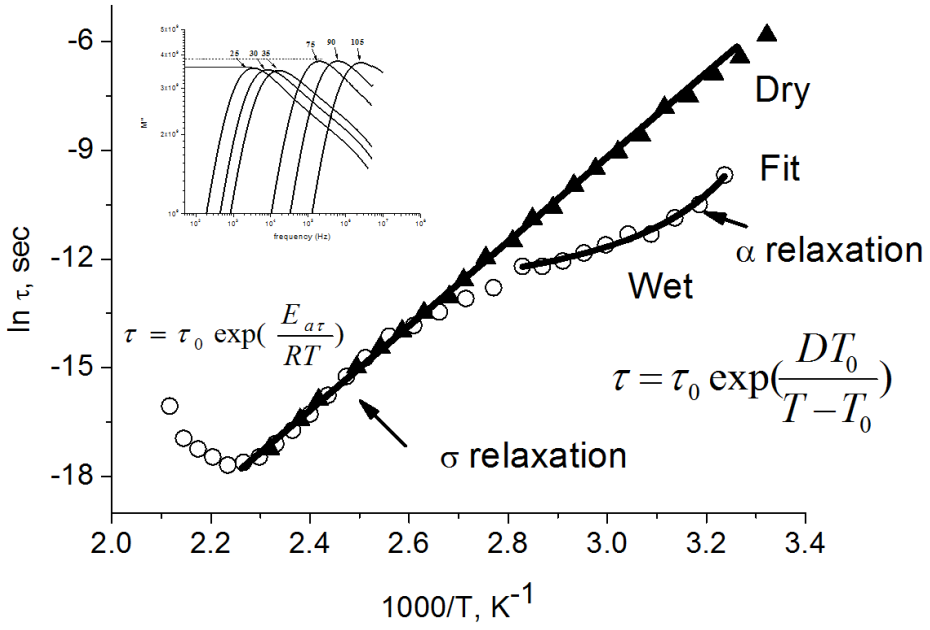

Fig. 5.5 Temperature dependence of relaxation time as-prepared (open circles) and annealed films (open triangular) obtained from 3 wt% CS/AgNPs film. Insert window shows frequency dependence of the imaginary part of the electric modulus at the temperature indicated on graphs.

In wet CS/AgNPs films in the temperature range between 80-160°C, in conductivity and relaxation time plots, an Arrhenius-type behavior (Fig. 5.5) have been observed with activation energies between 70 and 110 kJ/mol. This relaxation process is called σ-relaxation and can relate to local diffusion process of ions between high potential barriers in disordered systems [108]. σ-relaxation process does not depend on water content and observed in dry films in all investigated temperature range with the same activation energy as in wet samples. This kind of relaxation process has been found in the pure CS [110] and polysaccharides [47]. The activation energy of σ-relaxation process in CS/AgNPs films depends on the method of preparation and nanoparticles concentration (Fig.5.7). The ionic conductivity of the polymer is related to the number of ions. Conductive ions can be thermally excited from localized ionic states to free ion-like states when they have energy above barrier which equal to the activation energy and ions can propagate throughout the polymer.

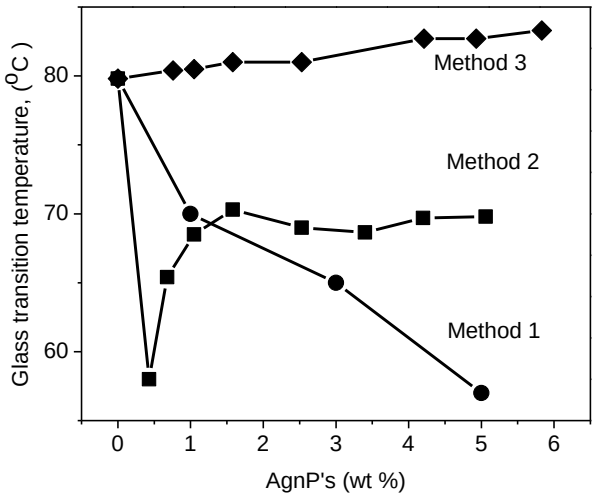

Fig. 5.6 Dependence of Vogel temperature T_0 on Ag nanoparticles wt %.

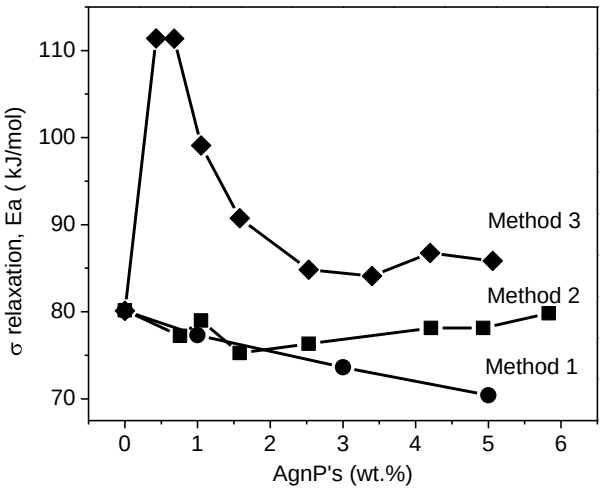

Fig. 5.7 Dependence activation energy of σ-relaxation on Ag nanoparticles wt%.

According to an Arrhenius-type dependence of σ-relaxation $\sigma = \sigma_0 \exp(-\frac{E_{a\sigma}}{RT})$ activation energy must decrease with increasing of conductivity (Fig. 5.4) as observed on Fig. 5.7. A negative slope in the films at the temperature above 160°C corresponds to the beginning of the degradation (Fig. 5.5). This value is closely related to the degradation temperature previously reported for CS [108].

5.7 XPS Analysis

The XPS analysis was used to examine the specific interaction of AgNPs with the chitosan matrix. All the spectra were fitted by multiple Gaussians and normalized. Fig. 5.8 shows the fitting components of binding energy (BE) of the Ag *3d* region for samples obtained by the three methods. Ag *3d* region is characterized by two peaks as consequence of spin orbital splitting that corresponds to Ag $3d_{3/2}$ and Ag $3d_{5/2}$ core levels. The CS/AgNPs composites in the Ag 3d region have shown four lines. Lines at BE 368.2 and 374.2 eV correspond to core levels of the metallic silver. Two new components at lower energy (366.4 and 372.4 eV) indicate the presence of Ag ions [112]. It is important to note that the Ag 3d region of Ag powder (not shown) indicates that the Ag exists only in metallic state and lines at BE 366.4 and 372.4 eV have not observed. The formation of Ag^+ in the CS/AgNPs composites (method 1) can be due to the interaction of AgNPs with the chitosan matrix and is not depends on method of preparation.

In the films prepared by method 2, Ag is in the same chemical state as in films prepared by method 1 (Fig.5.8). In sample prepared by method 3 a shift in BE of Ag $3d_{5/2}$ and Ag $3d_{3/2}$ from 368.2 and 374.2 eV to 368.7 and 374.7 eV have been observed. This shift can be attributed to different chemical interaction between AgNPs and CS. Necessary to note that the variation of the intensities of the peaks can be related to the different concentration of metallic silver and Ag ions.

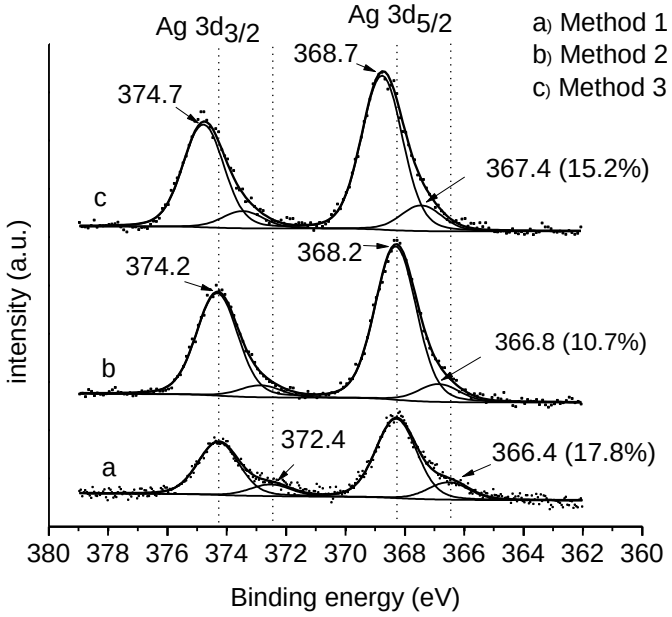

Fig. 5.8 XPS spectra for Ag *3d* region obtained on CS/AgNPs composites

For the further information about the mechanism of interaction between AgNPs and chitosan matrix can be obtained from the XPS spectra in the region nitrogen and oxygen. Figure.3-9 shows the XPS specra for the *N (1s)* region. The main peak at BE of 399.2 can be assigned to $–NH_3^+$ groups [48, 49]. It's important to note that, most of the literature assigns the peak at BE 399.2 region as $–NH_2$ groups [112]. By considering our material which is prepared from chitosan acetate films, the NH_3^+ groups must be dominant. Significant shifts of this peak from BE 399.2 eV to 399.6 eV for method 2 and 3 have been observed. This shift can be relate to stronger interaction of AgNP's with the $–NH_3^+$ groups of the chitosan, which are consistent with the FTIR results (Fig.5.2). In the method 1, a peak at BE of 397.2 eV can be assigned to $-NH_2$ groups which indicates that all nitrogen atoms exist in one valence state. In the method 2 and 3, a significant shift of this peak to higher BE of 398.4 eV have been observed. This shift of peak

position indicates that nitrogen atoms exist in a more oxidized state. During the chemical reduction process (method 2 and 3) nitrogen atoms in the amino groups of chitosan chelated agent for silver ions, which gave rise to the decrease of the electron density of the nitrogen atom, and thus increased BE to 398.4 eV [112]. Additional peak with BE of 406.4 eV can be attributed to the nitrate ions, which remain from the silver nitrate precursor in the method 2 and 3 [113]. It is important to note that such peak with BE of 406.4 eV not observed in the method 1.

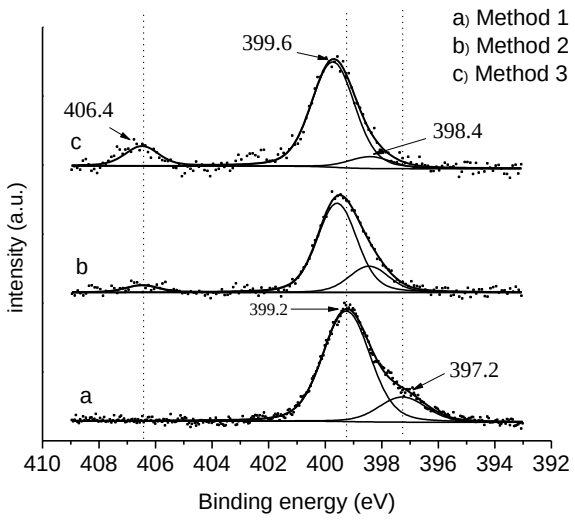

Fig. 5.9 XPS spectra for N (1s) obtained for (a) method 1 (b) method 2 (c) method 3.

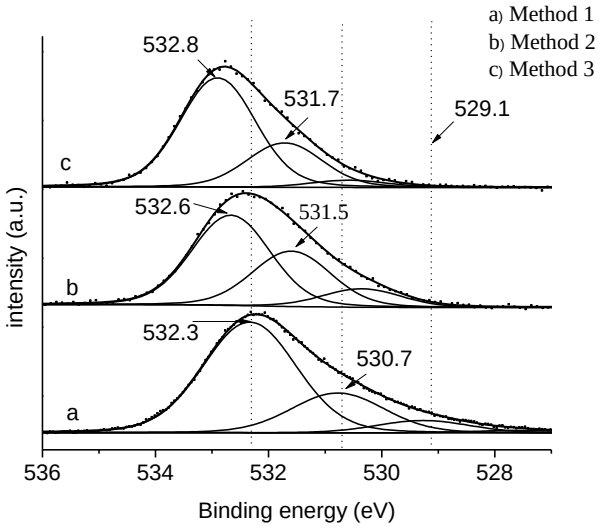

Fig. 5.10 XPS spectra for *O (1s)* obtained for (a) method 1 (b) method 2 (c) method 3.

Fig. 5.10 shows XPS spectra for *O1s* region. The peaks at BE of 532.3 eV according to the literature correspondent to the bond of Ag-O. The bond Ag-O were formed by the tight binding between a vacancy in the d-orbital of Ag and CS molecules [114]. The peak at the BE 531.7 eV can be related to C-O bonding. In the method 2 and 3 the peaks of *O1s* are shifted towards higher BE, implying a decrease of electron density due to existance of interaction between the oxygen

atoms of chitosan with AgNPs [110]. The XPS analysis, as all previous measurements, has shown influence of preparation methods on the specific interaction of AgNPs with the chitosan matrix.

5.8 Summary

Chitosan-silver nanoparticles (CS/AgNPs) composites films have been synthesized by three different methods. Dimensions of obtained AgNPs for method 1, 2 and 3 are approximately 25, 40 and 20 nm respectively. The FTIR and XPS analysis show the existence of strong interaction between free NH_3^+ and OH groups of chitosan and AgNPs which depends on method of preparation. But mechanism of this interaction is not clear and needs in investigation (see chapter 6). For fist time, new method of determination of wt. % of AgNPs, based on EDS analysis, has been proposed. This method allows to compare properties of nanocomposites obtained using method of preparation.

The DC conductivity and dielectric relaxation process of CS/AgNPs composite films investigated as a function of moisture content and AgNPs wt %. Two relaxation processes have been observed. Low temperature relaxation process (in the range 25-70°C) related to the α-relaxation associated with the glass transition and it can be described by the Vogel-Fulcher-Tammann dependence. The Vogel temperature dependents on water content, nanoparticles concentration and method of preparation. The glass transition vanishes in a dry material. The second relaxation was observed in the temperature range 80-160°C and it is identified as the σ-relaxation which often associated with the hopping motion of ions in the disordered structure. This relaxation exhibits Arrhenius-type dependence with activation energy of 70-110 kJ/mol and it is independent of water content, but dependent on AgNPs concentration and the method of preparation. This Arrhenius process is associated with a migration property of movable ions.

Additionally, the most important results obtained in this chapter for further work are:

- There is an relationship between electrical and structural properties of CS/AgNPs nanocomposites.
- Exist the strong interaction between free NH_3^+ and OH groups of chitosan and AgNPs which change vibration frequencies of these groups in FTIR measurements, but mechanism of this interaction in not known.
- Dimensions of nanoparticles obtained by these three methods are large for application in biomedicine. Therefore necessary another method of preparation, which will allow to obtain composite with less nanoparticles dimension.
- Therefore, in the next chapters we will study in detail:
    - Mechanism of relaxation process of chitosan side groups (-OH and -NH_2/NH_3^+) in neat chitosan and mechanism of interaction between AgNPs and chitosan matrix.
    - Chitosan mediated synthesis of CS/AgNPs nanocomposite.

Chapter 6. High frequency (GHz) dielectric relaxations in chitosan and CS/AgNPs nanocomposite films.

As has been shown in the previously chapter neat chitosan and CS/AgNPs nanocomposite films demonstrate high water absorption. It is noteworthy that in hydrated samples of polysaccharides, proteins and biopolymers water molecules can be directly bounded to give rise to additional relaxations [115]. The polymer chain restricts the orientation of water molecules such that the collective motions of the macromolecule-water are distorted giving rise to relaxation times about 100 times as slow as that of pure water [115]. It has been previously reported a dielectric relaxation at 1 GHz frequency for different hygroscopic solids [116]. This relaxation can be attributed to the breakage of hydrogen bonds between adjacent water molecules in thin films in microwave frequencies. The high frequency dielectric measurements of aqueous solutions and dynamical structure of free water around biopolymers also have been reported [115]. However, to our knowledge, there is no report in the literature about the molecular origin of the dielectric relaxation properties of biopolymer films in the gigahertz (GHz) frequency range. High frequency dielectric relaxations are important to fully understand the physicochemical and electrical properties of polymer material including the molecular mobility, dielectric relaxation and hydrogen bonding structure. Dielectric spectroscopy is a relevant technique to probe translational or rotational molecular motions and hydration properties with high sensitivity.

The objective of this chapter is to investigate the temperature-dependent dielectric relaxation behaviors of non-neutralized, neutralized chitosan films and CS/AgNPs nanocomposite films in the frequency range of 1 MHz to 3 GHz and temperature range of -10 to

110^{o}C using dielectric spectroscopy. Additionally, interpretation of dielectric spectra can be greatly aided with the use of complementary techniques such as TGA, FTIR and XRD measurements. All these techniques may prove useful in determining structural changes that undergo polymer films upon heating/cooling cycles.

6.1. Dielectric measurements

Typical dependence of dielectric loss ε" with frequency (1Hz to 3 GHz) of as-prepared non-neutralized and neutralized chitosan films (with water content about 11 wt % obtained from TGA measurements) are shown on Figure 6.1 at the two selected temperatures indicated on graphs. These dependencies have been obtained on three Impedance Analyzers. These spectra have been calculated from dielectric spectroscopy measurements using DC correction as described elsewhere [47, 49]. Figure 6.1 shows three relaxation processes: 1) low frequency α-relaxation, 2) β-relaxation (10^5-10^8 Hz) and 3) two additional new high frequency relaxation processes (10^8-3 10^9 Hz). It is noteworthy that α-relaxation observed in non-neutralized films has higher amplitude and it is observed at higher frequency range when compared with neutralized films. This effect can be related to fact that the α-relaxation process is highly dependent on acid content which changes viscosity of chitosan solution and act as plasticizer [117].

Figure 6.2 shows a typical dependence of the dielectric loss (ε″) with frequency of the as-prepared non-neutralized chitosan films at four different temperatures. The fitting of the complex permittivity in non-neutralized and neutralized films were carried out using the well-known Cole-Cole empirical model [118].

$$\varepsilon^{*} - \varepsilon_{\infty} = \frac{\varepsilon_{s} - \varepsilon_{\infty}}{[1 + (jw\tau)^{1-\alpha}]}$$

where ε_s-ε_∞ and ε_∞ are the dielectric relaxation strength and the dielectric constant at the high frequency limit, respectively; τ is relaxation time. The exponents α introduce a symmetric broadening of the relaxation.

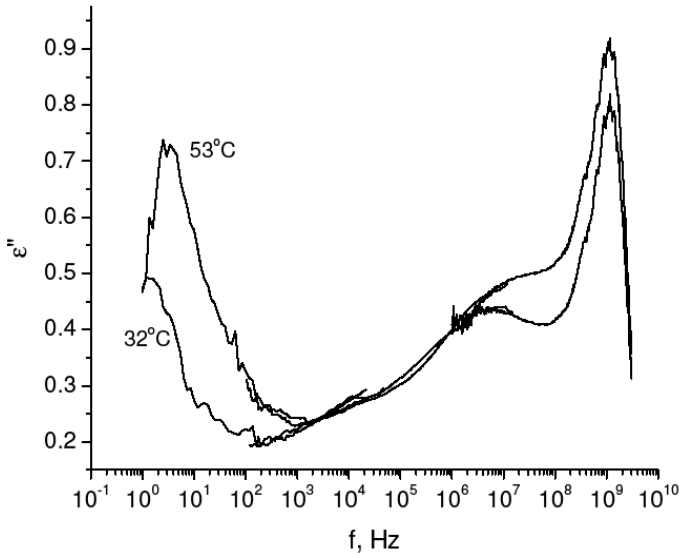

Figure 6.1: Dielectric loss factor (ε″) *versus* frequency for (a) non-neutralized and (b) neutralized chitosan films at the two indicated temperatures.

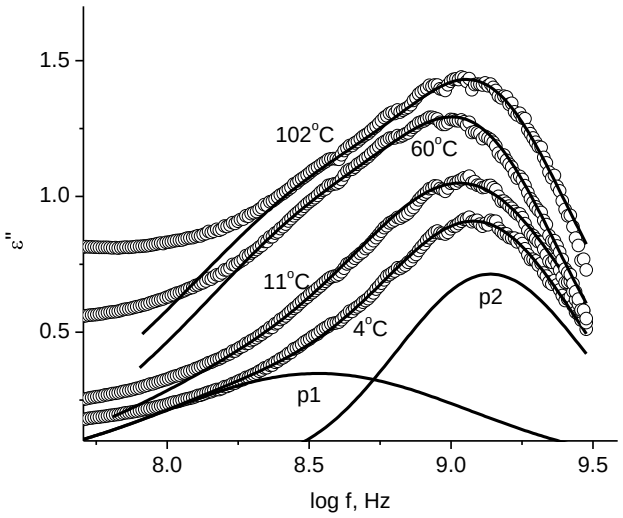

Figure 6.2: Dielectric loss factor (ε″) *versus* frequency for non-neutralized chitosan film measured at the indicated temperature (dashed-lines: fitting using Cole-Cole model).

Due to non symmetrical shape of the dependencies of the dielectric loss with frequency it is customarily to dissect the impedance response as the sum of two Cole-Cole contributions. As one can see from Fig. 6.2, the sum of two Cole-Cole peaks fits well the overall behavior (continuous lines; this gives rise to unsymmetrical shape). For illustrative purposes we show the deconvolution of the data at 4°C as the sum of two Cole-Cole peaks (tagged as p1 and p2). The dielectric loss (ε″) shows two maxima at frequencies *ca.* 5.8 10^8 and 1.3 10^9 Hz for non-neutralized chitosan polymer films; a similar behavior has been observed and in neutralized films. Figures 6.3a and 6.3b show that the dependencies of real part of permittivity measured at the frequency 1 MHz versus temperature for as-prepared wet and dry non-neutralized and neutralized chitosan films in the process of heating and cooling. This frequency has been chosen to avoid Maxwell-Wagner interface and electrode polarizations which is observed at high temperature in chitosan films below 10^5 Hz.

It is noteworthy that after heating to 110^0C, films were annealed at this temperature for 30 min to drive off any moisture. This procedure ensures that measurements during cooling were carried out on dry samples with water content less than 0.5 wt % (according to TGA measurements, insert on Fig. 6.3). As one can see real part of permittivity (or dielectric constant) for both wet films exhibit a peak at *ca.* 54^0C. Conversely, during the cooling process (dry films) dielectric constant decrease with decreasing of temperature. Figures 6.4 and 6.5 show the dependencies of relaxation time *versus* reciprocal temperature for as-prepared wet non-neutralized and neutralized chitosan films in the process of heating and cooling.

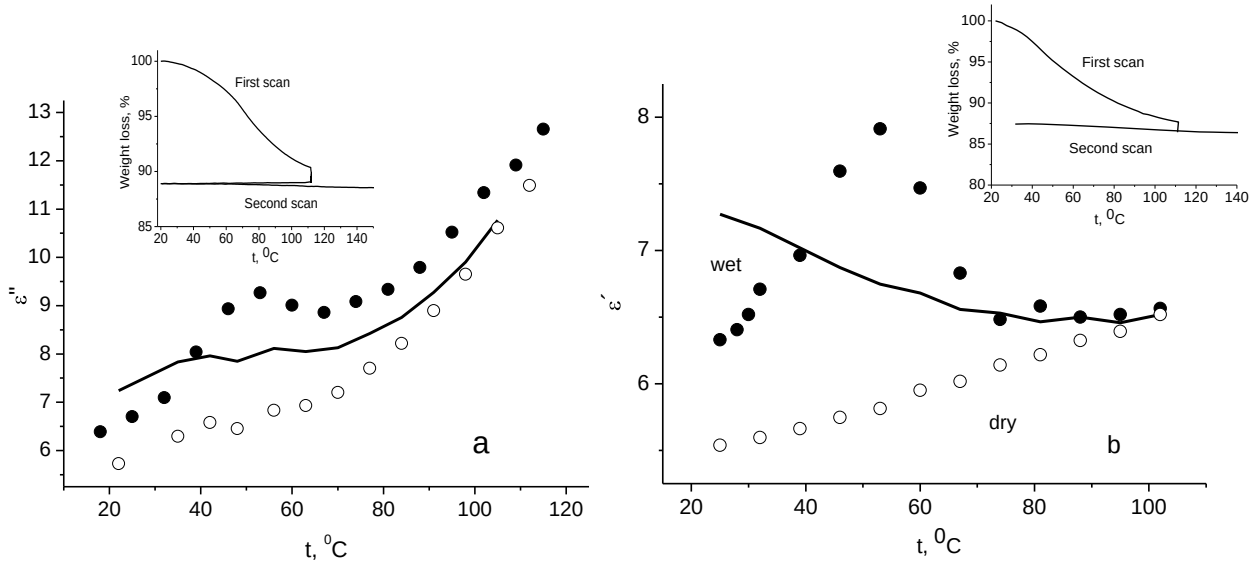

Fig. 6.3 Dependence of the temperature measured at the frequency of 1 MHz on as-prepared (wet) and dry films (a) non-neutralized and (b) neutralized chitosan films. The continuous lines are results of fitting using the Maxwell–Wagner equation. The inset shows TGA measurements on the as-prepared film during the first and second scans. The second scans have been obtained after annealing at the temperature of 110ºC for 30 min.

Below 54^0C in both non-neutralize and neutralize films, the temperature dependence of relaxation time τ_1 of process 1 can be described by Arrhenius-type dependence: $\tau = \tau_0 \exp\frac{E_a}{RT}$, with negative activation energy E_a. The values of E_a are -3.02±0.15 and -3.54±0.3 kJ/mol in non-neutralize and neutralize films, respectively. For higher temperatures, relaxation times decrease and E_a values change from the negative to positive with activation energy +3.41±0.17 kJ/mol and +3.89±0.35 kJ/mol for non-neutralize and neutralize films, respectively. For process 2 below 54^0C in non-neutralize films, the temperature dependence of relaxation time τ_2 is close to zero and at higher temperatures it becomes positive with activation energy +1.72±0.15 kJ/mol. In contrast, in neutralize films the relaxation time of process 2 at the temperature 54^0C changes value from negative (with Ea=-3.35±0.3 kJ/mol) to positive (with Ea=+4.61±0.2 kJ/mol).During

the process of cooling on both dry-non-neutralized and dry-neutralized films, the temperature dependence of relaxation times of process 1 and 2 exhibit practically zero activation energies.

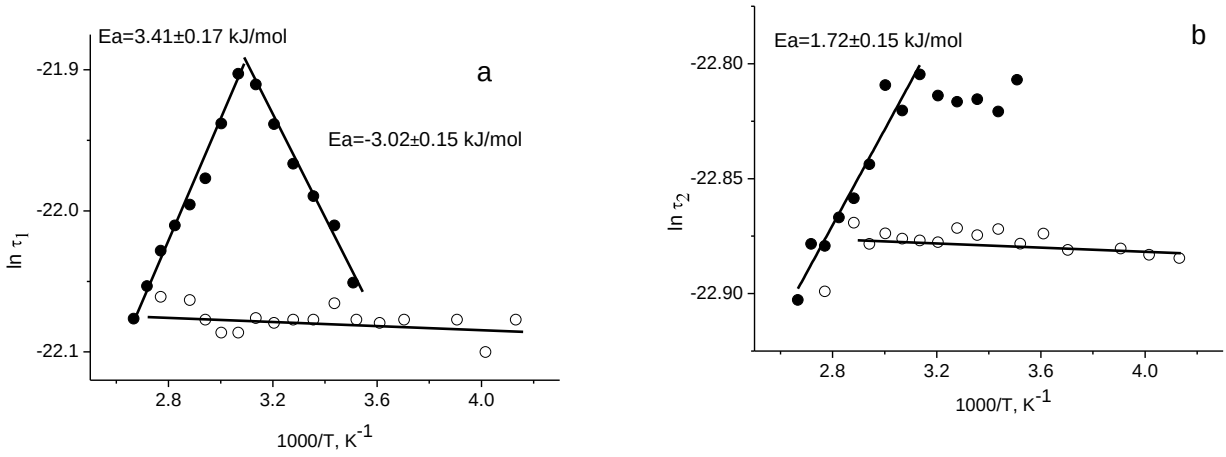

Fig. 6.4. Temperature dependence of relaxation time versus 1/T for the non-neutralized film (a) for the first relaxation process (p1) and (b) for the second relaxation process (p2). The lines represent Arrhenius-type dependence fitting.

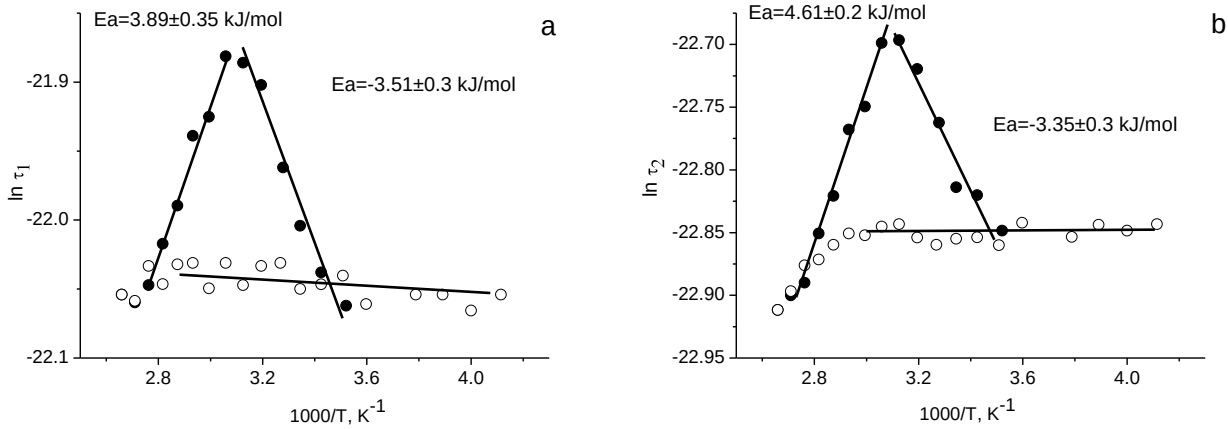

Fig. 6.5 Temperature dependence of relaxation time versus 1/T for the neutralized film (a) for the first relaxation process (p1) and (b) for the second relaxation process (p2). The lines represent Arrhenius-type dependence fitting.

6.2. DC conductivity

The values of DC (direct current) conductivity have been obtained from fitting of impedance spectra in low frequency range 1-10^4 Hz using Solartron 1260 and methodology descried in ref [119]. Fig. 6.6 shows dependence of DC conductivity σ versus 1000/T for wet (as prepare), and after annealed at temperature 110^0C for 30 min in the process of cooling for non-neutralized (Fig.6.6a) and neutralized (Fig.6.6b) films.Both non-neutralized and neutralized films show similar behavior: nonlinear dependence in wet samples and two linear dependencies in dry films in the cooling processes. Nonlinear dependence is a typical feature of the α-relaxation behavior related to glass transition [49]. The temperature dependence of conductivity is well described by the Vogel-Fulcher-Tammann-Hesse (VFT) equation [120].

$$\sigma = \sigma_0 \exp(-\frac{DT_0}{T - T_0}),$$

Results of fitting using VFT equation are shown on Fig. 6.6 as continuous lines. From this fitting the Vogel temperature is calculated as 277.1±1.2 K and 278±1.3K for non-neutralized and neutralized films, respectively. The same value of Vogel temperature have been obtained from dielectric spectroscopy measurements from fitting dependence of relation time of α process versus reciprocal temperature [49].

T_0 in many amorphous and semicrystalline polymers is usually 50^0C lower than glass transition temperature, Tg. [49]. Using this empiric relation Tg can be calculated as 54.1±1.2^{0}C and 55±1.3^{0}C for non-neutralized and neutralized films, respectively. In dry films during the cooling process the α-relaxation has not been observed because this relaxation is related to a plasticizing effect of water [49]. In dry samples and upon cooling from 105 to 46^0C, the DC dependence of the conductivity is well described by the Arrhenius model for both neutralized and non-neutralized chitosan. This relaxation, so-called σ-relaxation, has been widely studied

and it is associated with the hopping motion of ions in the disordered structure of the biomaterial [46, 49]. Further cooling from 46 to 20^0C, the DC dependence of conductivity with temperature in chitosan can be represented by the variable range hopping model proposed by Mott [98].

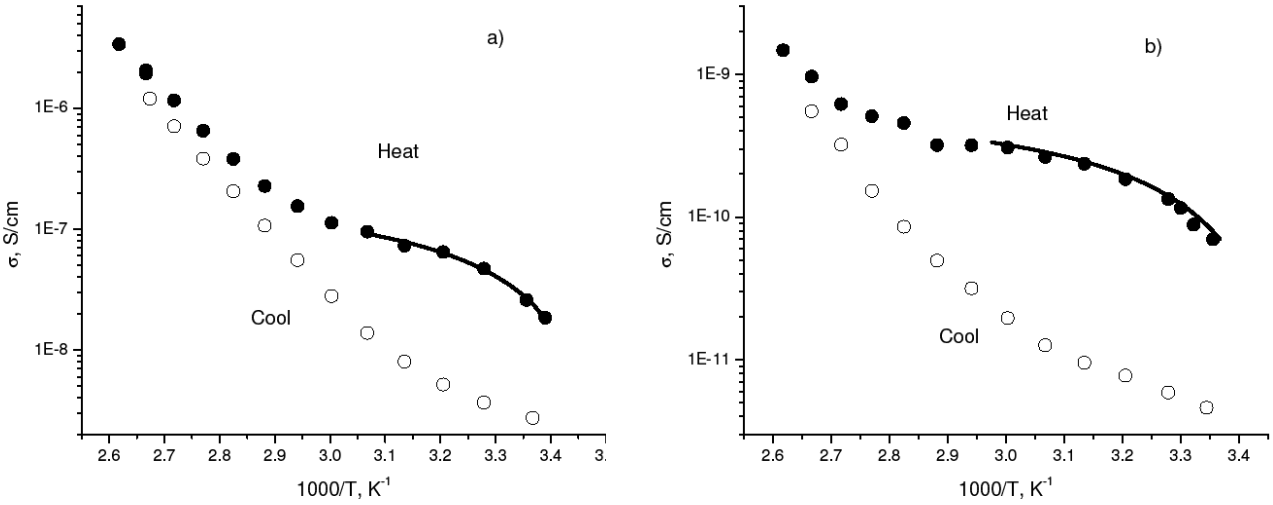

Fig. 6.6 Temperature dependence of DC conductivity versus 1/T for (a) non-neutralized film and (b) neutralized film. The lines represent fitting using the VFT equation.

6.3. *In situ* Infrared Spectroscopy

To understand mechanisms of interaction of the bound water molecules with chitosan film as a function of temperature additional FTIR measurements were carried out on non-neutralized and neutralized films under the same heating-cooling cycles (analogously to dielectric spectroscopy and TGA measurements). Figures 6.7a and 6.7b show FTIR spectra of the non-neutralized chitosan film in the process of heating and cooling. Firstly, the non-neutralized chitosan film spectra (see Fig.6.7a) is observed by confirming the appearance of the $-NH_3^+$ band at 1545 cm^{-1} (note that there is no apparent $-NH_2$ band at 1590 cm^{-1} in neutralized

films). One may conclude that this film is essentially in the acetate (non-neutralized) form [121]. The characteristic 3700-3000 cm^{-1} vibration bands corresponds to the amine and hydroxyl groups and the characteristic peaks at 1639 cm^{-1} (amide I group) and 1549 cm^{-1} (bending vibrations of NH_3) are also observed. The absorption band centered at 3350 cm^{-1} (Fig.6.7a) confirms the presence of broad O-H and N-H stretching in which the O-H bands overlap by N-H stretching [122].

In case of non-neutralized films, during the process of heating, there are two relevant changes observed: 1) reduction of intensity and broadening of the band centered at 3350 cm^{-1} which shifts to 3445 cm^{-1} (upon heating); and 2) the band at 1635 cm^{-1} shifts to 1654 cm^{-1}. These changes could be affecting the hydrogen bonded structure of the chitosan film due to elimination of adsorbed water and the breaking of intra-chain hydrogen bonds between water molecules and NH or OH groups of the chitosan molecule. It is noteworthy the appearance of a new band at 1710 cm^{-1} above 70^0C. This new band at 1710 cm^{-1} is ascribed to the interaction of NH_3^+ groups of chitosan with $-COO^-$ in the process of drying of film [122].

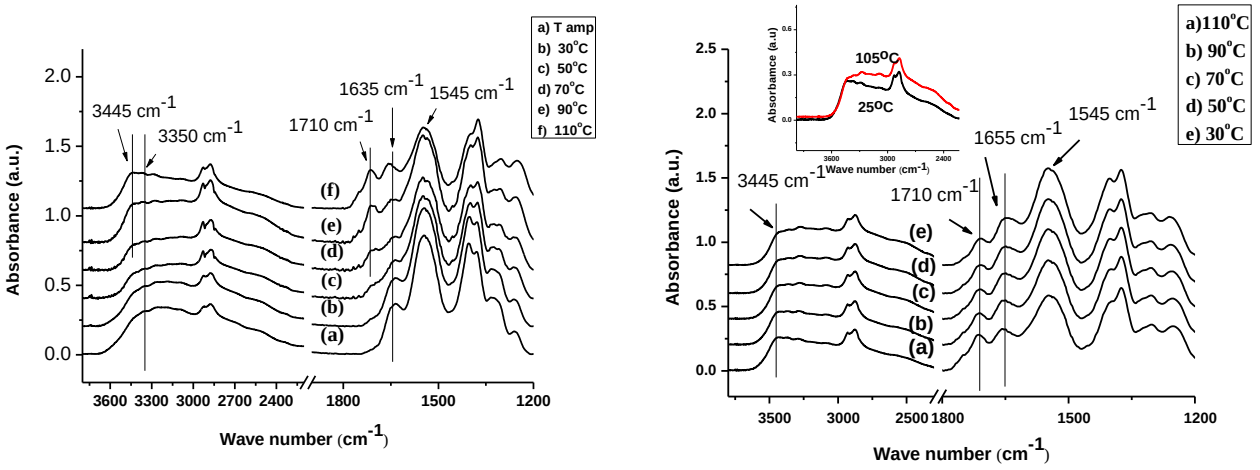

Figure 6.7: FTIR Spectra of non-neutralized chitosan film (a) in the process of heating and (b) in the process of cooling.

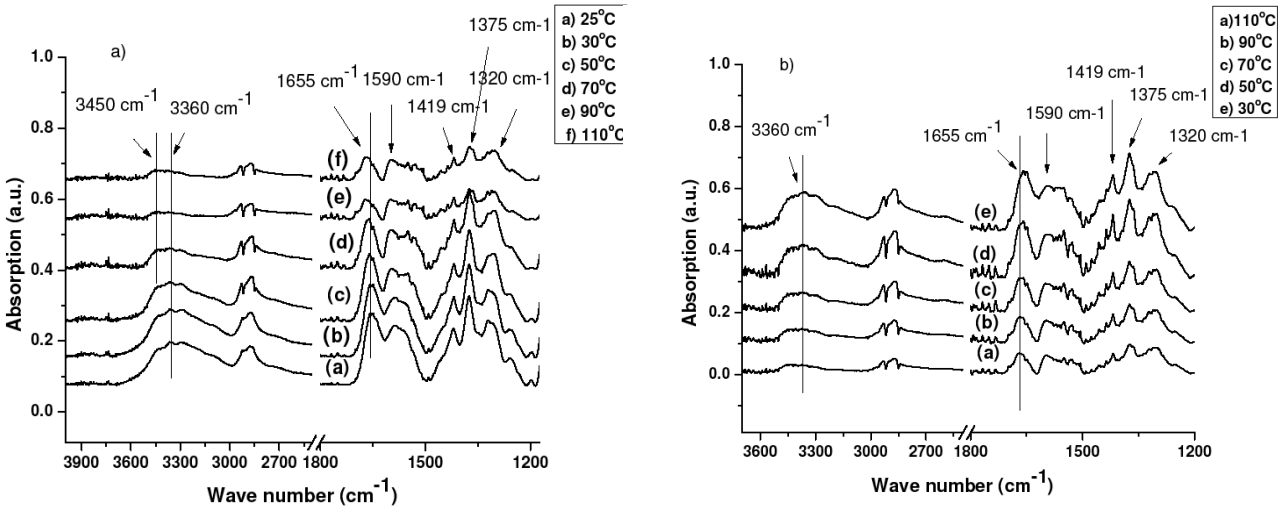

Figure 6.8: FTIR spectra of neutralized chitosan films (a) upon heating, and (b) upon cooling.

Fig. 6.7b shows FTIR spectra of non-neutralized chitosan films during the process of cooling. The absorption band at 3445 cm^{-1} has a relatively constant intensity and broadening. This observation indicates a possible overlapping of hydrogen bonding with –OH and NH groups. Additionally, the band at 1654 cm^{-1} shifts to 1649 cm^{-1}.

Figures 6.8a and 6.8b show FTIR spectra of neutralized chitosan film during the heating and cooling cycles. The most important feature of the FTIR spectra of neutralized films is the presence of a band at 1590 cm^{-1} which corresponds to the N-H stretching of the amine group. The removal of acetate counter ion (by neutralization) is further confirmed by the appearance of the bands at 1419 cm^{-1}, 1375 cm^{-1} and 1320 cm^{-1} corresponding to CH_2 bending, CH_3 deformation and CH bending, and CH_2 wagging, respectively [123]. For neutralized films upon heating (Fig. 5.7a), the broad band centered at 3360 cm^{-1} shifts to 3450 cm^{-1} with significant reduction in intensity and the band at 1655 cm^{-1} shifts to higher wavenumber values. The shift of

these characteristic vibrations to higher wavenumbers and decrease in intensity is associated with elimination water from neutralized film. It is noteworthy that in neutralized film the peak at 1710 cm^{-1} has not been observed.

In the cooling process (Fig. 6.8b), the band centered at 3450 cm^{-1} shifts to 3360 cm^{-1} with increasing of intensity and the band at wave number 1655 cm^{-1} shifts to lower wave number. These changes are likely due to new types of hydrogen bonding in the swollen chitosan environment. It is notable that for neutralized films there is a large increase of intensity of the band at 3360 cm^{-1} during the cooling process. The changes observed in the FTIR spectra for both non-neutralized and neutralized films in the heating-cooling process will help explain the temperature-dependence of relaxation times obtained in impedance measurements.

6.4. X-Ray Diffraction

The X-ray diffraction patterns of chitosan non-neutralized film under different temperatures are presented on Fig. 6.9. At room temperature (25 °C), the corresponding diffractogram shows a mixture of two crystalline phases and an amorphous one. After applying a whole-pattern deconvolution with Gaussian peaks, the area below the broadest peak (with a center located at $2\theta = 18° \pm 0.05°$) is associated to amorphous fraction (*ca.* 67%). On the other hand, crystalline fraction is characterized by two hydrated crystalline phases: *tendon* or hydrated Form I (hereafter *T*), and hydrated *L*-2 or Form II (hereafter *L*-2) which is observed in non-neutralized acetate films [45]. The procedure for indexing them is based on the calculated diffraction pattern extracted from the structures modeled in reference 30. Phase *T* is usually reported as the stable polymorph in chitosan systems, either if they are neutralized or not [124]. In the present work the distinguishing reflections of *T* are: (001), (110), (200) and (032). Three peaks of phase *L*-2 have been identified in pattern at room temperature as: (003), (200) and

(121). It is a metastable phase and previous studies noted that it spontaneously transforms into the phase Annealed (hereafter An).

On heating, the occurrence of the An phase is detected from 60 °C up to 105 °C. This transition (i.e., *T* —> An) is concomitantly noticed with an increasing of intensity and sharpening of the complex peak at central part of XRD patterns. It is presumed that this behavior is not only a direct consequence of the change in the crystal structure and decreasing the amount of amorphous fraction (about 57% at 105 ºC), but it is chiefly caused by the progressive increasing of the An fraction (peaks (110) and overlapped reflections (200) with respect to those of the hydrated phases *L-2* (reflections (200). Also there is an intensity decrease in direction (003) and *T* phase (decrease reflections (110) and the disappearing of peak (032). Table 6.1 shows the association of the (*hkl*) indices with the corresponding 2θ positions and the different phases encountered (i.e., *T, L-2* and An).

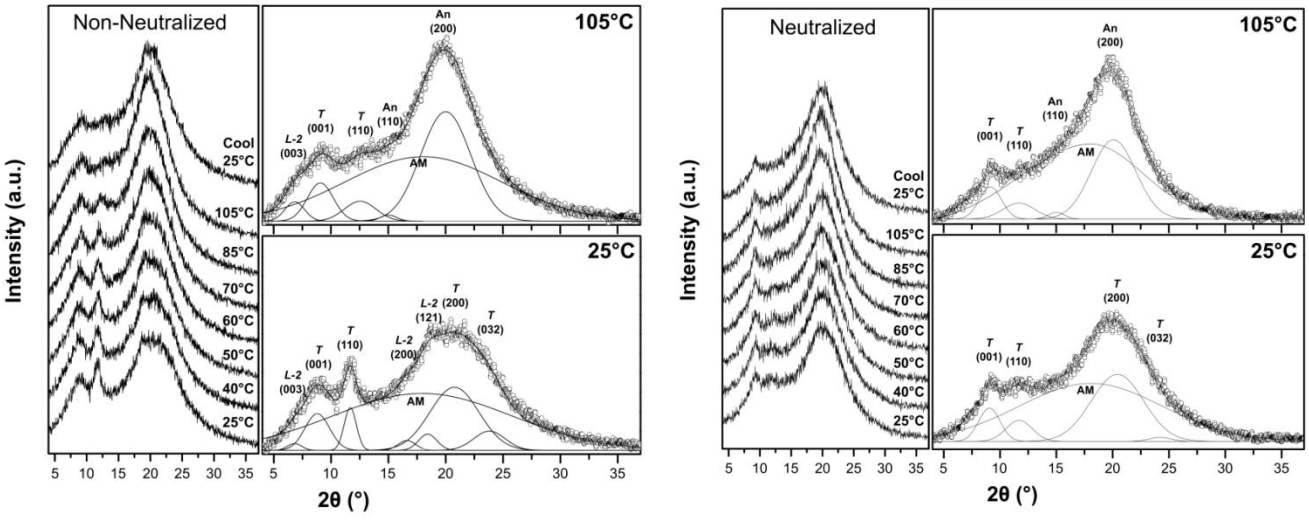

Figure 6.9. X-ray diffraction patterns at different temperatures for: non-neutralized film and for neutralized film. Right figures show results of fitting (see text). *T, L-2* and *An* referred to the crystalline phases; *AM* indicates the amorphous fraction.

The decreasing of the amount of amorphous phase (or the crystallization process) on heating is caused by the loss of water as reported in reference [125]. It is important to emphasize that the predominant phase at high temperature is An and that it is a product of three dynamical related-processes: 1) non-isothermal crystallization of amorphous fraction by progressive loss of weakly-bonded water on heating; 2) transition from *T* phase to An phase, and 3) spontaneous transition from metastable *L-2* phase to An phase. In reference to this latter transition, it is restrained during the heating process in view of the persistence of the characteristic reflection (003) of *L-2* up to 105 °C (Fig.6.9). In a first approximation, a likely explanation for this phenomenon is the competition between water and acetic acid during hydrolysis of non-neutralized chitosan acetate films. In other words, an increment of the loss of water molecules obstructs the loss of acetic acid and, subsequently, the permanence of that limits the advance of transition *L2* —> An. In this sense, the kinetic of this latter transition is directly related with the dependence of non-neutralized chitosan hydrolysis on water content in the films [126]. Lack of *L-2* Form in neutralized films (Fig. 5.9b) directly relates with the absence of acetic acid[42] that increases amorphous fraction (about 70% at 25 ºC and 63% at 105 ºC). Thus, the crystallization of neutralized films by heating is only represented by two processes 1) non-isothermal crystallization of amorphous fraction by progressive loss of weakly-bonded water on heating and 2) transition from *T* phase to An phase. Table 6.1 shows the association of the (hkl) indices with the corresponding 2θ positions and the different phases of non-neutralized and neutralized chitosan films at the extreme values of the temperature range studied.

Table 6.1 (*hkl*) indices and 2θ positions of T, *L-2* and An phases of non-neutralized and neutralized chitosan films at the extreme values of the temperature range studied. Mean X-ray wavelength of Cu Kα1,2 = 1.54187 Å

Sample	Temperature (ºC)	Phase	2θ (º)	(*hkl*)
Non-neutralized	25	L-2	6.81	(003)
			16.61	(200)
			18.43	(121)
		T	8.79	(001)
			11.66	(110)
			20.75	(200)
			23.81	(032)
	105	L-2	6.80	(003)
		T	9.05	(001)
			12.52	(110)
		An	15.00	(110)
			20.00	(200)
Neutralized	25	T	9.03	(001)
			11.67	(110)
			20.42	(200)
			24.23	(032)
	105	T	9.14	(001)
			11.68	(110)
		An	15.00	(110)
			20.09	(200)

It is noteworthy that after annealing at the temperature 110^0C during 30 min in the diffractograms of cooled samples at 25^0C (Fig. 6.9, upper dependencies), there are not significant changes when compared with diffractograms obtained at 105^0C. This means that in the cooling process, high water absorbance does not take place; this observation is confirmed by TGA measurements (water content in the annealing samples is about 0.5%). We note that all of our previous measurements (DC, X-ray and TGA) were run in the same heating-cooling cycles (analogously to dielectric spectroscopy). This strategy will help understand molecular structure changes upon heating-cooling and explain features of the high frequency relaxation.

6.5 Mechanism of high frequency relaxation.

High frequency dielectric measurements in chitosan films allowed to observed two new relaxation processes in the frequency range 10^8-3x10^9 Hz which exhibit a complex dependence on temperature. Upon heating below 54^0C a negative activation energy has been observed. However, for temperatures higher than 54^0C activation energy changes from the negative to positive (Figs.6.4 and 6.5). Negative activation energy at the frequency of *ca.* 300 MHz has been observed in hydrated lysozyme [127] and serum albumin [128]; in hydrate collagen at *ca.* 200 MHz [129] and *ca.* 100 kHz [130]; β-cyclodextrin complex with 4-*t*-butylbenzyl alcohol at *ca.* 1 MHz and calcified and decalcified bone at *ca.* 100 kHz [131]. Despite many studies of different materials, the explanation of observed negative activation energy has been based on the suggestion that the activation process involves the breaking of a hydrogen bond between surrounding molecules and water molecules in their primary hydration shell. This hydration shell is followed by the formation of other hydrogen bonds between the reorienting water molecule and its neighbors or the formation of more stable hydrogen bonds between reoriented water molecules [132]. However, explanations proposed in the literature could not be directly applied to chitosan films due to a more complex dependences of activation energy on temperature (changing the slope from the negative to positive values) and the high frequency range (between 10^8-3 10^9 GHz). It is noteworthy that the relaxation frequency of bound water in different biomaterials is typically found at 100 MHz, whereas the relaxation of free water is *ca.* 16 GHz [133].

It is well known that water molecules can be bonded through hydrogen bonding with both -OH and -NH_2 (or NH_3^+ in non-neutralized) groups of chitosan [49] According to FTIR measurements for the entire temperature range, the most significant changes are observed in

absorption band related to these groups. One can conclude that these groups are responsible for observed high frequency relaxation processes in both non-neutralized and neutralized films. An important question arises: why does the activation energy changes from negative to positive at temperatures above 54°C? According to DC conductivity measurements this value equals to the glass transition temperature (54.1 ± 1.2^0C and 55 ± 1.3^0C for non-neutralized and neutralized films, respectively).

Additionally, the confirmation that this temperature corresponds to the glass transition is the appearance of peaks about 50°C which has been observed in wet films by analyzing the dependence of ε´ versus temperature (Fig. 6.3). To make sure that this peak has no relation with water evaporation, a simple estimation has been performed using the Maxwell-Wagner effective medium model that considers a single inclusion (in our case water with ε_2) surrounded by continuous matrix of polymer (with ε_1). This model is often used in the polymer composites for estimation of effective dielectric constant $\varepsilon_{eff.}$ [134]. Due to the relatively low water content about 10 wt. %, this approximation can give a realistic estimation. The Maxwell-Wagner equation is given by [134]

$$\varepsilon_{eff} = \varepsilon_1 \frac{\varepsilon_2 + 2\varepsilon_1 - 2(1-\phi_1)(\varepsilon_1 - \varepsilon_2)}{\varepsilon_2 + 2\varepsilon_1 + (1-\phi_1)(\varepsilon_1 - \varepsilon_2)}$$

Were $1-\Phi_1$ is volume fraction of water in the chitosan matrix.

To put our results in perspective, we now calculate the temperature-dependence of effective dielectric constant at the frequency 1 MHz of chitosan films according to Maxwell-Wagner equation. In this calculation we use temperature dependence of water dielectric constant (ε_2) and taken in account that dielectric constant of water at the frequencies below 1 GHz practically constant [135] and dependent only on the temperature [135]. For calculation the temperature-dependent ε_1 at 1 MHz in dry chitosan films (see Fig. 6.3, open circles) has been used. Water

volume fraction was obtained from TGA measurements. This calculation gives rise a monotonically dependence on the real part of permittivity with decreasing of water content (continuous lines on Fig. 6.3). The same estimation has been performed for calculating the effective conductivity of chitosan-water complex by taking into account that the conductivity of ultra pure water is *ca.* 5.5 10^{-8} S/cm. The results obtained have shown that the water evaporation practically do not affected on conductivity of chitosan films.

Consequently the peak observed in the dependencies of ε′ versus temperature can be related to the glass transition. It is well known that when the temperature increases above the glass transition temperature, ε′ typically exhibits peaks that tend to decrease with a further temperature increasing. This type of behavior is due to the random thermal motions of chains which makes it more difficult for dipoles to align in the direction of an applied electric field [136]. Conversely, in dry films and upon cooling, those peaks and the glass transition have not been observed due to water evaporation (water act as plasticizer in the wet material) [49].

For amorphous materials, the glass transition temperature (T_g) is the temperature that separates glassy and rubbery states. As result, at T_g pronounced changes are observed in the mechanical, thermal and dielectric properties. In the hydrophilic chitosan, at the temperatures higher than T_g, there is an additional dehydration process (TGA measurements, insert on Fig. 6.3) and transformation of crystalline phase due to water evaporation (transition from hydrated to annealed form and increasing volume fraction of crystalline phase, Fig. 6.9). All these effects responsible for changes in the thermal motions of -NH and -OH chains.

It is noteworthy that the well-known model of thermal dipolar relaxation is based upon the presence of two states of dipolar group orientation separated by potential-energy barrier which approximately equals activation energy [137]. Molecular dynamics of site groups in chitosan is

not well known; however, the molecular dynamics simulation of hydroxymethyl side groups in cellulose [138] and OH side groups in poly(vinyl alcohol) (PVA) [139] considers a motion of these groups between two sites separated by an energy barrier which appears due to the presence of intermolecular and intramolecular hydrogen bonds. For example, in PVA the presence of intermolecular and intermolecular hydrogen bonds are responsible for hydroxyl side groups to have two energy minima with difference in energy of 5.5 kJ/mol and only 8% of groups have average energy 10 kJ/mol [139]. Consequently, this model suits well for explaining experimental results in chitosan films. At temperatures below glass transition temperature (54^0C), the initial structure of wet films, according to XRD measurements, are likely tendon structure consisting of a polymeric water structure comprised of a network of water molecules that are hydrogen bonded [49].

To identify the nature of the two observed relaxation processes it is important to emphasize on the chemical structure of chitosan; it has an -OH and a $-NH_2$ (neutralized form) and NH_3^+ (non-neutralize films). The relaxation process 1 in both films centered at the frequency *ca.* 5.8 10^8 Hz and according to Fig. 6.4a and 6.4b has approximately the same negative and positive activation energies. Therefore, it is possible to conclude that process 1 relate to relaxation of -OH side groups (note that these groups are relatively unchanged by the neutralization of films). These conclusion is also confirmed by FTIR data: a similar shift of characteristic band associated with the –OH stretching vibration from 3350 cm^{-1} to 3445 cm^{-1} has been observed for both non-neutralized and neutralized films. It is noteworthy that PVA also possess -OH side groups and the relaxation frequency of such groups is centered at *ca.* 10^8 Hz [140].

In contrast, the relaxation process 2 is observed at the frequency *ca.* 1.3 10^9 Hz for both non-neutralized and neutralized films; however, they exhibit different dependencies on the

temperature and activation energies. These differences can be related to the mobility of different side groups that change during the neutralization of films: NH_2 (neutralized) and NH_3^+ (non-neutralized). Additionally, it must be considered the presence of acetic acid in the non-neutralized film and the interaction of the COO^- groups with the NH_3^+ groups of chitosan [141]. This interaction can be detected by FTIR measurements: appearance of new band at 1710 cm^{-1}. Therefore, one may conclude that relaxation process 2 can be related to relaxation of NH_2/NH_3^+ side groups. We now discuss the nature of observed negative activation energy. The negative activation energy can be related to the reorientation of weak intermolecular hydrogen bonds between bound water and NH_2/NH_3^+ and OH groups; this changes the build-up symmetry of hydrogen bonding of the side groups NH and OH and as a result, energy of these groups is lowered [142]. We now give a plausible scenario to help explain the observed phenomena.

1. Fig. 6.10 shows the schematic of proposed structure of neutralized (Fig. 5.10a) and non-neutralized (Fig. 5.10b) chitosan films below 54^0C. According to the literature hydrated form of chitosan has bonded and free water in chitosan matrix. Additionally, non-neutralize films have COO^- groups which interact with the NH_3^+ groups of chitosan [139]. Upon heating (below glass transition), water molecules rearrange in such a way that build-up of hydrogen bonding is affected, i.e. the symmetry of hydrogen bonding changes. This event is thermodynamically favorable such that it frees side group mobility to evolve to another state. Consequently, a negative (favorable) activation energy is observed. Such effects have been observed in proteins: hydrogen bonds of hydroxyl groups with side groups of protein can generate molecular asymmetry in hydrogen bonding build-up with difference in energy of *ca.* 2.5 kJ/hydrogen bond [140]. This energy is higher than the potential energy in equilibrium state such that lateral NH_2 and OH groups pushes the system to a lower energy state; this relaxation is responsible for

observed negative activation energy. We propose that only reorientation of hydrogen bonds with side groups of chitosan are promoted upon heating (not broken hydrogen bounds) as probed by FTIR spectra; it is observed that only: 1) a small reduction of intensity of band centered at 3350 cm^{-1} and band at 1655 cm^{-1} and 2) a small shift of T peak (110) of hydrated Form I to the higher 2θ observed in XRD spectra.

2. In the temperature range 54^0C (glass transition) to 110^0C, activation energy of relaxation process changes slope from negative to positive values. At a temperature above the glass transition the amplitude of the random thermal motions of chains increase leading to breaking of weak hydrogen bonds between water molecules and NH or OH groups of chitosan (Fig. 5.10c and 5.10d). Additionally, according to TGA measurements (Fig. 6.3, insert) the loss of water molecules has been observed. XRD measurements have shown the change in the crystal structure (from hydrate to annealing forms) by decreasing the amount of amorphous fraction and decreasing of interchain distances due to loss of water. The breaking of the H-bonds between water molecules and side groups of chitosan were responsible for: the high reduction of intensity and shift to higher values of band centered at 3350 cm^{-1}; reduction and shift to higher values of the band at 1635 cm^{-1} for non-neutralize films (and band at 1655 cm^{-1} in neutralized films). We propose that at temperatures above 54^0C (glass transition), side groups of chitosan posses energies higher than potential energy barrier between the two states: hydrate to annealing forms. Theses changes are due to the breaking of hydrogen bonds, water loss and as a result, the relaxations of the lateral groups exhibiting normal process with positive activation energy.

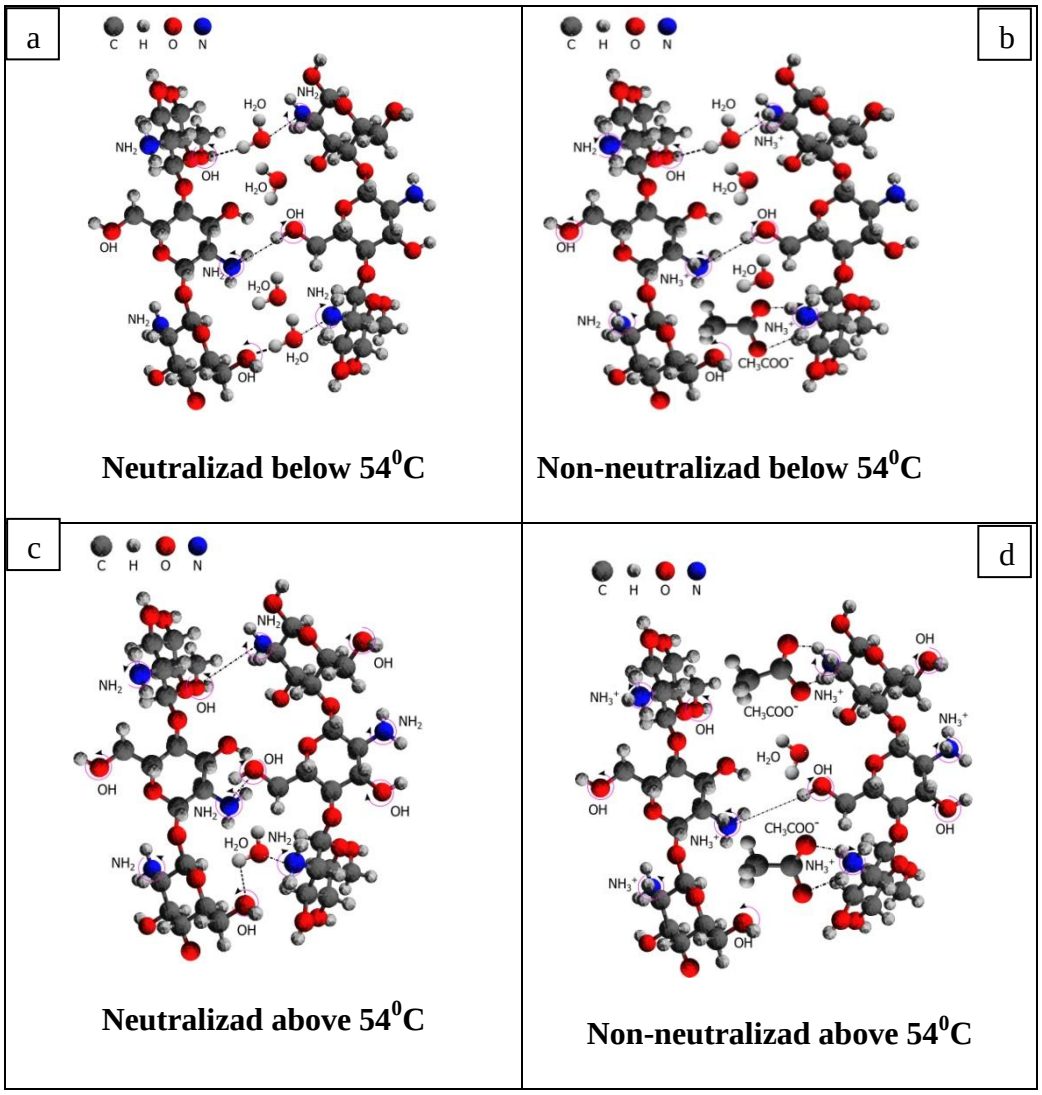

Figure 6.10: Schematic of the structure of neutralized (a, c) and non-neutralized (b, d) chitosan at the temperatures below glass transition (a, b) and above glass transition temperature (c, d).

3. In the process of cooling, the activation energies of both relaxation processes are practically about zero or exhibit a very little negative slope (less than -0.02 kJ/mol). According to TGA data (insert on Fig. 6.3), it has not been observed a significant water absorbance (water content in the annealing samples is about 0.5%). According to XRD measurements (Fig. 6.9) it has not been observed changes in the crystalline structure of chitosan films (it practically does not change XRD pattern when compared with patterns at 105^{0}C). Dielectric constant in the

cooling process decrease with decreasing of temperature (Fig. 6.3) due to lower freedom of movement of dipole molecular chains. FTIR spectra for both neutralized and non-neutralized films in dry and wet state at 30^0C showed a difference due to the different types of hydrogen bonding in dry and wet films. The measurements in the cooling process confirmed the determining role of H-bonding and free water in the relaxation processes in chitosan films. Based upon the above analyses, it is possible to conclude that two high frequency relaxation processes are related to the changes of energy and freedom of movement of the side groups OH and NH_2/NH_3^+, respectively.

6.6. High frequency relaxation of CS/AgNPs composites.

The above results demonstrated that the new relaxation process about 1 GHz attributed by the side groups (OH, NH_3^+/NH_2) of chitosan. Thus, it's interesting to investigate the high frequency relaxation process of CS/AgNPs composites and the influence of molecular motion and activation energy of the respective relaxation process. We have performed the temperature dependant impedance measurement over high frequency by taking the direct comparison with the CS biopolymer. Fig. 6.11 shows the temperature dependent relaxation peaks about 1 GHz frequencies. It's evident from the Fig. 10, the peak maximum is constant (no shifts in the peak position) have been observed. According to the TGA measurements (chapter 5) with increasing AgNPs content decrease water absorption. This means that AgNPs replace water molecules in chitosan matrix due and form more strong hydrogen bonds between AgNPs and CS side groups. Such strong bonds do not allow to rotate the side groups, which confirmed by the zero activation energy. Fig. 6.11 shows the schematic of proposed CS/AgNPs structure which based on high frequency measurements.

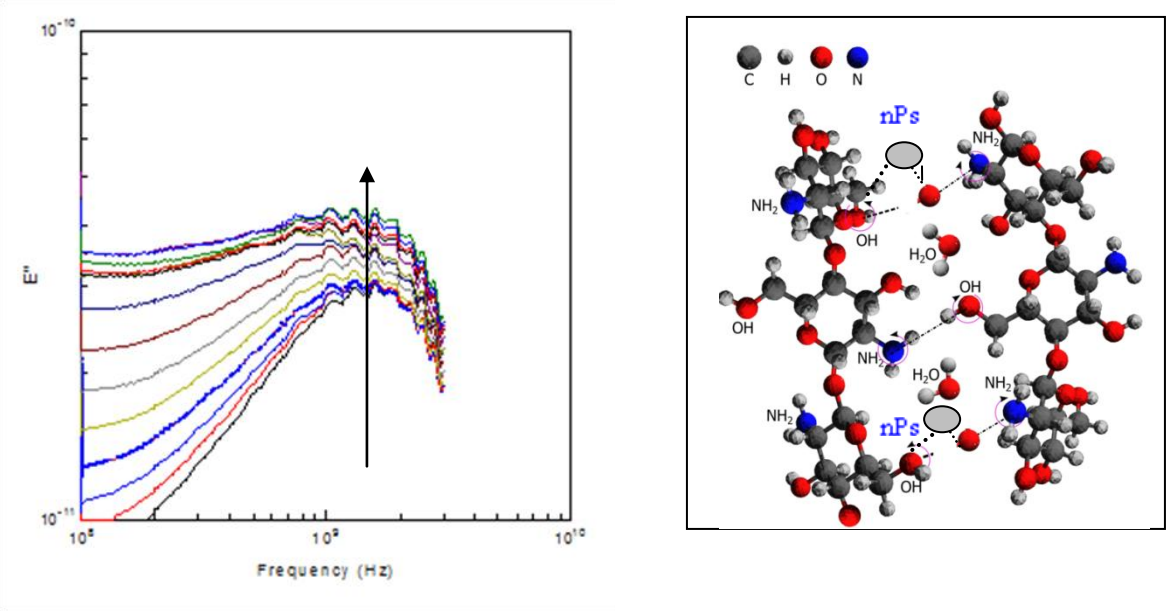

Figure. 6.11 a) Dielectric loss factor (ε″) *versus* frequency for CS/AgNWs composite with different temperatures.b) schematic of mechanism of interaction between CS side groups and AgNPs.

6.7. Summary

The temperature dependence of high frequency (in GHz range) dielectric relaxation behavior of neat chitosan films have been investigated using dielectric spectroscopy, TGA, FTIR and XRD measurements. For the first time, two new relaxation processes in the gigahertz frequency range has been reported. The relaxation process centered at the frequency *ca.* 5.8×10^8 Hz relate to the mobility of OH side groups. The relaxation process observed at the frequency *ca.* 1.3×10^9 Hz related to mobility of NH_2/NH_3^+ side groups. In wet films, glass transition phenomena is observed by performing temperature-dependent measurements of DC conductivity and dielectric constant. Upon heating and below the glass transition temperature, chitosan films exhibit an Arrhenius-like dependence with negative activation energy due to the disruption of the symmetry of hydrogen bonding (not H-bonding breakage). Upon further heating (above the glass transition) the activation energy changes slope from negative to positive because of water

molecules are expelled from the vicinity of chain molecules and H-bonding breakage. After this thermal treatment, films are cooled to *ca.* 10°C and the activation energy is practically zero. FTIR spectra for both non-neutralized and neutralized films in the heating-cooling process have shown changes in vibration frequencies and intensities of side OH, and NH_2/NH_3^+ groups, respectively. XRD analysis reveals associated structural changes upon heating and cooling in the following fashion: 1) non-isothermal crystallization of amorphous fraction by progressive loss of weakly-bonded water on heating (above glass transition), and 2) transition from *Tendon* phase to *Annealed* phase. Based upon these changes in the chitosan structure the new model of high frequency relaxation has been proposed which can be attributed to the interaction of the bounded water molecules and the changes of energy and freedom of movement of side groups, namely OH and NH_2/ NH_3^+. It is noteworthy that in many applications, OH and NH_2/NH_3^+ groups strongly interact with water molecules but also in the formation of chitosan-based composites and nanocomposites.

In addition, the high frequency relaxation process of CS/AgNPs nanocomposite have been investigated with different temperatures as of chitosan films. It was found that the high frequency relaxations have zero activation energy due to the strong interaction between AgNPs and the CS side groups. In many cases, the nature of the molecular interaction of side groups with nanoparticles is still not known. Therefore, the proposed high frequency method and model for the determination of energy and freedom of movement of side groups will allow understanding mechanism of interaction of chitosan with Ag nanoparticles. These new finding could open up the promising platform to complete understanding the interaction mechanism for various biomedical and biosensing applications.

Chapter 7. Chitosan mediated synthesis of CS/AgNPs nanocomposite: investigation of properties and antibacterial activity.

As has been shown in Chapter 5, CS/AgNPs composite obtained by three methods (direct dissolved AgNPs in chitosan solution, chemical reduction using ascorbic acid and sodium citrate and chemical reduction using ascorbic acid and sodium dodecil sulfate) demonstrate relate high dimensions of nanoparticles. Additionally, residuals of the chemical reduction processes could also affect on properties of composites due to the interaction with -OH and $-NH_3/NH_2$ functional groups of chitosan. Therefore, in this chapter properties and antibacterial activity of another simple and efficient greener route to synthesize CS/AgNPs composite films will be presented using dilute acetic acid as a reducing agent, mediated by the biopolymer chitosan (see 3.4).

7.1. UV-Vis spectroscopy analysis

The formation of AgNP obtained by reduction of different concentrations of $AgNO_3$ in the chitosan-dilute acetic acid solution at 95^0C was monitored by UV-vis spectroscopy. Typical UV-vis absorption spectra of the resulting solution are shown in Figure 7.1. Specifically, in the case of sample prepared at 95°C, the final solution starts to change from colorless to light yellow color within 20 minutes of reaction and further change to stable dark yellow color in 8 hours after addition of $AgNO_3$ solution. It can be observed that all spectra display the characteristic surface plasmon resonance (SPR) absorption maximum between 412 nm-416 nm, indicating the formation of spherical silver nanoparticles [143]. At the same time, it is evident from Figure 7.1 that, as the concentration of precursor ($AgNO_3$) increases, a progressive increment in the intensity of the SPR band is observed which is related with an increase of AgNP concentration in

the chitosan solution. It was found that the concentration of acetic acid in CS and temperature play an important role in the reduction process. These results are consistent with the previous studies of AgNP synthesis by dilute acetic acid used as reducing agent and chitosan as mediator of the reaction [42].

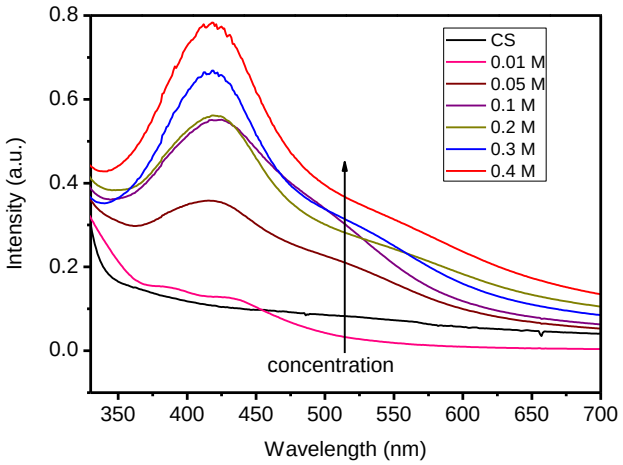

Fig. 7.1. UV-vis absorption spectrum of CS/AgNP's films obtained by reduction under different concentration of precursor ($AgNO_3$) at 95^oC.

7.2 Morphology Analysis (TEM)

Transmission Electron Microscope (TEM) images obtained for CS/AgNP composite films are shown in Figure7.2. TEM results revealed that in films with low concentration of silver (0.5 wt. %) the formation of spherical silver nanoparticles with size ranging from 3 to 11 nm are distributed homogeneously on CS matrix (Figure 7.2a). However, for 1 wt. % (Fig. 7.2b and 7.2c) AgNP agglomerates have been observed. As mentioned above, the nanocomposite films have been prepared from precursor solutions with different $AgNO_3$ concentration. In order to compare the electrical and antibacterial properties wt % of AgNPs was calculated using EDS analysis (the same as in chapter 5).

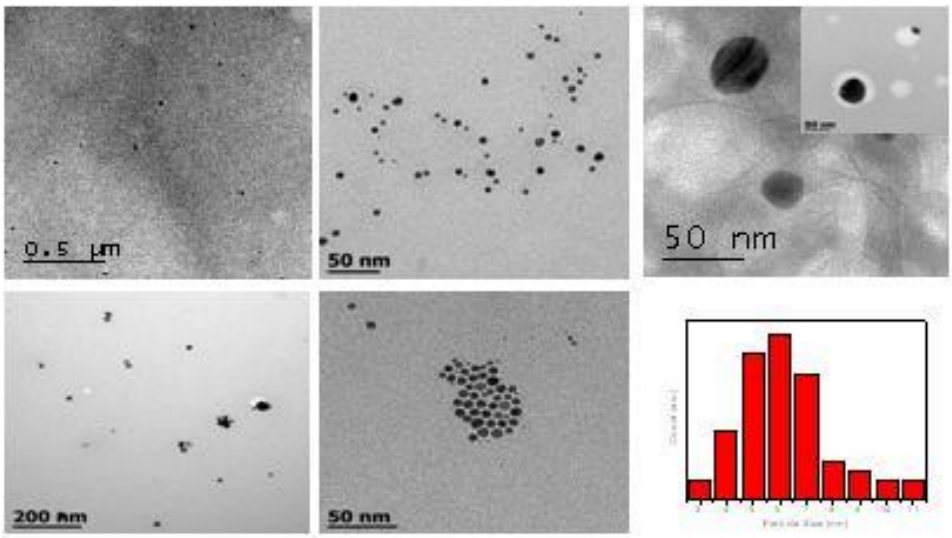

Fig.7.2. TEM microphotograph of synthesized CS/AgNP composites: a) 0.5 wt% AgnP, b) 1 wt% AgnP c) high magnification of 1 wt% AgnP and d) Size distribution of AgnP's.

7.3 FTIR and XRD analysis

In order to understand the molecular interactions of AgNP with chitosan, Fourier-transform infrared spectroscopy (FTIR) analysis was performed. Figure 7.3 shows FTIR spectra of pristine CS and CS/AgNP. The pure chitosan films exhibits characteristic transmittance band at 3000-3500 cm^{-1} assigned to the N-H stretching vibrations as well as vibration band at 1643 cm^{-1} band for amide I (C=O stretching); 1556 cm^{-1} for amide II (N-H bending); bands at 1410 cm^{-1} for OH bending vibrations; 1326 cm^{-1} for CH_2 wagging vibration; 1261 cm^{-1} for amide III vibration mode due to combination of N-H deformation and C-N stretching; and 1154 cm^{-1} for anti-symmetrical stretching of C-O-C bridge [144].

In the FTIR spectra of CS/AgNP nanocomposite film, the bands at 3370 cm^{-1} (amine and hydroxyl groups) and 1556 cm^{-1} (bending vibrations of NH_3) decrease in intensity and slightly shift to lower wave number evidencing the interaction of primary amino groups in chitosan with

AgNP surface [145]. Other transmittance bands at 1643 cm^{-1} (amide I group), 1410 cm^{-1} (bending vibration of OH group) and 1326 cm^{-1} (CH_2 wagging vibration) were not changed, suggesting that these transmittance bands are not sensitive to the metal nanoparticle surface [144].

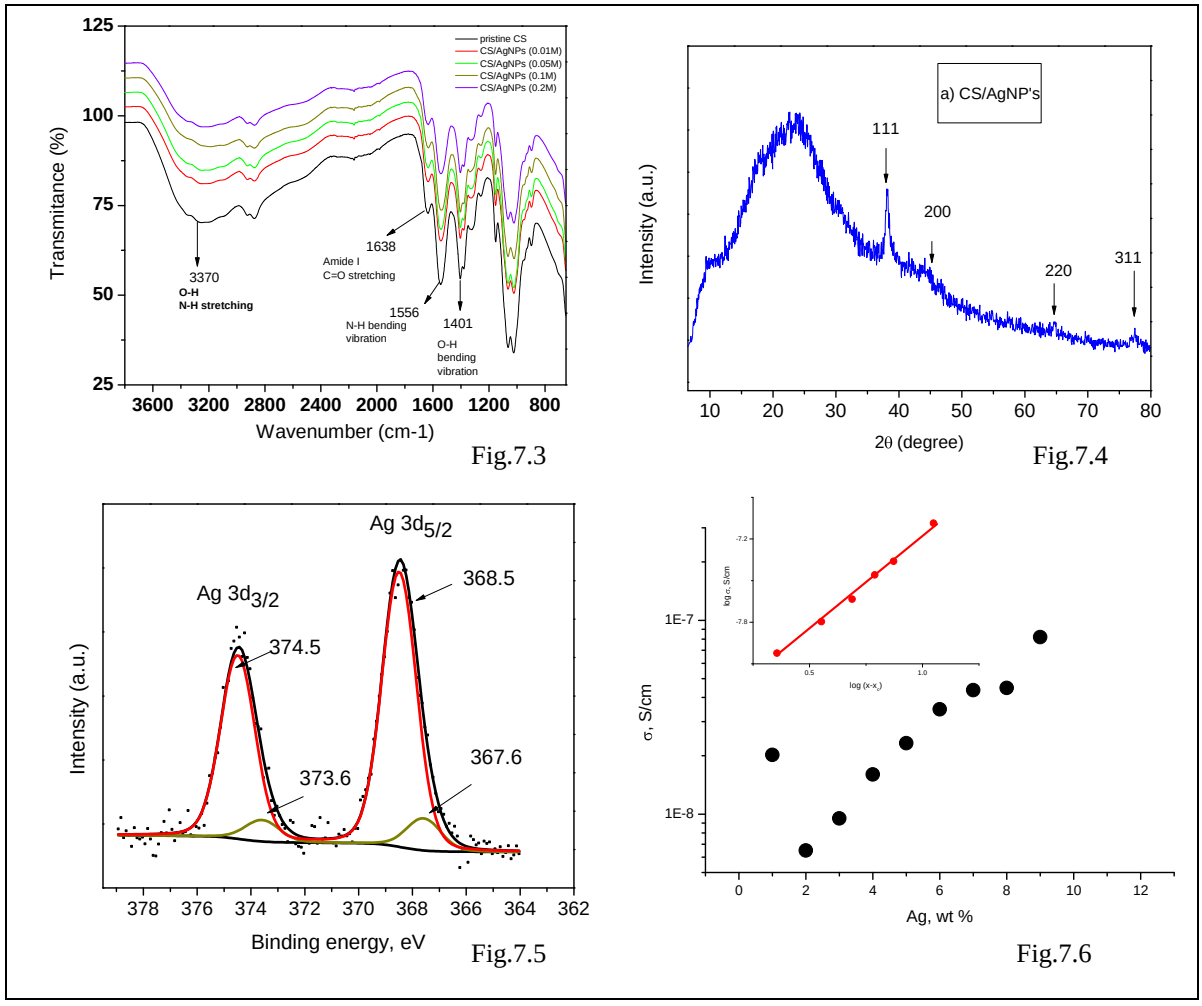

Fig.7.3. FTIR spectra of pristine CS and CS/AgNP's with different concentration of AgNPs. Fig.7.4. X-ray diffraction pattern of CS/AgNP's composites. Fig.7.5. XPS spectra for Ag 3d region obtained from CS/AgNP's composite film. Fig.7.6. Electrical conductivity of CS/AgNP's films as a function of the AgNP's wt % .Inserts show a double log-log plot of the electrical conductivity vs $x-x_c$.

Figure 7.4 shows the X-ray diffraction patterns of CS/AgNP Typical XRD pattern of CS/AgNP composite film (5 wt. % of AgNP's) shows peaks at 2θ values of 38^0, 44.2^0, 64.3^0 and 77.7^0 that correspond to the (111), (200), (220) and (311) planes of face centered cubic (fcc) for Ag^0 [146]. The broad peak at 2θ equal 22.5^o relates to crystalline form of chitosan. The crystalline size of nanoparticles *d* was estimated from XRD measurements using the Scherer formula. The calculated value of *d* was about of 9±0.5 nm, which is close to TEM measurements.

7.4 XPS Analysis

X-ray photoelectron spectroscopy (XPS) analysis was performed by focusing on the changes of silver spectra to gain further insight into the specific interaction of AgNP with chitosan. The Ag 3d region of the silver is characterized by two peaks as a consequence of spin orbital splitting that corresponds to $Ag3d_{3/2}$ and $Ag3d_{5/2}$ core levels. The same two peaks are observed in the Ag 3d region in CS/AgNP composite (Figure 7.5). Each peak can be further resolved into another two peaks at lower binding energy. In Figure 6.5, the peaks at 368.5 and 374.5 eV correspond to $3d_{5/2}$ and $3d_{3/2}$ core levels of metallic silver respectively [147], and the new two peaks at lower binding energy (367.6 and 373.6 eV) indicate the presence of silver ions in Ag_2O with binding energy between 367.3-367.6 [148]. These results mean that 89.5% of silver is in metallic state.

7.5 Conductivity measurements

The DC conductivity of the composites was obtained from the extrapolation of impedance measurements to zero frequency and by using the dimensions of each film [149]. Neat chitosan exhibits low ionic conductivity that can be related to the presence of small concentration of conductive species in the form of NH_3^+ groups and H^+ ions [149]. At ambient conditions, film's

water content is ca. 10 wt. %, which reduces the resistance of films and masks the real conductivity behavior of composites. Figure 7.6 shows the plots of the DC electrical conductivity obtained from impedance measurements as a function of the AgNP wt. % in dry films at room temperature [149]. At low concentration of AgNP, a decreasing in conductivity was observed. The decrease of condutivity in low concentraction is explained by the strong interactions of AgNP with free NH_3^+ groups of CS film, which in turns decrease the free NH_3^+ and -OH and are responsible for the conduction in CS [52]. An abrupt increasing of conductivity with increasing of AgNP wt. % and a subsequent saturation is typically observed for percolation phenomena (Figure 7.6).

It is important to note that CS-silver nanocomposites demonstrate low conductivity even in saturation region with high weight percent of silver. Such effect has been observed in films obtained by direct dissolved of silver nanoparticles in chitosan solution and has been explained by the presence of a thin polymer layer that coexists between silver nanoparticles [111].

In the vicinity of the percolation threshold a simple power law describes the DC conductivity as follow:

$$\sigma \propto (x - x_c)^t, \qquad \text{for } x > x_c \qquad (1)$$

Where, x is the wt. % of conductivity phase, x_c is the critical AgNP concentration at the percolation threshold, and t is a critical exponent that only depends on the dimensionality of the percolation system. The insert in Figure 7.6 shows the log-log dependence of the conductivity of the CS composites on x-x_c. The least-square fitting analysis according to equation (1) results in a percolation threshold of 0.85 ± 0.31 wt. % of silver nanoparticles and a critical exponent t equals to 1.24 ± 0.11 for CS/AgNP films; Values of critical imply that the CS/silver nanoparticles system is two-dimensional according to well-established values [111]. The same value of critical

exponent (1.32 ±0.09) has been calculated in films obtained by direct dissolved silver nanoparticles in chitosan solution. Such low value of the critical exponent clearly suggests that a 2D conductive network is formed and that the charge must flow along surfaces and interstitial spaces of polymer matrix [150].

7.6 Antibacterial analysis

The antibacterial activity of as-synthesized CS/AgNP nanocomposite films was evaluated against Gram-positive bacteria *Staphylococcus aureus*, and Gram-negative bacteria *Escherichia coli*. In order to ensure the accuracy of the measurement, all films were subjected to antibacterial test simultaneously and under the same conditions. Additionally, our previous study demonstrated that dilute acetic acid present in the CS significantly influences the bacterial growth, so neutralization of films was carried out by washing them with deionized water until neutral pH (pH=7).

The antibacterial activity of neat chitosan was reported previously. However, the exact mechanism of antibacterial action of neat chitosan is poorly understood while several hypotheses have been proposed. Interaction of the protonated amino groups of chitosan with the negatively charged cell membranes surface; penetration into the phospholipid bilayer of membranes; and disruption of the cytoplasmic membrane are common explanations of the action of neat chitosan [151]. For instance it has been observed a remarkably decreasing about two orders of magnitude of CFU/cm^2 of *Staphylococcus aureus* after 48 h of cell culture in pristine chitosan films.

The antibacterial effect of CS/AgNP composite films against *Staphylococcus aureus* and *Escherichia coli* incubated after 48 h are shown in Figure 7.7. It can be seen that there is a slight difference in antibacterial effectiveness of both films against investigated Gram-positive *Staphylococcus aureus*, suggesting that the relatively ten times thicker Gram positive cell wall

with multiple murein layers and teichoic acid prevents the interaction of AgNP with thiol group, resulting in a decrement in bactericidal effect [152].

Additionally, Figure 7.7 shows that the antibacterial effect for CS/AgNP films composite films clearly increased as increasing concentration of AgNP's until it reaches a maximum at a critical concentration that correlates well with the percolation threshold concentration determined by conductivity measurements (Figure 5.6). For CS/AgNP films (approximately 1 wt. % of silver content) showed minimum in CFU/cm^2, denoting a maximum in bactericide effectiveness, thus suggesting that low concentration of AgNP's is sufficient for cell death. These values correlated well with the percolation thresholds obtained from electrical measurements (0.85 ± 0.31 wt.%). Above this critical concentration the antibacterial activity saturates or decreases against both Gram-positive *Staphylococcus aureus* and Gram-negative *Escherichia coli*. The composite film showed the maximum bactericidal effectiveness close to percolation thresholds. The percolation effect helps to explain the observed maximum bactericide activity of the CS/AgNP's composites, i.e. once the system percolate, a physical path is formed through which the current can flow thus decreasing the effective surface area of nanoparticles [59]. Additionally, at higher silver concentrations, clusters start to appear which further decrease the surface area of nanoparticles (See Figure 7.2). A similar observation has been reported in our previous studies of commercial AgNP embedded into chitosan matrix [59].

The results published in the literature is controversial about antibacterial properties of silver nanoparticles and silver ions. The various observed and hypothesized interactions between AgNP, Ag^+ ions and bacteria cells have been discussed in a large number of publication [24, 48, 49]. Some investigation showed that AgNP affects more the bacteria than silver ions, and the dominated factor is the direct contact of bacteria with nanoparticles. In other publications it is

proposed that nanosilver alone has minimal toxicity and it serves mostly as a source of Ag^+ ions. Other publications supported the hypothesis of similar biological response of AgNP and Ag^+ ions. *Sotiriou and Pratsinis et al.* [153] proposed that the mechanism of antibacterial activity depends on nanoparticle size: the smaller AgNP releases higher concentration of Ag^+ ions. Thus, the antibacterial activity is dominated by the release of Ag^+ ions rather than by the AgNP itself. Herein, the results showed that CS/AgNP films (AgNP size less than 10 nm) have superior antibacterial activity. In other investigation, CS/Ag^0 membrane surface (metallic Ag produced by chemical reduction with ascorbic acid) exhibited better antibacterial performance than the after 4 days of inoculation, in agreement with our work [59]. In Ag/SiO_2 composite, the antibacterial activity of nanosilver was dominated by Ag^+ ions when Ag nanoparticles were less than about 10 nm in average diameter [153].

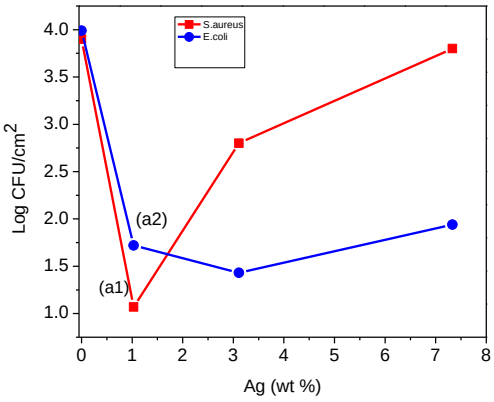

Figure 7.7. Log CFU/cm^2 versus Ag concentration for CS/AgNP composites after 48 h of culture.

The exact mechanism in which silver nanoparticles operate to cause antimicrobial effect is not clearly known. One possible antibacterial mechanism involves the interaction of silver with the bacteria cell wall and subsequent penetration; thereby causing structural changes in the cell

membrane. Another plausible scenario is that, because the DNA of the bacteria has sulfur and phosphorus as its major components, the nanoparticles can act on these soft bases destroying the DNA and causing cell death [59].

CS/AgNP antibacterial properties can be explained as a synergistic effect of chitosan (which causes a decrease of about two orders of magnitude of CFU/cm^2 of *Staphylococcus aureus* after 48 h of cell culture) and silver nanoparticles. Chitosan stabilize the AgNP and prevent silver nanoparticle agglomeration below a critical concentration. It also confers a positive charge to nanoparticles surface, enhancing their binding to the negative charges present at the cell surface. Moreover, the antibacterial activity increases with the concentration of AgNP. We proved that close to percolation threshold, the antibacterial activity attained a maximum, suggesting higher effective surface area of silver nanoparticles because chitosan prevents AgNP aggregation. This in turns results in an effective interaction against bacteria cell wall. Above percolation concentration the presence of agglomerates dramatically lowers the effective surface area of AgNP and thus the antibacterial efficacy greatly decreased.

7.7 Cell viability analysis

Fig. 7.8 shows the cell viability analysis of obtained from the florescence microscopy. As seen in the Fig. 7.8, control samples (CS) did not show any dead cells. The cells were treated with increasing concentration of AgNPs showed a progressive death of the fibroblast cells which highly associated with the time and the dose. About 0.1mM (approx. 1 wt %), the majority of the cells found to be dead, suggesting the optimum concentration for the cell death. These results consistent with the antibacterial and electrical measurements.

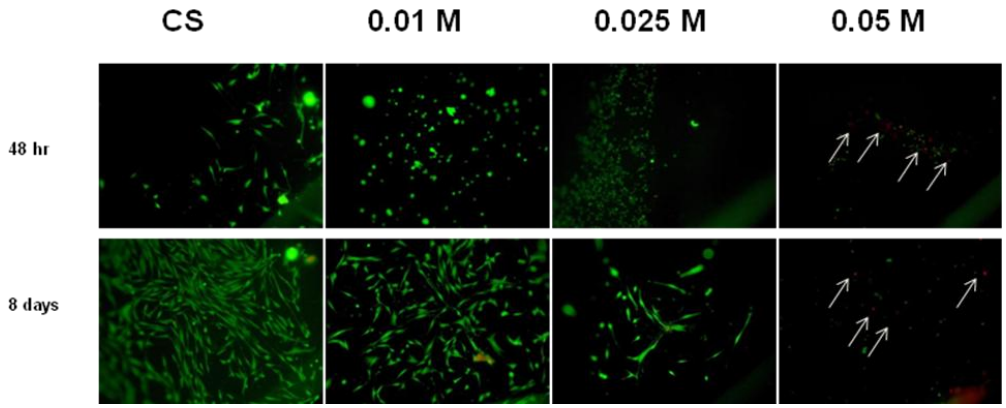

Fig.7.8. Cell viability, live/dead assay. Human fibroblasts isolated from foreskin were seeded on the scaffolds at HIGH density and maintained in culture for 48 hours and 8 days with medium changing every other day.

7.8 Summary

In summary, stable CS/AgNP bionanocomposite were successfully synthesized by a greener *in situ* chemical approach with dimension of nanoparticles about of 6 nm. The resulting bionanocomposites exhibit enhanced antibacterial activity against Gram-positive *Staphylococcus aureus* and Gram-negative *Escherichia coli* bacteria. The CS/AgNP composite showed synergetic antibacterial action (*ca.* two orders of magnitude). Thus, collective action of AgNP and Ag^{+} ions facilitated the enhancement of synergetic antibacterial activity below critical concentration. On the other hand, chitosan helps stabilize the AgNP and prevents AgNP agglomeration below a critical concentration. Chitosan also confers a positive charge to nanoparticles surface, enhancing their binding to the negative charges present in the cell wall. The cell viability analysis showed that the about 1 wt% of AgNPs, cells were found to be dead. The electrical and antibacterial properties of CS/AgNP bionanocomposite depend on the concentration. Above percolation threshold concentration, agglomeration of AgNP is responsible for a decreasing in the effective surface area of AgNP and consequently the antibacterial activity.

Chapter 8. Electrochemical detection of glucose based on chitosan stabilized silver nanoparticles (AgNPs) and silver nanowires (AgNWs) modified electrodes: a comparative study.

CS/AgNPs nanocomposites can find application for the development of glucose sensors. For such application material prepared by method 1 (direct dispersion of nanoparticles in CS solution) have been chosen due to the fact that this material had not reaction residues. Additionally CS/silver nanowires composite has been used due to their higher surface area compare with nanoparticles. Among different nanostructured materials, one-dimensional (1D) metallic nanostructures, such as Ag nanowires, have drawn considerable interest for the development of electrochemical sensors for H_2O_2 and glucose detection [79, 154]. They exhibit elevated electrical conductivity and due to its high aspect ratio, Ag nanowires could form conductive paths between the active center of the enzymes and electrodes, allowing the adequate electron transfer required for enzyme-based biosensors. Different innovative approaches have been developed to rectify the problem associated with their stability and surface oxidation [155]. Among the detection methods to sense glucose, electrochemical approaches are considered to be the most promising because of their instrumental simplicity, portability, high sensitivity and specificity. Diverse studies have been carried out using different materials such as ionic liquids [156], graphene [157], and chitosan [78] as versatile matrix materials to immobilize enzymes and to promote electron transfer of redox enzymes on the surface of modified electrodes. Among them, chitosan biopolymer displays an ideal matrix properties that helps stabilize AgNWs and also, to immobilize enzymes with efficient electrical communication while maintaining their biological activities. Additionally, chitosan offers higher stability, good biocompatibility and excellent film-forming ability [158]. Based upon these advantages, in this chapter, the possible

application of CS/AgNPs and CS/ AgNWs based electrochemical biosensor for glucose detection has been investigated.

8.1 Electrochemical glucose biosensing based on CS/AgNPS nanocomposite.

The glassy carbon electrodes used in this work were homemade in our lab. They were carefully polished until obtain a mirror surface and corroborated that they are clean and have a reversible electron transfer. After that, 35 µl of CS/AgNPs solution was dropped onto the surface of the pretreated GCE and left to dry at room temperature to obtain a CS/AgNPs-modified GCE, referred to as CS/AgNPs/GCE. The immobilization of GOx onto the surface of the CS/AgNWs/GCE was obtained by dropping 5 µL of 20 mgmL^{-1} GOD aqueous solutions onto the resultant CS/AgNPs/GCE and left to dry at 4^{o}C for at least 2 h, it was referred to as the CS/AgNWs/GOx/GCE. The enzyme modified electrodes were stored in refrigerator at 4^{o}C when not in use. CS/AgNW/GOx/GCE electrode was prepared in the same fashion.

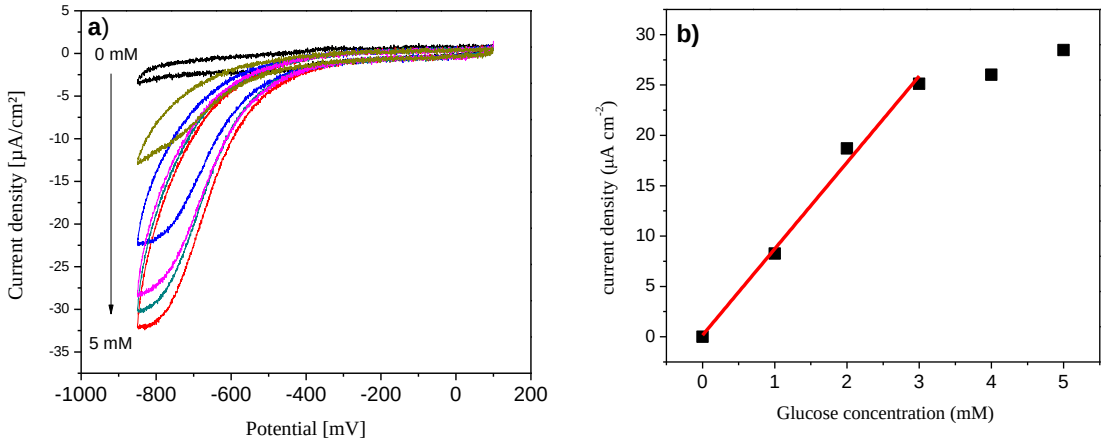

Fig. 8.1 (a) CVs of the CS/AgNPs/GOx-GCE modified electrode in O_2 saturated 0.1 M PBS solution (pH 7.4) containing different concentrations of glucose. Scan rate: 50 mV s^{-1}. b) The calibration plot obtained from the voltamperometric response at a constant 0.8 V potential.

The gulcose biosensing properties of the CS/AgNPs/GOx-GCE midified electrode was studied using standard three electrode electrochemical cell described in the section 3.6.9. The measurement was performed in PBS solution (pH 7.4) at scan rate of 50 mV in a oxygen (O_2) saturated condition. Figure 8.1a shows the cyclic voltamograms (CVs) of CS/AgNPs/GOx-GCE modified electrode obtained in the presence of different concentration of glucose. A cathodic peak at -0.8 V was clearly observed. Furthermore, the reduction current gradually increses with the glucose concentration, in a linear range of (1-3) mM of glucose concentration (Fig. 8.1b). The sensitivity of the modified electrode, obtained from the calibration plot was 8.57 $\mu A\ mM^{-1}\ cm^{-2}$. The relative small linear range and low sensitivity obtained for this CS/AgNPs/GOx-GCE modified electrode could be attributed to the reduction of the electron transfer between the redox centre of the enzyme and the electrode surface. In addition, not effective immobilization of enzyme could also be responsible for the low linear range toward glucose detection. That is why for biosensor application CS/Ag nanowire composites has been synthesized and investigated.

8.2. Enhancement of glucose sensing using chitosan stabilized silver nanowire (AgNW) modified electrodes

8.2.1. Structural characterization of CS/AgNW composite

The morphology of as-prepared AgNWs was examined with SEM and TEM analysis. Fig. 8.2a shows TEM images of Ag nanowires stabilized by chitosan polymer on the modified electrode surface. As is shown in Fig. 8.2a, the silver nanowires are well dispersed and stabilized with chitosan. The high magnification image of Ag nanowires, exhibit a clear view of AgNWs with average diameter of 60-70 nm and lengths range of 3-10 μm. In inset of 8.2b, the Selected Area Electron Diffraction (SAED) pattern of AgNWs reveals that the crystals have ordered crystallographic orientation.

The crystalline nature of the synthesized AgNWs was also investigated by X-ray powder diffraction (XRD). Fig. 8.3a shows the typical X-ray diffraction pattern of AgNWs (powder samples). The pattern displays sharp peaks at 2θ values of 38^0, 44.2^0, 64.3^0 and 77.7^0. The indentified peaks corresponds to the (111), (200), (220) and (311) planes of the face centered cubic (fcc) structure of Ag [159]. The high intensity diffraction peaks of (111) plane can be indicative that silver nanowires may have a preferred orientation along the (111) crystalline plane. It should be noted that no additional peaks were detected from this XRD pattern which suggests that the final product was essentially present in a pure form.

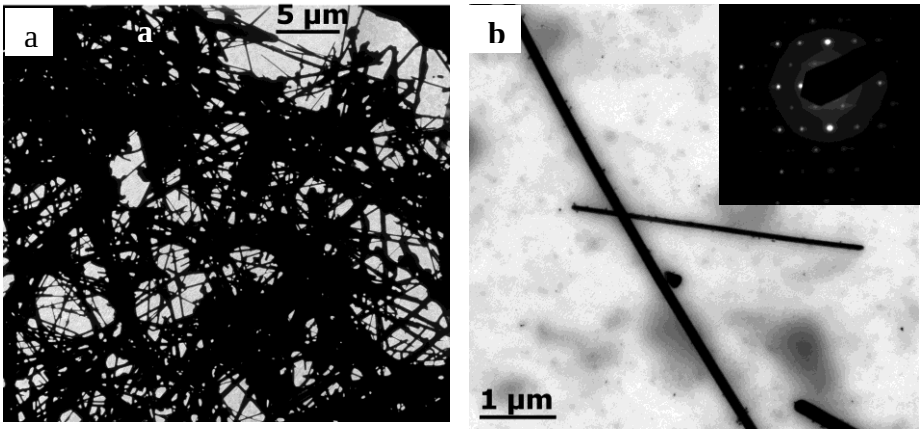

Fig.8.2. TEM images of: (a) chitosan stabilized AgNWs (b) High-magnification TEM image of AgNWs. Inset: the corresponding SAED pattern.

In order to obtain information about the specific interaction and effectiveness of enzyme immobilization on the AgNWs surface, Fourier-transform infrared spectroscopy (FTIR) analysis was performed. Fig. 8.3b shows representative FTIR spectra of pure GOx, CS/AgNWs composite and CS/AgNWs/GOx. The pure GOx molecule exhibits characteristic transmittance bands at 1658 and 1542 cm^{-1} and 1103 cm^{-1}, assigned to the amide I and amide II adsorption

bands of proteins, and the C-O stretching vibration of GOx, respectively [160]. The CS/AgNW composite has peaks at 1643 cm^{-1} band for amide I (C=O stretching); at 1556 cm^{-1} band for amide II (N-H bending) and at 1410 cm^{-1} band for -OH bending vibrations [59]. After immobilization of GOx on the AgNW surface, appearance of both amide I and amide II peaks of GOx, indicating the effective immobilization of GOx on the AgNW surface by retaining its secondary structure.

The effective immobilization of GOx could be a combination of two components. The first one due via electrostatic interaction between positively charged AgNWs and negatively charged GOx. The second one related to the presence of biocompatible CS that may allow to maintain the native structure of GOx and stabilize it on the AgNW surface, thus preventing the enzyme denaturation.

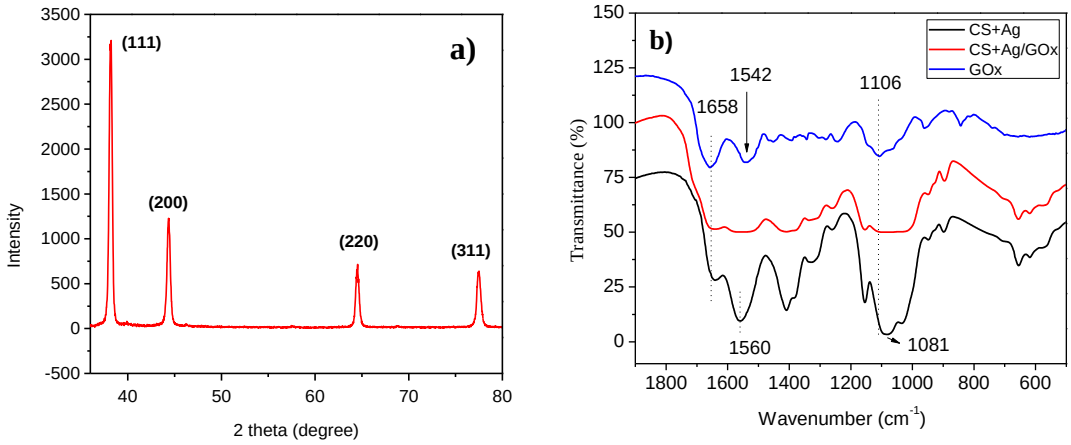

Fig 8.3. a) XRD pattern of AgNWs b) FTIR spectra of GOx, CS/AgNWs and CS/AgNWs/GOx composites.

8.2.2. Electrochemical glucose biosensing based on CS/AgNWs nanocomposite.

To investigate the direct electron transfer kinetics of GOx immobilized on AgNWs and stabilized by chitosan (CS), cyclic voltammetry measurements were performed. Fig. 8.4a shows that the CVs obtained at bare GCE (black curve), GCE/CS (red curve), AgNWs/CS-GCE (blue curve) and AgNWs/GOx/CS-GCE modified electrodes in 0.1 M nitrogen-saturated phosphate-buffered saline (PBS) solution (pH 7.4) at a scan rate of 50 mVs^{-1} in the presence of 3 mM of glucose.

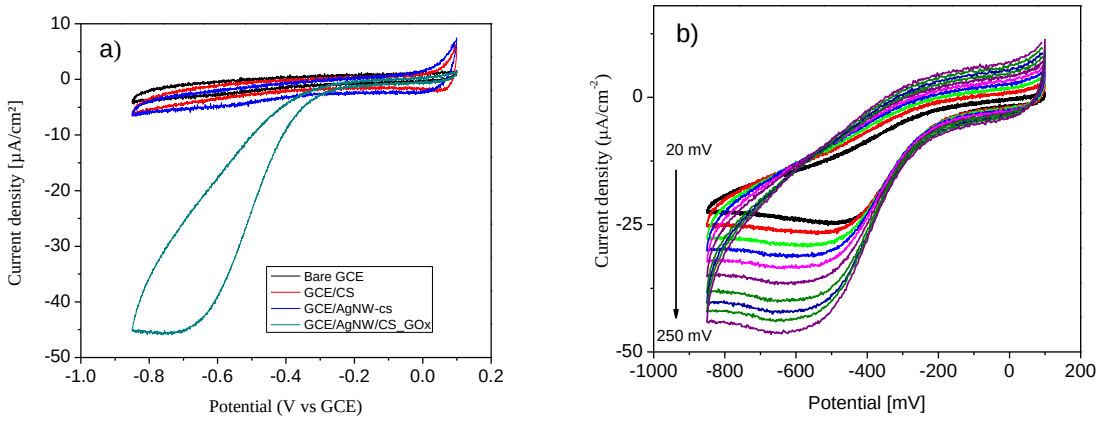

Fig 8.4. a) CVs of different modified electrodes b) CVs of CS/AgNWs/GOx-GCE in a 3 mM of glucose in PBS (pH 7.4) solution at various scan rates (20 to 250 mV s^{-1})

From the CVs of the same figure it is possible to see that bare GCE, CS and AgNWs/CS modified electrodes did not show any reduction peaks, suggesting that these electrodes are electrochemically inactive to glucose detection over the measured potential range. In contrast, the AgNWs/GOx/CS modified electrode displays well defined reduction peak at -0.65 V, suggesting the direct electron transfer ability between GOx and the modified electrode surface in comparison with the other modified electrodes (Fig. 8.4a). The reduction potential peak about -0.65 V should correspond to the reduction of O_2 and H_2O_2 and is consistent with previous report

[154]. The influence of varying the scan rate on the CV performance of the resulting CS/AgNWs/GOx-GCE electrode is shown on Fig. 8.4b. The cathodic peak current increase linearly with an increase of the scan rate from 20 to 250 mVs^{-1}) and shift to negative potentials, indicating that process of the immobilized GOD is a diffusion surface-controlled process mediated electron hopping process between GOx and electrode surface [161].

In order to determine the optimal concentration of GOx immobilized on the silver nanowires, experiments with different initial concentration of GOx (mg/ml) were done and the sensitivity to detect glucose of the different electrodes was estimated. Fig. 8.5a shows the calibration plots obtained for glucose determination of the modified electrodes containing different GOx concentrations. Fig. 8.5b shows the sensitivity values of the different electrodes versus the GOx concentration.

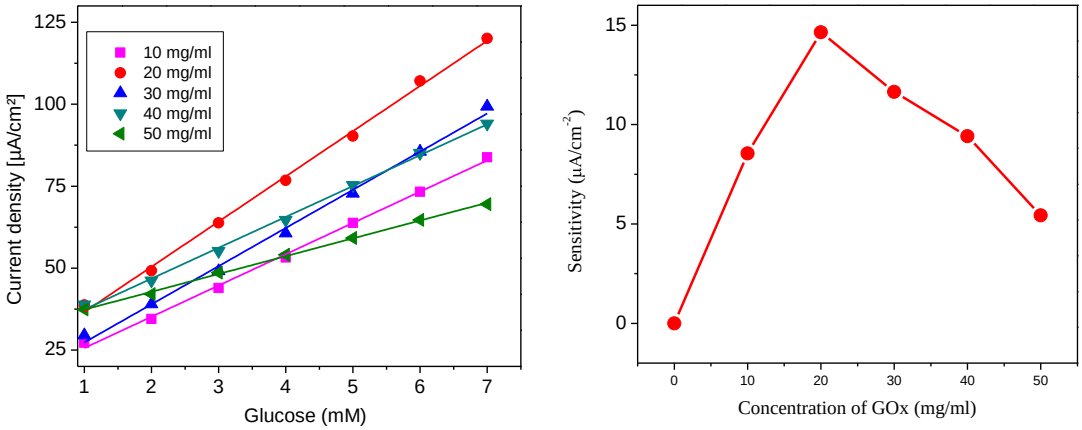

Fig 8.5. a) Calibration curves for glucose (1-9 mM) obtained from CVs of CS-AgNWs/GOx/GCE modified electrode with different GOx concentrations. b) Dependences of glucose sensitivity for different concentration of GOx immobilized on the electrode surface.

The results demonstrated that the sensitivity increases with GOx concentration and reaches the maximum value about 20 mg/ml of GOx. Above this critical GOx concentration, sensitivity is dramatically decreased. This may be caused because at low GOx concentration there will be limited availability of immobilized enzyme to give response. At higher concentration the significant decrease in the sensitivity could be caused by the insufficient chitosan to immobilize this quantity of GOx on the electrode surface resulting in an electronic diffusivity decreasing.

This result confirms that the sensitivity is predominantly controlled by the electronic conductivity on the electrode surface. Therefore, the optimum concentration of GOx was found in 20 mg/ml and this concentration was chosen for constructing the modified electrodes.

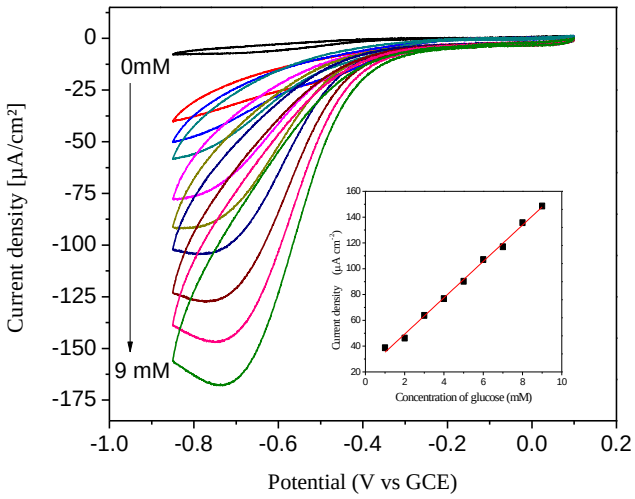

Fig. 8.6. CVs demonstrating the electrochemical detection of glucose over a concentration range of 1-9 mM using CS/AgNWs/GOx/GCE modified electrode at a scan rate of 50 mVs^{-1}. Inset: the corresponding calibration curve of the amperometric response varying glucose concentration (R^2 = 0.99).Sensitivity 14.6 µA m M^{-1} cm^{-2}.

Figure 8.6 shows the CVs of CS/AgNWs/GOx-GCE modified electrode for various concentration of glucose (1-9 mM) in 0.1 M phosphate buffered solution (PBS, pH 7.4) under

O_2-saturation condition. The modified electrode displays a strong reduction peak around -0.7 V and an evident increase in the reduction current upon successive addition of glucose. A calibration plot of glucose concentration versus their respective peak currents calculated at fixed potential (-0.65 V) is shown in the inset of Fig. 8.6. It shows the linear relationship between the catalytic current and the increased glucose concentration from 1 to 9 mM (R^2= 0.99) with sensitivity of 14.6 μA mM^{-1} cm^{-2}. Figure 8.7 shows the schematic illustration of the modified electrode consisting of CS/AgNWs/GOx casted on the GCE electrode.The possible mechanism, of observed well defined reduction peak at -0.7 V, is due to the AgNWs mediated reduction of H_2O_2 produced by the following reactions of glucose and glucose oxidase in presence of O_2.

$$glucose + GO_x(FAD) \rightarrow gluconolactone + GO_x(FADH_2)$$

$$GO_x(FADH_2) + O_2 \rightarrow GO_x(FAD) + H_2O_2$$

By addition of glucose, glucose oxidase (GOx) reacts with glucose and converts into gluconolactone following reduction of the flavin adenine dinucleotide (FAD) prosthetic group. Then, the reduced FAD is reoxidized by the oxygen present in the solution yielding hydrogen peroxide (H_2O_2). The H_2O_2 produced near de GOx molecule is catalyzed by the AgNWs that are well dispersed onto the electrode surface by the chitosan, allowing the charge transfer to the GCE and thus the detection of the reduction current. The high aspect ratio of the nanowires gives the possibilities to react with all H_2O_2 generated by the glucose reaction and at the same time owing its high conductivity increased the current output and the sensitivity of the glucose sensor based on CS/AgNWs/GOx [162]. A comparison of the sensor performance obtained in this work with glucose sensors based on the one-dimensional nanomaterial's reported in the literature is shown in Table 8.1.

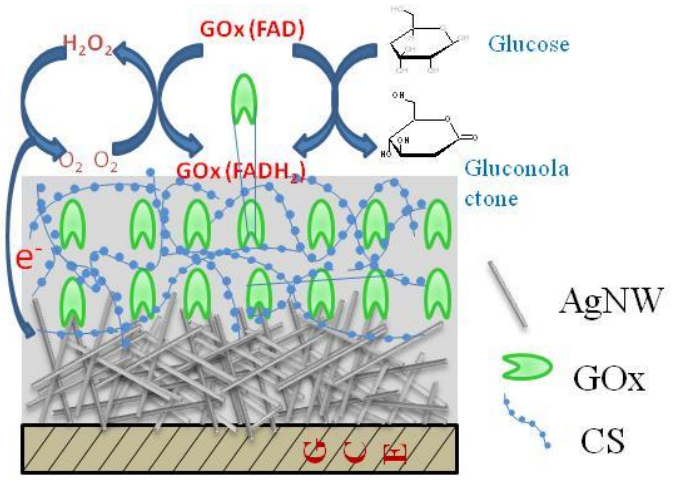

Fig.8.7. Schematic illustration of modified AgNWS/CS/GOx-GCE stabilization structure and the process occurring during the enzymatic electrochemical oxidation of glucose.

Table.8.1 Comparison of the sensor performance of one-dimensional nanomaterial's based glucose sensors.

Electrode material	**Sensitivity ($\mu A\ mM^{-1}\ cm^{-2}$)**	**Linear range**	**Detection limit (μM)**	**ref**
AgNW/CS/GOx	14.72	1-15 mM	2.1	present work
AgNW-GOx	N/A	10 μM to 0.8 mM	2.83	79
AgNW-GOx	15.86	2 to 20 mM	N/A	154
SiNWs@AuNPs-GOx	N/A	1-16 mM	50	163
PtNWAE/GOx	4.21	83 μM-182 mM	83.23	164
1DHS TiO_2/GOx	9.90	0.15 mM-1.5 mM	1.29	165
GR–CNT@ZnO–GOx	5.36 (±0.072)	0.01-6.5	4.5	166

NW: nanowire, PtNWAE: platinum nanowire array electrode, 1DHS: one-dimensional hierarchically structured, CNT: carbon nantube, GR: Graphene.

Is evident from the Table 8.1 remarkable sensitivity of 14.6 μA $mM^{-1}cm^{-2}$, wide linear range (1-15 mM) and significantly lower detection limit 2.1μM of the CS/AgNWs/GOx/GCE modified electrode. These parameter werehigher than that of recently, developed other electrochemical biosensors based on 1-D nanomaterials as listed in Table 1. [79,154,163,164-

166]. The enhancement obtained could be ascribed due to high electrical conductivity of the AgNWs, that allows the formation of electrical wiring network between redox centre and the electrode surface thus, providingthis necessary direct electrical communication. Furthermore, the strong electrostatic interaction between AgNWs and GOx enzymes could facilitate the direct electron transfer rate between electrode surface and immobilized GOx molecules. Other important reason can be due because chitosan possess highly active -OH and $-HN_2/NH_3^+$ functional groups that interacts with the GOx enzymes, thus forming highly stable immobilization on the AgNWs surface which enhance the electron transfer rate.

8.2.3. Stability and interference studies of the modified enzyme electrode

The stability of the CS/AgNWs/GOx/GCE modified electrode was investigated by amperometric measurements in the presence of 5 mM glucose in O_2 saturated PBS solution (pH 7.4). Figure 8.8a shows that the current response of the biosensor retained about 80% of its original response over 7 days, indicating excellent stability and reproducibility of fabricated biosensor. To verify the practical applicability of the modified electrode, the CVs for glucose determination were carried out with different interfering substances, such as ascorbic acid (AA) citric acid (CA) and uric acid (UA). Fig. 8b shows the current response of the CS/AgNWs/GOx/GCE modified electrode to 3 mM glucose in presence of the more frequently possible interfering substances in the real blood samples, like ascorbic acid (AA), citric acid (CA) and uric acid (UA). Fig. 8.8b shows that the current response of the biosensor is not significantly affected by the interfering agents, added in concentration higher than their normal concentration in blood, suggesting the excellent selectivity of the glucose biosensor to the practical determination of glucose.

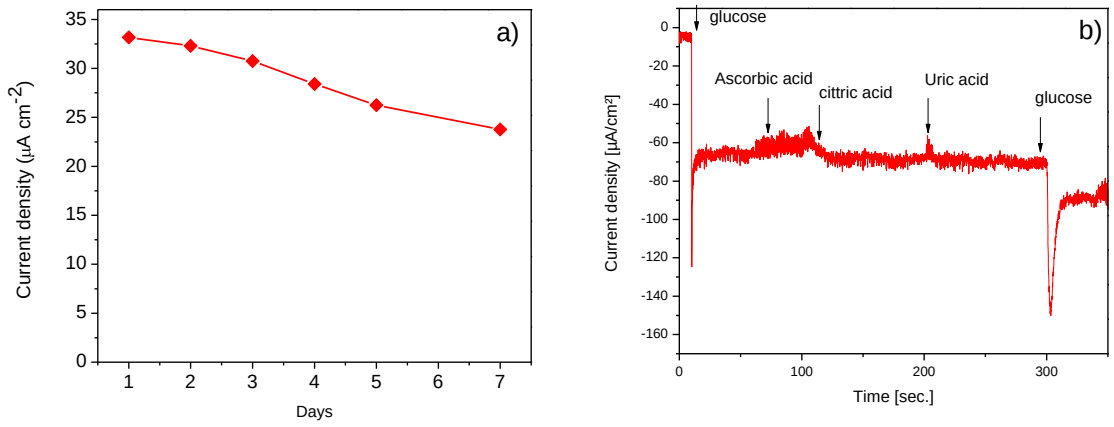

Figure 8.8. a) The stability of the CS/AgNWs/GOx-GCE modified electrode over a week storage period. b) Amperogram showing the effect of interfering substances (3mM) of ascorbic acid (AA), citric acid (CA), uric acid (UA).

8.2.4. Comparsion of glucose biosensing performance based CS/AgNPs and CS/AgNWs modidied electrodes.

Table 8.2. Comparsion of glucose sensing based CS/AgNPs and CS/AgNWs modidied electrodes.

Modified electrode	Sensitivity ($\mu A\ mM^{-1}\ cm^{-2}$)	Linear range	Detection limit
CS/AgNPs/GOx-GCE	8.57	1.4 mM	1 mM
CS/AgNWs/GOx-GCE	14.72	1-15 mM	2.1 μM

Table.8.2 shows that the glucose sensing performance of of two different modified electrodes based on CS/AgNPs and CS/AgNWs under same conditions of measurements. The modified electrode based on CS/AgNWs exhibits remarkably higher sensitivity, wide linear range and low detection limit compared to the CS/AgNPs modified electrode.

8.3. Summary

In summary, the enzymatic electrochemical biosensor based on CS/AgNPs/GOx/GCE and AgNWs/Cs/GOx/GCE has been developed. It was demonstrated that, it was possible to construct an electrochemical enzyme based biosensor for glucose adding glucose oxidase (GOx) enzyme to the previously modified GCE. The effective immobilization of GOx on the AgNPs and AgNWs is possible in the presence of CS. The CS/AgNWs/GOx/GCE modified electrode exhibits excellent enzyme accommodation and support direct electron transfer of redox centres of the enzyme with the modified electrode surface. In comparison with CS/AgNPs/GCE modified electode, CS/AgNWs/GOx/GCE modified electrode showed significantly enhanced sensitivity (two fold). The significant enhancement of sensitivity, stability and linear range could be attributed by the high specific surface area of AgNWs and higher electrical conductivity, facilitate direct electron transfer between redox centre of the enzyme and electrode surface. Moreover, the chitosan plays curicial role in stabilizing GOx and promote the electron transfer kinetics. The excellent electrocatalytic activity of modified electrode with high sensitivity may open promising platform for its exploitation in various diagnosis methods and biosensing applications.

Chapter 9. Conclusions and recommendations

9.1. Conclusions

In this work CS/AgNPs composites have been synthesized using different methods for potential antibacterial and biosensing applications. Besides, different preparation methods, it was found that the similar properties of nanocomposites as:

- Presence of α and σ relaxations;
- Dependence of moisture content in the films on concentration of nanoparticles;
- Interaction of AgNPs with chitosan matrix;
- Relation between electrical and antibacterial properties of nanocomposites.

Additionally, based on this present study the following new results have been obtained:

- A new, simple and efficient extracellular biosynthesis of silver nanoparticles using anaerobic enriched mixed bacteria has been proposed. This simple and green protocol could be used to prepare other metallic nanoparticles.
- The Ag particles size, shape and their distribution in chitosan matrix are highly depend on the synthesis methods, the type of reducing and stabilizing agents used for the synthesis.
- New method based on EDS analysis has been proposed which allow comparing the properties of nanocomposites obtained by different preparation method.
- For the first time, the molecular relaxation process in chitosan and chiotsan/silver nanocompopsites at high frequency range (1 GHz) have been investigated. This new

relaxation process in chitosan based polymers is attributed by the freedom of rotation of side groups (-OH, $-NH_2/NH_3^+$).

- In CS/AgNPs nanocomposite due to interaction of AgNPs with the side groups of chitosan decrease the freedom of side group's rotation.
- For the first time, the correlation between electrical percolation effect and maximum bactericide activity have been found. This can helps to fabricate nanocomposite with well defined concentration with maximum antibacterial properties using electrical measurements.
- The effective immobilization strategies and direct electron transfer methods have been developed for the enzymatic glucose biosensing based on chitosan stabilized silver nanoparticles (AgNPs) and silver nanowires (AgNWs).
- The developed modified electrode of CS/AgNWs/GOx-GCE in this work, exhibited excellent sensitivity with higher stability, showed potential candidate for biosensor platform compared to CS/AgNPs/GCE modified electrodes.

Based on the results obtained in this work, further recommendations towards the future research are discussed in the next section.

9.2. Recommendations

- The new observed high frequency relaxation process in GHz frequency range attributed to the side group rotation of chitosan polymer films. Such method can be potentially applied to other polymer films to estimate the activation energy of side group motion as well as to investigate the interaction mechanism of metal nanoparticles with polymer.
- Another important result is related to antibacterial properties of AgNPs. It was shown to be superior antibacterial activity near electrical percolation concentration of AgNPs. Therefore, this method is the potential platform to design the material by correlating of electrical properties with the antibacterial activity and can be used for the other polymer-metal nanocomposites.
- The modified CS/AgNWs/GOD/GCE electrode exhibited high sensitive detection of blood glucose levels. Therefore, to modify the electrode surface by vertically aligned AgNWs in order to have higher specific surface for direct electrical communication to enhance the biosensor performance has potentially encouraged for the biosensing community.
- Finally, observed excellent antibacterial activity of CS/AgNPs (low particle size) and destruction of fibroblast cells with low concentration of AgNPs, could potentally applied to test the for cancer cells.

List of Publications

Articles in international journals

1. **S. Kumar-Krishnan**, E. Prokhorov, M. Ramirez, M. A. Hernandez-Landaverde, D. G. Zarate-Triviño, Y. Kovalenko, I. Sanchez, J. Mendez-Nonell and G. L. Barcenas, Novel gigahertz frequency dielectric relaxations in chitosan films. ***Soft Matter*, 2014, 10, 8673-8684.**

2. **S. Kumar-Krishnan**, G. Kumar, E. Prokhorov, G. Luna-Bárcenas, German Buitron, Isaac C. Sanchez. Exploitation of anaerobic enriched mixed bacteria (AEMB) for the silver and gold nanoparticles synthesis.***Colloids and Surfaces A: Physicochem. Eng. Aspects*, 2014, 462, 264–270.**

3. **S. Kumar-Krishnan**, D. Zarate-Triviño, E. Prokhorov, G. Luna Barcenas, M. Vazquez Lepe, J.B. Gonzalez Campos., Structure and properties of chitosan-silver nanoparticles nanocomposites. ***Current nanoscience*, 2014**. **DOI:** 10.2174/1573413710666141013223549.

4. J. Betzabe Gonzalez-Camposa, Josue D. Mota-Moralesb, **Siva Kumar**, M. Hernández-Iturriaga[2], E. Prokhorov, G. Luna-Bárcenas, M. Vázquez Lepe, J. Mota-Morales and Z. Y. García-Carvajal., New insights into the bactericidal activity of chitosan-Ag bionanocomposite: The role of the electrical conductivity., ***Colloids and Surfaces B: Biointerfaces* 2013, 111, 741– 746.**

5. **S. Kumar-Krishnan**, E. Prokhorov, G. Luna-Bárcenas, C. Velasquillo, M. Hernández-Iturriaga, M. Vázquez Lepe, Yu. Kovalenko and I.C. Sanchez. Chitosan/silver nanocomposites: Synergistic antibacterial action of silver nanoparticles and silver ions. ***European Polymer Journal. (Under review).***

Conference proceedings

1. **Siva Kumar-Krishnan**, Evgen Prokhorov and Gabriel Luna-Barcenas. Molecular relaxation in chitosan films in GHz frequency range**. Mater. Res. Soc. Symp. Proc. 2014.**

2. **S. Kumar-Krishnan**, E. Prokhorov, G. Luna-Barcenas, A. Mauricio-Sanchez, O. Arias de Fuentes. New High frequency Relaxation in Chitosan and PVA. Proceedings of *3rd* Binational Meeting Mexico-USA in Advances in Polymer Science, **MACROMEX 2014**. Mexico. 3-6 December, 2014.

3. **Siva Kumar-Krishnan**, Olimpia L. Arias de Fuentes, Evgen Prokhorov, Araceli Mauricio-Sanchez, Moisés Oviedo Mendoza and Gabriel Luna-Barcenas., Molecular Relaxation of the Side Groups in Poly (vinyl alcohol) Films in GHz Frequency Range**, Mater. Res. Soc. Symp. Proc. 2015. (*acepted for publication)***

4. **Siva Kumar- Krishnan**. Olimpia Arias de Fuentes., Evgen Prokhorov, J. Gabriel Luna-Barcenas, Electrochemical detection of hydrogen peroxide and glucose based on chitosan stabilized silver nanowire modified electrodes., **IEEE Xplore, 2015. (*accepted for publication).***

Presentation on international conferences

1. **Siva Kumar. K,** E. Prokhorov, G. Luna-Barcenas, Hernadez Itrriage, J.Gonzalez-Campos. Chitosan-Silver Nanostructures for medical applications. *8TH INTERNATIONAL CONFERENCE ON NANOSCIENCES AND NANOTECHNOLOGy*. 9-16th July, 2011, Thessaloniki, Greece.

2. **Siva Kumar. K**, E. Prokhorov, G. Luna-Barcenas, Hernadez Itrriage, D.zarate-Trivino J.Gonzalez-Campos. Structure and Properties of Chitosan-Silver nanoparticles nanocomposite, MACROMEX 2012, *SECOND US-MEXICO MEETING IN POLYMER SCIENCE*., 7-10th December, 2011, Cancun, Mexico.

3. **Siva Kumar. K,** E. Prokhorov, G. Luna-Barcenas, Hernadez Itrriage, J. Gonzalez-Campos**.** Structure and Properties of Chitosan-Silver nanoparticles nanocomposite. *GORDEN RESEARCH CONFERENCE ON POLYMER PHYSICS*. 20-28th July 2012, Boston, United States.

4. **Siva Kumar-Krishnan**, Evgen Prokhorov and Gabriel Luna-Barcenas. Molecular relaxation in chitosan films in GHz frequency range**.** *XXII INTERNATIONAL MATERIALS RESEARCH CONGRESS*, 10-15th August, 2013, Cancun, Mexico.

5. **Siva Kumar-Krishnan**, Olimpia L. Arias de Fuentes, E. Prokhorov, A. Mauricio‐Sanchez, M. Oviedo Mendoza, G. Luna-Barcenas. Molecular Relaxation of the Side Groups in Poly (vinyl alcohol) films in GHz Frequency Range., *XXIII INTERNATIONAL MATERIALS RESEARCH CONGRESS*. 17–21 August, 2014, Cancún, Mexico.

6. **Siva Kumar- Krishnan**. Olimpia Arias de Fuentes., Evgen Prokhorov, J. Gabriel Luna-Barcenas., Electrochemical detection of hydrogen peroxide and glucose based on chitosan stabilized silver nanowire modified electrodes. *9TH IBEROAMERICAN* CONGRESS *ON* SENSORS, 15-19, October, 2014, Bogotá, Colombia.

7. **Siva Kumar-Krishnan**, E. Prokhorov, G. Luna-Barcenas, A. Mauricio-Sanchez, O. Arias de Fuentes. New High frequency Relaxation in Chitosan and PVA. *3rd Binational Meeting Mexico-USA in Advances in Polymer Science, MACROMEX 2014.* Mexico. 3-6 December, 2014.

References

1. H. W. Boucher, *Clin. Infect. Dis*. 50 (2010) 4-9.
2. A. Chen and S.Chatterjee *Chem. Soc. Rev.* 42 (2013) 5425-5438.
3. M. Ahamed, M.S. AlSalhi , M.K.J. Siddiqui., *Clinica Chimica Acta* 411 (2010) 1841-1848.
4. A.M. Schrand, L.K. Braydich-Stollel, J.J. Schlager, L. Dai, S.M. Hussain. *Nanotechnol.* 19 (2008) 235104.
5. B. Nowack, H. F. Krug, M. Height, *Environ. Sci. Technol*. 45 (2011) 1177.
6. C.M. Jones and E. M. V. Hoek J. *Nanopart. Res.* 12 (2010) 1531.
7. J. R. Morones, J. L. Elechiguerra, A. Camacho, K. Holt, J. B. Kouri, J. T. Ramirez and M. J. Yacaman, *Nanotechnol*, 16 (2005) 2346-2353.
8. Q. H. Tran, V. Q. Nguyen and A.T. Le *Adv. Nat. Sci.: Nanosci. Nanotechnol*. 4 (2013) 033001.
9. O. Choi and Z. Q. Hu, *Environ. Sci. Technol*., 42(2008) 4583-4588.
10. C. N. Lok, C. M. Ho, R. Chen, Q. Y. He, W. Y. Yu, H. Z. Sun, P. K. H. Tam, J. F. Chiu and C. M. Che, *J. Proteome Res*, 5 (2006) 916-924.
11. Sondi and B. Salopek-Sondi, *J. Colloid Interface Sci*., 275(2004) 177-182.
12. C. Greulich, D. Braun, A. Peetsch, J. Diendorf, B. Siebers, M. Epple, M. Koller, *RSC Adv*. 2 (2012) 6981.
13. J. Jain, S. Arora, J. M. Rajwade, P. Omray, S. Khandelwal, K. M. Paknikar, *Mol. Pharm*. 6 (2009) 1388.
14. G. A. Martnez-Casta, N. NiÇo-Martnez, F. Martnez- Gutierrez, J. R. Martnez-Mendoza, F. Ruiz, *J. Nanopart. Res*. 10 (2008) 1343.
15. O. Choi, K. K. Deng, N. J. Kim, L. Ross, Jr., R. Y. Surampalli, Z. Hu, *Water Res.* 42 (2008) 3066.
16. S. W. Kim, Y.W. Baek, Y. *J. An, Appl. Microbiol. Biotechnol*. 92 (2011) 1045.
17. E. Navarro, F. Piccapietra, B. Wagner, F. Marconi, R. Kaegi, N. Odzak, L. Sigg, R. Behra, *Environ. Sci. Technol*. 42 (2008) 8959.
18. A. Panacek, M. Kolar, R. Vecerova , R. Prucek, J. Soukupova, V. Krystof, P. Hamal, R. Zboril, L. Kvitek, *Biomaterials* 30 (2009) 6333.
19. J. S. Kim, E. Kuk, K. N. Yu, J. H. Kim, S. J. Park, H. J. Lee, S. H. Kim, Y. K. Park, Y. H. Park, C. Y. Hwang, Y. K. Kim, Y. S. Lee, D. H. Jeong and M. H. Cho, *J. Nanomed. Nanotechnol*, 3 (2007) 95.
20. S. Pal, Y. K. Tak and J. M. Song. *Appl. Environ. Microbiol.*73 (2007) 1712.
21. A.T. Le *et al Adv. Nat. Sci. Nanosci. Nanotechnol.*4 0 (2012) 45007.
22. M. Guzman, J. Dille and S. Godet., *Nanomed. Nanotechnol.* 8 (2012) 37.
23. Kim K J, Sung W S, Moon S K, Choi J S, Kim J G and Lee D G. *J. Microbiol. Biotechnol.* 18 (2008) 1482.
24. A. Pamacek, M. Kola, R. Vec, R. Prucek, J. Soukupova, P. Hamal and R. Zbor *Biomaterials* 30 (2009) 6333.
25. D. R. Monteiro, L. F Gorup, S. Silva, M. Negri, E .R. Camargo and R. Oliveira ., *Biofouling* 27 (2011) 37.
26. M. G. Hwang, H. Katayama, S. Ohgaki, *Environ. Sci. Technol.* 40 (2006) 7434.
27. M. Rai, A. Yadav and A. Gade, *Biotechnol. Adv*., 27 (2009) 76.
28. Q. L. Feng, J. Wu, G. Q. Chen, F. Z. Cui, T. N. Kim and J. O. Kim, *J. Biomed. Mater. Res.*, 52 (2000) 662.

29. M. Raffi, F. Hussain, T. M. Bhatti, J. I. Akhter, A. Hameed and M. M. Hasan, *J. Mater. Sci. Technol*., 24 (2008) 192-196.
30. A.B. Smetana, K. J. Klabunde, G. R. Marchin and C. M. Sorensen, *Langmuir*, 24 (2008) 7457-7464.
31. G. K. Vertelov, Y. A. Krutyakov, O. V. Efremenkova, A. Y. Olenin and G. V. Lisichkin, *Nanotechnol*, 19 (2008) 355707.
32. A.G. Orpen, L. Brammer, F. H. Allen, O. Kennard, D. G. Watson and R. Taylor, J. *Chem. Soc., Dalton Trans*., 1989, 1-83.
33. A.Nel, T. Xia, L. Madler and N. Li, *Science*, 311(2006) 622-627.
34. J. Imlay, S. Chin and S. Linn, *Science*, 240 (1988) 640-642.
35. S. Chairam, E. Somsook, *J. Magn. Magn. Mater*. 320 (2008) 2039-2043.
36. C.C. Berry, S. Wells, S. Charles, A.S.G. Curtis, *Biomaterials* 24 (2003) 4551-4557.
37. J.H. Park, K.H. Im, S.H. Lee, D.H. Kim, D.Y. Lee, Y.K. Lee, et al., *J. Magn. Magn. Mater*. 293 (2005) 328-333.
38. F.-L. Mi, S.-S. Shyu, Y.-B. Wu, S.-T. Lee, J.-Y. Shyong and R.-N. Huang, *Biomaterials*, 22(2001) 165.
39. M. K¨oping-H¨oggard, Y. S. Mel'nikova, K. M. Varum, B. Lindman and P. Artursson, *J. Gene Med.*, 5 (2003) 130.
40. Z. Li, H. R. Ramay, K. D. Hauch, D. Xiao and M. Zhang, *Biomaterials*, 26 (2005) 3919.
41. H.H. Shuai, C.Y. Yang, H. I-Chen Harn, R. L. York, Tzu-Chun Liao, W.S. Chen, J. Andrew Yeh and Chao-Min Cheng., *Chem. Sci*., 4 (2013) 3058-3067
42. D. S. dos Santos, P.J. G. Goulet, N.P. W. Pieczonka, O. N. Oliveira,, and Ricardo F. Aroca., *Langmuir* 20 (2004) 10273-10277.
43. P.C. Bersch, B. Nies, A. Liebendorfer, *J.Mater. Sci. Mater.Med*. 6 (1995) 231-240.
44. K. Sakurai, T. Shibano, K. kimura, T. Takahashi. *sen-iGakkaishi*, 41 (1985) 85.
45. K. Ogawa, T. Yui., M. Miya. Boisci.Biotech.Biochem, 56 (1992) 858-62.
46. D. Maissner, J. Einfeldt, A.K. Wasniewski, *J. Non- Cryst. Solids* 320 (2003) 40-55.
47. J. Einfeldt, D. Maissner, A. Kwasniewski, *Prog. Polym. Sci.* 26 (2001)1419-1472.
48. A.Nogales, T.A. Ezquerra, D.R. Rueda, M. Retuert, *J. Colloid Polym Sci.* 275, (1997) 419-425.
49. B. J. González-Campos, E. Prokhorov, G. Luna-Bárcenas, A. Fonseca-García, I.C. Sanchez. *J. Polym. Sci., Part B: Polym. Phys.* 47 (2009) 2259-2271**.**
50. Y. Hayashi, N. Shinyashiki, S. Yagihara. *J. Non-Cryst.Solids*. 305 (2002) 328-332.
51. A.Ravindran, P. Chandran and S. S. Khan, *Colloids Surf. B*, 55 (2013) 342-352.
52. M. Potara, E. Jakab, A. Damert, O. Popescu, V. Canpean and S. Astilean., *Nanotechnol.* 22 (2011) 135101.
53. X. L. Cao, C. Cheng , Y. L. Ma , C. S. Zhao., *J Mater Sci: Mater Med* 21 (2010) 2861-2868.
54. J. An, Q. Luo, X. Yuan, D. Wang, L. Xueyan., *J. Appl. Polym. Sci*., 120, (2011) 3180-3189.
55. D.Wei, W. Qian., *Colloids. Surface.B: Biointer*. 62 (2008) 136-142.
56. D. Wei, W. Sun, W. Qian , Y. Ye , X.Ma, *Carbohydr.Res*. 344 (2009) 2375-2382.

57. A.Murugadossa, P. Goswamia, A. Paul, A. Chattopadhyaya *J.Molecular Catalysis A: Chemical* 304 (2009) 153-158.
58. A.Regiel, S. Irusta, A. Kyzioł, M.Arruebo and J. Santamaria . *Nanotechnol*. 24 (2013) 015101
59. J. Betzabe Gonzalez-Campos, Josue D. Mota-Morales, Siva Kumar, Diana Zarate-Trivi˜no, Montserrat Hernandez-Iturriaga, Yevgen Prokhorov, Milton Vazquez Lepe, Zaira Y. Garcia-Carvajal, Isaac C. Sanchez, Gabriel Luna-Barcenas., *Colloids and Surfaces B: Biointerfaces* 111 (2013) 741-746.
60. D.L. Tran, G. D. Pham, X. P. Nguyen, D. H.Vu, N. T. Nguyen, V. H. Tran, T. T.Trang Mai, H. B. Nguyen, Q.D. Le, T. N. Nguyen and T. Cham ., *Adv. Nat. Sci.: Nanosci. Nanotechnol.* 2 (2011) 045004.
61. R. Yoksan, S. Chirachanchai., Mater. Chem. Phys. 115 (2009) 296-302
62. H. V. Tran, L. D. Tran, C. T. Ba, H. D. Vu, T.N. Nguyen, D. G. Pham, P. X. Nguyen., Coll .Surfaces A: Physicochem. Eng. Aspects 360 (2010) 32-40
63. R. J.B. Pinto, S. C.M. Fernandes, C. S.R. Freire, P. Sadocco, J. Causio, C. Pascoal Neto, T. Trindade., *Carbohydr. Res*. 348 (2012) 77-83.
64. S Honary, K Ghajar1, P Khazaeli and P Shalchian Tropical., *J. Pharmaceut.Res*. 10 (2011) 69-74.
65. S. Ghosh, T. K. Ranebennur, and H. N. Vasan., *Int.J. Carbohydr. Chem*. 2011.
66. P. Sanpui, A. Murugadoss, P.V. Durga Prasad, S. S.Ghosh, A. Chattopadhyay., *Int. J. Food Microbiol*. 124 (2008) 142-146.
67. M. Banerjee, S. Mallick, A. Paul, A. Chattopadhyay, and S.Sankar Ghosh., *Langmuir* 26 (2010) 5901-5908
68. P. Kaur, A.Choudharyand, R. Thakur. *Int. J.Scientific & Eng. Res*., 4 (2013).
69. K. Vimalaa, Y. Murali Mohana,1, K. Samba Sivudua, K. Varaprasada, S. Ravindraa, N. Narayana Reddya,Y. Padmab, B. Sreedharc, K. MohanaRaju, *Colloids and Surfaces B: Biointerfaces* 76 (2010) 248-258.
70. K. Shameli, M. B.Ahmad, W. M. Zin, W. Yunus, A. Rustaiyan, N.A. Ibrahim, M.Zargar, Y. Abdollahi, *Int. J.Nanomedicine* 5 (2010) 875-887 .
71. J. Hernandez-Vargas, J. Betzabe Gonzalez-Campos, J. Lara-Romero, E. Prokhorov, Gabriel Luna-Barcenas, Judit A. Avina-Verduzco, Juan Carlos Gonzalez-Hernandez *J. Appl. Polym. Sci*. 2014.
72. S.K. Lan Levengood and M. Zhang., *J. Mater. Chem. B*, 2 (2014) 3161-3184.
73. S. Jana, S.J. Florczyk, M. Leung and M. Zhang *J. Mater. Chem*., 22 (2012) 6291-6299
74. L.Zhang, T. J. Webster., *Nano Today* 4 (2009) 66-80.
75. R. Jayakumar, Deepthy Menon, K. Manzoor, S.V. Nair, H. Tamura., *Carbohydr.Polym*. 82 (2010) 227-232.
76. R. G. Sibbald, J. Contreras-Ruiz, P. Coutts, M. Fierheller, A. Rothman and K. Woo, *Advances in Skin & Wound Care*, 20 (2007) 549-58.
77. Z. F. He, Y. H. Song, L. Wang, L. L. Wan, H. Z. Zhu and S. Gao, *Asian J. Chem.*, 24 (2012) 3837-3841.
78. W. Shi, Z. Ma., *Biosen. Bioelectron*.26 (2010) 1098-1103.
79. L.Wang, X. Gao, L. Jin, Q. Wu, Z. Chen, X. Lin., *Sensors .Actuators* 176 (2013) 9-14.
80. H.H. Shuai, C.Y. Yang, H. I.Chen Harn, Roger L. York, Tzu-Chun Liao, W.Shiang Chen, J. Andrew Yeh and C.M.Cheng., *Chem. Sci.*, 4 (2013) 3058-3067.

81. J. L. Arias, L. H. Reddy and P.Couvreur.,*J. Mater. Chem*., 22 (2012)7622-7632.
82. M. Perfezou, A. Turner and A.Merkoc¸ *Chem. Soc. Rev.*, 41 (2012) 2606-2622.
83. Y. F. Huang, H. T. Chang and W. H. Tan, *Anal. Chem*., 80 (2008) 567-572.
84. S. J. Kwon and A. J. Bard, *J. Am. Chem. Soc*., 134 (2012) 10777-10779.
85. Y.Lu, Y.Mei, M. Schrinner, M. Ballauff, M. W.MÖ1ller, N. Breu,. *J. Phys. Chem*. C. *111* (2007) 7676-7681.
86. Willner, I.; Baron, R.; Willner, B. *Adv. Mater*., 18 (2006**)** 1109-1120.
87. Reiad, N. A., Abdel Salam, O. E.; Abadir, E. F.; Harraz, F. A. *Chinese J. Polym. Sci*. 31 (2013) 984-990.
88. J. Virkutyte, R. S. Varma. *Chem. Sci*. 2 (2011) 837-846.
89. R. S. Varma. *Green Chem*. 16 (2014) 2027-2041.
90. D. Hebbalalu, J. Lalley, M. N. Nadagouda, R. S. Varma, *ACS Sustainable Chem. Eng*. 1 (2013) 703-712.
91. M. Akhtar, J. Panwar, Y.S. Yun, ACS Sustainable Chem. Eng. 1 (2013) 591-602.
92. D. I. Gittins, D. Bethell, D. J. Schiffrin, R. J. Nichols, *Nat.* 408 (2000) 67-69.
93. Z. M. Davoudi, A.E. Kandjani, A. I. Bhatt, I. L. Kyratzis, A. P. O'Mullane, and V. Bansal. *Adv. Funct. Mater*. 24 (2014) 1047-1053.
94. L. Liu, C. He, J. Li, J. Guo, D. Yangb, W. Jie. *New J. Chem*. 37 (2013) 2179-2185.
95. H.Yang Mi, Z. Li, L. Sheng Turng, Y. Sun, S. Gong. *Mater. Design*. 56 (2014) 398-404.
96. I. Moreno, N. Navascues, M. Arruebo, S. Irusta, J. Santamaria. *Nanotech*. 24 (2013) 275603-275614.
97. J.J. Zhu, C.X. Kan, J. G. Wan, M. Han, and G.H.Wang., *J.Nanomaterials* (2011)1-7.
98. K. Kalishwaralal, V. Deepak, S. R. Pandian, M. Kottaisamy, S. BarathManiKanth, B. Kartikeyan, S. Gurunathan, *Colloids. Surf. B*. 77 (2010) 257-262.
99. J. Huang, Q. Li, D. Sun, Y. Lu, Y. Su,X. Yang,H. Wang, W. Shao,N. He, J. Hong, C. Chen, *Nanotech.*18 (2007) 105104-105115
100. N. Jain, A. Bhargava, S. Majumdar, J.C. Tarafdar, J. Panwar. *Nanoscale*, 3 (2011) 635-641.
101. P. R. Selvakannan, R. Ramanathan, B. J. Plowman,Y. M. Sabri, H. K. Daima, A. P. Omullane, V. Bansal, S. K. Bhargava. *Phys. Chem. Chem, Phys*. 15 (2013) 12920-12929.
102. A. Ahmad, P. Mukherjee, S. Senapati, D. Mandal, M. I. Khan, R. Kumar, M. Sastry, *Colloids. Surf. B.* 28 (2003) 313-318.
103. R. Ramanathan, A. P. Omullane, R. Y. Parikh, P.M. Smooker, S. K. Bhargava, V. Bansal. *Langmuir*, 27 (2010) 714-719.
104. R. Ramanathan, M. R. Field, A. P. Omullane, P.M. Smooker, S. K. Bhargava, V. Bansal. *Nanoscale*. 5 (2013) 2300-2306.
105. E.Hutter, J.H.Fendler,. *Adv. Mater*. *16* (2004) 1685-1706.
106. J .Zhang, Y.L.Yuan, J.Shen, S.C Lin,. *Eu. Polym J. 39* (2003) 847-850.
107. N. Vigneshwaran, N.M. Ashtaputre, P.V.Varadarajan, R.P. Nachane, K.M. Paralikar, R.H. Balasubramanya, *Mater Let. 61* (2007**)** 1413-1419.

108. J. B.Gonzalez-Campos, E. Prokhorov, J.G Luna-Barcenas, I. C. Sanchez,. *J. Polym Sci. B.48* (2010**)** 739-748.

109.Caires, F.J. Lima, L.S. Carvalho, C.T. Ionashiro, M. *Thermochim. Acta*. *500* (2010) 6-11.

110.M.T.Viciosa, M.Dionısio, R.M. Silva, R.L.Reis,J. F.Mano. *Biomacromol. 5 (*2004) 2073-2082.

111. E. Prokhorov, J. G. Luna-Barcenas, J. B. Gonzalez-Campos, I. C. Sanchez,.. *Mol. Cryst. Liq. Cryst. 536* (2011**)** 24-32.

112. X. Zhu, R. Bai, K.H.Wee, C.Liu,.S.L.Tang,. *J. Membrane Sci.* 363 (2010) 278-286.

113.V. K. Kaushik,. *J. Electron Spect.&Rel. Phen.* 56 (1991**)** 273-277.

114. J.An, X.Yuan, Q.Luo, D.Wang,. *Polym. Int*, 5, (2010) 62-70.

115.Y. Hayashi, N. Shinyashiki, S. Yagihara. J. Non-Cryst.Solids. 305 (2002) 328-332.

116.J. H. Christie, S.H. Krenek, I.M. Woodhead. *Biosystems. Eng*. 102 (2009) 143-152.

117.Z. Osman. *Ionics*, 11 **(**2005) 397-400.

118.S. Havriliak, S. Negami. *J. Polym. Sci. C*., 14 **(**1966) 99-117.

119. C. Chatelet, O. Damour, A. Domard. *Biomater*. 22 **(**2001) 261-268.

120. K. S.Cole, R. H. Cole. *J. Chem. Phys.* 9 **(**1941) 341-352.

121. E. Sandra, Noriega, A. Subramanian. *Int. J.Carbohydr. Chem*.(2011) 1-13.

122.J. Zawadzki, H. Kaczmarek. *Carbohydr. Polym.* 80 **(**2010) 394-400.

123. Y. Dong , C. Xu, M. Wang, Y. Wu, Y. Ruan, *Sci. china. series* B. 44 **(**2001) 216-224.

124.K. Ogawa, T. Yui, K. Okuyama, *Int. J. Biol. Macromol.* 34 **(**2004) 1-8.

125. K. Ogawa. *Agric. Biol.Chem*. 55 **(**1991) 2375-2379.

126. S. Demarger-Andre, A. Domard. *Carbohydr.Polym.* 23 **(**1994) 211-219

127.S. C. Harvey, P. Hoekstra, *J. Phys. Chem*. 76 **(**1972) 2987-94.

128.W. S. Wallace, T. E. Evans, L. H. Hitzrot. *J. Colloid. Interface Sci.* 26 **(**1968) 306-316.

129.J. R.Grigera, F.Vericat, K. Hallenga, H. J. C.Berendsen,. *Biopolym.* 18 **(**1979) 35-45.

130.E. Marzec. *J. Mat. Sci*. 30 **(**1995) 5237 5240.

131.J. C. Papaioannou, N. D. Papadimitropoulos, I. M. Mavridis. *Mol. Phys*. 97 **(**1999) 611- 627.

132. R. Pethig. *Annu. Rev. Phys. Chem*. 43 **(**1992) 177-205.

133.J. Bicerano. Prediction of polymer properties. *Marcel Dekker*, Inc. 2002.

134. P. Barber, S. Balasubramanian, Y. Anguchamy, S. Gong, A. Wibowo, H. Gao, H. J. Ploehn, H-C Loye. *Materials* 2 **(**2009) 1697-1733.

135.W. J. Ellison, K. Lamkaouchi, J.M. Moreau. *J. Mol. Liquids* 6 (1996) 171-279.

136.H. Frohlick, *Theory of Dielectrics*, Oxford University press. 1956.

137.T. Blythe, D. Bloor. Electrical properties of polymers. *Ed. Cambridge University Press*. 2005.

138. H. Montes, K. Mazeau, J. Y. Cavaille. *Macromol.* 30 (1997) 6977-6984.

139.A. De La Rosa, L. Heuxa, J.Y. Cavaille, K. Mazeau. *Polym.* 43 (2002) 5665–5677.

140. A. Lian, S. Besner, L. H. Dao. *Materials Letters* 21 **(**1994) 215-220.

141.G. P. Mikhailov, S. V. Tuchkov, V. V. Lazarev, and E. I. Kulish. *Russian J. Phys. Chem. A,* 88 **(**2014) 936-941.

142.J. F. Nagle, M. Mille, H. J. Morowitz. *J. Chem. Phys*. 72 **(**1980) 3959-3971.

143. X.P. Jia, X.Y. Ma, D.W. Wei, J. Dong, W.P. Qiam, Colloids. Surf.A: Physicochem. Eng.Aspects. 330 (2008) 234-240.

144. G. A. Gaddy, J. L. McLain, E. S. Steigerwalt, R. Broughton, B. L. Slaten, G. Mills. *J.Cluster. Sci*. 12 (2001) 457-471.

145.E. Guibal. *Sep. Pur. Tech*. 38 (2004) 43-74.

146.A. J. Varma, S.V. Deshpande, J.F. Kennedy. *Carbohydr. Polym*. 55 (2004) 77-93

147.F. M. Reicha, A. Sarhan, M. I. Abdel-Hamid, I. M. El-Sherbiny. *Carbohydr. Polym*. 89 (2012) 236-244.

148.Y. Hu, Y. Wu, J. Cai, Y. Ma, B. W, K Xia, X. He. Int. *J. Mol. Sci*. 8 (2007) 1-12.

149.L.Jin, R.B.Bai, *Langmuir*. 18 (2002) 9765-9770.

150.K. Mikhaylichenko, C. Riehn, L. Valachovic, A. Sanov, C. Wittig. *J. Chem. Phys*. 16 (1996) 6807-6817.

151.L.H. Fan, Y.M. Du, B.Z. Zhang, J.H.Yang, J.P. Zhou, J.F. Kennedy, *Carbhohydr. Polym*. 65 (2006) 447

152.P. Prietoa, V. Nistora, K. Nounehb, M. Oyamac, M. Abd-Lefdild, R. Diaz. *Appl.Surf. Sci*. 258 (2012) 8807-8813.

153.G. A. Sotiriou, S. E. Pratsinis, *Environ.Sci.Technol*. 44 (2010) 5649-5654.

154. X.Yang, J. Bai, Y. Wang, X. Jiang and X. He, *Analyst*, 137 (2012) 4362- 4367.

155.C. Chen, Q. Xie, D. Yang, H. Xiao, Y. Fu, Y. Tan and S. Yao, *RSC Adv*., 3 (2013) 4473-4491.

156. K. Kwak, S. Senthil Kumar, K. pyo, and. Lee., *ACS Nano* , In press.

157.X. Kang, J. Wang, H. Wu, I. A. Aksay, J. Liu, Y. Lin., *Biosens. Bioelectron*. 25 (2009) 901-905.

158.L. F. Ang, L. Y. Por, M. F. Yam, *Plos one*, 8 (2013) 70597-70597.

159.I. Moreno, N. Navascues, M. Arruebo, S. Irusta, J. Santamaria. *Nanotech*. 24 (2013) 275603-275614.

160.S. J. Bao, C.M. Li, J.F.Zang, X. Q. Cui, Y. Qiao, and J. Guo, *Adv. Funct. Mater*. 18 (2008) 591-599.

161. S. S .Kumar, K K. Waak, D. Lee,. *Anal. Chem*. 83 (2011) 3244-3247.

162.D. Zhai, B. Liu,Y. Shi, L. Pan, Y.Wang, W. Li, R. Zhang, and G. Yu.,*ACS nano* 7 (2013) 3540-3546.

163. S. Su, Y. He, S. Song, D. Li, L. Wang, C. Fan, S.T. Lee, *Nanoscale*, 2 (2010) 1704-1707.

164.Y. Wang, Y. Zhu, J. Chen and Y. Zeng, *Analyst* 4 (2012) 6025-6031

165.P. Si, S. Ding, J. Yuan, X.Wen (David) Lou, and D.-H. Kim. *ACS nano*, 5 (2011) 7617-7626.

166.K.Y.Hwa, B. Subramani., *Biosen. Bioelectron*. 62 (2014)127-133.